SANDIA REPORT
SAND2022-13028
Printed September 2022

Sandia National Laboratories

Quantifying the Known Unknown: Including Marine Sources of Greenhouse Gases in Climate Modeling

Jennifer M. Frederick[1], Ethan W. Conley[1], Michael A. Nole[1], Thomas Marchitto[2], and Benjamin M. Wagman[1]

[1] Sandia National Laboratories, Albuquerque, NM
[2] University of Colorado, Boulder, CO

Prepared by
Sandia National Laboratories
Albuquerque, New Mexico
87185 and Livermore,
California 94550

Issued by Sandia National Laboratories, operated for the United States Department of Energy by National Technology & Engineering Solutions of Sandia, LLC.

Available to DOE and DOE contractors from
U.S. Department of Energy
Office of Scientific and Technical Information
P.O. Box 62
Oak Ridge, TN 37831

Telephone: (865) 576-8401
Facsimile: (865) 576-5728
E-Mail: reports@osti.gov
Online ordering: http://www.osti.gov/scitech

Available to the public from
U.S. Department of Commerce
National Technical Information Service
5301 Shawnee Rd
Alexandria, VA 22312

Telephone: (800) 553-6847
Facsimile: (703) 605-6900
E-Mail: orders@ntis.gov
Online order: https://classic.ntis.gov/help/order-methods/

ABSTRACT

Researchers have recently estimated that Arctic submarine permafrost currently traps 60 billion tons of methane and contains 560 billion tons of organic carbon in seafloor sediments and soil, a giant pool of carbon with potentially large feedbacks on the climate system. Unlike terrestrial permafrost, the submarine permafrost system has remained a "known unknown" because of the difficulty in acquiring samples and measurements. Consequently, this potentially large carbon stock never yet considered in global climate models or policy discussions, represents a real wildcard in our understanding of Earth's climate. This report summarizes our group's effort at developing a numerical modeling framework designed to produce a first-of-its-kind estimate of Arctic methane gas releases from the marine sediments to the water column, and potentially to the atmosphere, where positive climate feedback may occur. Newly developed modeling capability supported by the Laboratory Directed Research and Development (LDRD) program at Sandia National Laboratories now gives us the ability to probabilistically map gas distribution and quantity in the seabed by using a hybrid approach of geospatial machine learning, and predictive numerical thermodynamic ensemble modeling. The novelty in this approach is its ability to produce maps of useful data in regions that are only sparsely sampled, a common challenge in the Arctic, and a major obstacle to progress in the past. By applying this model to the circum-Arctic continental shelves and integrating the flux of free gas from *in situ* methanogenesis and dissociating gas hydrates from the sediment column under climate forcing, we can provide the most reliable estimate of a spatially and temporally varying source term for greenhouse gas flux that can be used by global oceanographic circulation and Earth system models (such as DOE's E3SM). The result will allow us to finally tackle the wildcard of the submarine permafrost carbon system, and better inform us about the severity of future national security threats that sustained climate change poses.

CONTENTS

LIST OF FIGURES

LIST OF TABLES

ACRONYMS AND TERMS

Acronym/Term	Definition
AOM	anaerobic oxidation of methane
BP	before present
DOE	Department of Energy
ESAS	East Siberian Arctic Shelf
E^3SM	Energy Exascale Earth System Model
IGHCC2	2nd International Gas Hydrate Code Comparison Study
GHG	greenhouse gas
kA	kilo annum (thousand years)
KNN	k-nearest neighbors
LDRD	Laboratory Directed Research and Development
LGM	Last Glacial Maximum
MAAT	mean annual air temperature
MIS	Marine Isotope Stage
RSL	relative sea level
TOC	total organic content

1. MOTIVATION

Researchers have recently estimated that Arctic submarine permafrost currently traps 60 billion tons of methane and contains 560 billion tons of organic carbon in seafloor sediments and soil [1], a giant pool of carbon with potentially large feedbacks on the climate system. For comparison, humans have released a total of ~500 billion tons of carbon into the atmosphere since the Industrial Revolution. Unlike terrestrial permafrost, the submarine permafrost system has remained a "known unknown" because of the difficulty in acquiring samples and measurements. Consequently, this potentially large carbon stock never yet considered in global climate models or policy discussions, represents a real wildcard in our understanding of Earth's climate.

> "Arctic methane is underestimated in current carbon budgets, increasing its already significant global climate impact. Arctic methane should play an important role in global climate policy decisions and actions. However, the Global Methane Pledge does not fully address permafrost sources of methane release and warming. Permafrost methane has significant potential to drive accelerated warming. We currently have no integrated, strategic approach to track and predict carbon emissions from thawing permafrost. Major scientific and technical gaps in measurement, monitoring and modeling capabilities produce large uncertainties in current and future trajectories of Arctic methane emissions. Current Earth system models have very limited capability for modeling permafrost thaw and associated methane emissions. Important recommendations emerging from this Arctic methane workshop include: Acceleration of collaboration among scientists and policymakers on the needed upgrades in spatial and temporal coverage of various monitoring and modeling assets; Rigorous assessment requiring improved modeling, both in terms of fundamental methane physical/chemical/biological processes and at multiple spatial and temporal resolutions."
>
> - *Arctic Methane — Situational Awareness, Assessment & Policy Directions* Workshop hosted by the Wilson Center Polar Institute and Sandia National Laboratories, June 23, 2022.

This report summarizes our group's effort at developing a numerical modeling framework designed to produce a first-of-its-kind estimate of Arctic methane gas releases from the marine sediments to the water column, and potentially to the atmosphere, where positive climate feedback may occur. Newly developed modeling capability supported by the Laboratory Directed Research and Development (LDRD) program at Sandia National Laboratories now gives us the ability to probabilistically map gas distribution and quantity in the seabed by using a hybrid approach of geospatial machine learning, and predictive numerical thermodynamic ensemble modeling [2]. The novelty in this approach is its ability to produce maps of useful data in regions that are only sparsely sampled, a common challenge in the Arctic, and a major obstacle to progress in the past. By applying this model to the circum-Arctic continental shelves and integrating the flux of free gas from *in situ* methanogenesis and dissociating gas hydrates from the sediment column under climate forcing, we can provide the most reliable estimate of a spatially and temporally varying source term for greenhouse gas (GHG) flux that can be used by global oceanographic circulation and Earth system models (such as DOE's E^3SM). The result will allow us to finally tackle the wildcard of the submarine permafrost carbon system, and better inform us about the severity of future national security threats that sustained climate change poses.

1.1. Greenhouse Gases Sequestered in Arctic Marine Sediments

As summarized in [1], during the last glacial period (~115,000–11,700 years BP), permafrost formed on exposed portions of the continental shelves surrounding the Arctic Ocean [3],[4]. Unglaciated portions of the exposed continental shelves accumulated billions of tons of undecomposed plant material in frozen sediment [5],[6],[7]. Methane (CH_4) from biogenic and thermogenic sources accumulated within and below permafrost deposits, with some in gas hydrate form [8][9],[10]. After the Last Glacial Maximum (LGM, ~26,500 years BP), climate warming melted ice sheets and glaciers, which increased global sea level by ~134 m on average [5][11], inundating more than 3 million km^2 of permafrost [7][12], roughly $1/5^{th}$ the size of the present-day terrestrial permafrost region [13],[14] and containing similar density in soil organic carbon [1]. This marine transgression changed the thermal conditions of inundated permafrost, initiating warming and thawing of submarine permafrost that continues today [15],[16][17]. Like terrestrial permafrost, warming of the submarine permafrost makes the carbon stocks available to methanotrophic communities in the marine sediments which release CH_4 as a metabolic product of organic matter degradation. Warming of the sediments may also destabilize relict methane hydrate deposits which dissociate into water and methane gas. Because neither the amount nor the climate sensitivity of subsea carbon stocks is truly known, the submarine permafrost domain remains one of the least-constrained ecosystem feedbacks in the Earth's climate system [18][14][9].

1.2. Gas Escape at the Sediment-Water Interface

Not all gas produced in the marine sediments from methanogenesis or gas hydrate dissociation will make its escape into the water column. Geochemical [19][20] and microbiological evidence [21], together with mass balance calculations [22], nonetheless suggest that up to 90-100% of the dissolved methane produced in marine sediments is consumed *in situ* before reaching the water column by a process known as the anaerobic oxidation of methane (AOM) [23]. AOM is mediated by a consortium of methane-oxidizing Archaea and sulfate-reducing bacteria [21] and requires an alternate electron acceptor other than oxygen. In marine systems this electron acceptor is usually sulphate which comes from the overlying water column [22]. The reaction produces sulphide and the dissolved methane is oxidized to CO_2, which contributes to the formation of carbonates in the sediments near methane seeps [24].

The efficiency of the AOM community may vary under certain conditions, such as in active sediments where upward fluid fluxes are very high, or in areas with high sedimentation rates [27]. Such scenarios may occur after the onset of sudden submarine permafrost thaw, sudden methane hydrate dissociation, or near river mouths. However, for the majority of shelf sediments, as exemplified in a study at the Laptev Sea, [25] show the seawater intrusion and supply of sulphate is sufficient to keep pace with the release of dissolved methane from the thawing submarine permafrost below, fueling an efficient microbial biofilter that prevents much of the dissolved methane from reaching the water column.

On the other hand, methane is much more likely to pass through this biofilter entirely if it is rapidly advected towards the surface in the form of a bubble [26], also known as ebullition. Because methane in gaseous form is not directly accessible to the AOM community [27], it is assumed that the entire amount of methane transported within the gas phase can reach the water column. Such bubbling gas seeps are not uncommon, although quantifying their distribution in space and time is still the focus of ongoing research [28].

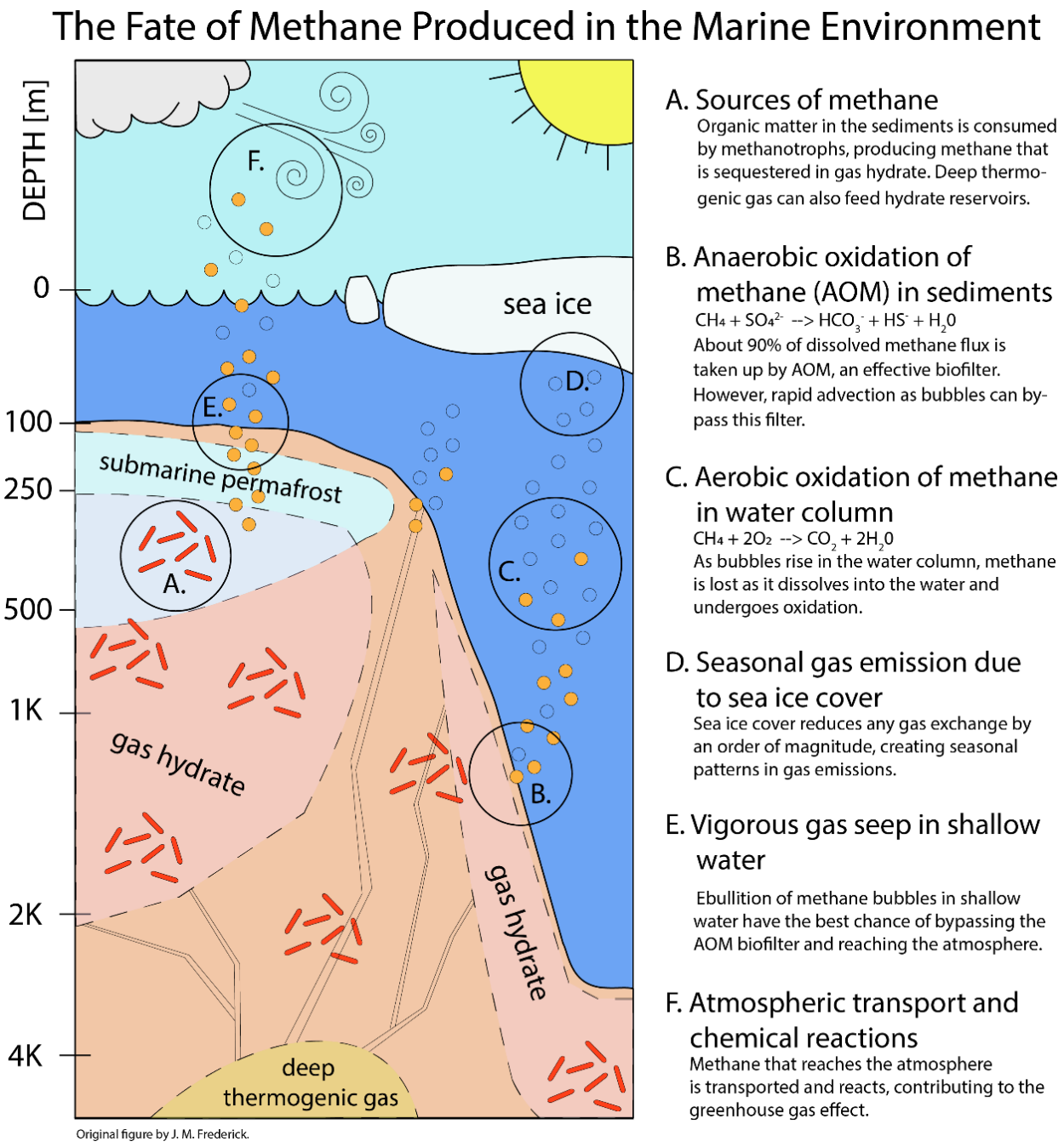

Figure 1. A visual summary of the fate of methane produced in the marine environment. Methane sources and reservoirs in the sediment include: deep thermogenic reservoirs, in-situ methanogenesis of organic matter, and gas hydrate reservoirs. Gas can migrate from the sediments to the water column by diffusion, or ebullition (bubbling). Anaerobic oxidation of methane, mediated by sulfate-reducing bacteria, acts as an effective biofilter for dissolved gas, but vigorous advective transport (ebullition) can bypass this filter and enter the water column. As bubbles rise in the water column, methane is lost to diffusion, and gets aerobically oxidated. Only bubbles released from less than ~100m depth have a chance of surviving to the atmosphere with some methane left. Once in the atmosphere, transport and chemical reactions occur. Sea ice coverage can reduce gas exchange by more than an order of magnitude, creating seasonality to methane emissions. The greenhouse gas effect can lead to a positive climate feedback, potentially accelerating methane emissions.

1.3. Gas Transport in the Ocean Water Column

Methane released from marine sediments can reach the ocean surface or surface mixed layer via turbulent diffusion or rising bubbles. While turbulent transport dominates in deep systems, the release of methane bubbles (ebullition) is the most important pathway in shallow waters, such as the pan-Arctic continental shelf (average water depth ~ 50 m), where they are most likely to reach the atmosphere [29],[30]. As previously described, ebullition is the most effective way for gas to pass through the sediment biofilter as well.

Once in the water column, the larger the bubble, or the shallower the release depth, the more CH_4 will survive the journey to the ocean surface. This is because as the bubble rises, dissolution (methane gas escaping the bubble) and exsolution (other gas species present in the water invading the bubble) will eventually change the composition of gas species inside the bubble [31]. For small bubbles or deep release depths, it is entirely possible for a bubble (consisting entirely of methane when released) to be composed of nothing but "air" when it finally reaches the water surface (air being predominantly nitrogen, oxygen, and carbon dioxide). In a seminal study, [32] have quantified methane gas bubble dissolution using a combination of bubble modeling and acoustic observations of rising bubbles to determine what fraction of the methane transported by bubbles will reach the atmosphere as a function of bubble release depth and bubble diameter. This study can provide bounds on the ebullitive flux of gas required for CH_4 to reach the atmosphere. For example, they found (for a 50 m release depth) that bubbles larger than 4 mm in diameter will reach the atmosphere with some CH_4 left [32]. Simple yet highly predictive 1D models of free and dissolved gas transport in the shallow water column toward the atmosphere have recently been developed [31] and can also be adopted to all of the pan-Arctic continental shelves to provide estimates for how much methane released at the seafloor can survive the journey to the ocean surface.

At bubble seep sites, bottom water is often highly concentrated in methane relative to the surroundings. It has been traditionally understood that dissolved methane in these bottom waters does not influence the atmosphere. For example, in a study conducted west of Svalbard in the summer of 2014, [33] observed high concentrations of dissolved CH_4 in the ocean above the seafloor with a sharp decrease above the pycnocline and very little CH_4 in the atmosphere directly above the seep site. They suggest that dissolved methane captured below the pycnocline may only be released to the atmosphere when physical processes remove this dynamic barrier. Storms that cause large mixing events are one mechanism which may facilitate transport of methane-bearing bottom waters to the surface, resulting in episodic but potentially large methane emissions to the atmosphere [34].

1.4. Gas Emission from the Ocean Surface to the Atmosphere and The Ongoing Scientific Debate

Although the Arctic Ocean constitutes just 4.3% of the global ocean surface area, according to [1] the conservative ocean-atmosphere flux of CH_4 from the submarine permafrost domain is ~15% of CH_4 emissions from global ocean estimates [35]. This flux is dominated by shallow environments, where CH_4 released from the seafloor can more efficiently escape to the atmosphere before oxidation. Moreover, fluxes from submarine permafrost represent 10%–40% of CH_4 release from the five-fold larger terrestrial permafrost zone [36]. Clearly, if these estimates are reliable, methane is being released from the thawing Arctic Ocean seabed at disproportionately larger quantities than from terrestrial permafrost (albeit the proportion that reaches the atmosphere is certainly lower but still highly debated).

Estimates of the annual methane emissions from the ocean to the atmosphere vary widely, with the most hotly contested area being the East Siberian Arctic Shelf (ESAS). The largest shelf in the world and comprising ~25% of all the Arctic shelves, methane emissions have been reported as high as 17 Tg yr^{-1} from the ESAS alone, attributed to degrading submarine permafrost and gas hydrates [37][38]. A large community continues to question the magnitudes of methane emissions previously reported. For example, based on a comprehensive statistical analysis of atmospheric observations and simulations, annual methane emissions from the ESAS were estimated to range from 0.0 to 4.5 Tg yr^{-1} [39]. The same study reported isotopic observations that suggest a biogenic origin (either terrestrial or marine) of the methane in air masses originating from the ESAS. However, a more recent study based on triple-isotope fingerprinting suggests, on the contrary, that ESAS methane may not primarily originate directly from the submarine permafrost (which would have a biogenic origin) but rather the continuous leakage of an old geological reservoir to the water column through degraded regions of the submarine permafrost, serving as conduits of deeper methane to gas-charged shallow sediments [40]. These are just a few examples of the scientific controversy surrounding seabed methane emissions in the ESAS.

The debate is ongoing among the rest of the Arctic too, as nicely summarized by [27], in terms of the significance of submarine permafrost thaw and hydrate destabilization for GHG emissions from Arctic sediments [41],[10], the methane concentrations in Arctic Ocean waters [42][44] and, ultimately, the methane emissions from the Arctic waters [10][43]. Yet methane emissions from warming Arctic shelves remain poorly quantified today [45],[46] and the truth is still far from being known.

Recent satellite observations provide a different perspective in our understanding of GHG emissions from the Arctic Ocean. Using three thermal infrared space-borne spectrometers, [47] estimates the annual CH_4 emission from the Arctic seas is roughly 18 Tg yr^{-1}, with the ESAS contributing 1.3–3.5 Tg yr^{-1}. Because this study was based on remote sensing data, available year-round, it was able to highlight the seasonality associated with methane emissions. [47] found that ocean-atmosphere exchange was correlated to deep mixing events in the Arctic seas, which tended to happen in winter (a time field work is rarely done) and depended on sea ice coverage. Sea ice cover effectively puts a lid on most gas exchange, reducing fluxes by at least an order of magnitude [48], and can cause build-up of gas beneath the ice, which escapes only after break-up, or through large fractures such as polynyas. Similar patterns in modeled methane emissions have been reported by [49], who found that spatial variability of methane fluxes into the atmosphere were primarily due to the peculiarities of the water circulation and ice conditions. Furthermore, increasing periods and areas of ice-free water and decreasing ice concentration have contributed to a steady increase in methane emissions since the middle of the first decade of the current century

1.5. Global Climate Modeling

Global climate models allow us to better understand how the Earth's climate will evolve as an interconnected, complex system. Models such as the DOE's E^3SM, an advanced Earth system model, do this through the coupled simulation of land, ocean, and atmospheric physics, and require the world's most powerful supercomputers to run. While E^3SM does not currently have the capability to accept spatially varying methane sources, researchers are currently working on several critical improvements for the next phase (V3). These include the capability to: (i) simulate methane based on surface emissions and climate feedbacks, and (ii) simulate methane gas in the stratosphere, which is critical to simulating the climate impact of its evolving emissions. Once this capability is in place, the framework developed in this LDRD study will be well positioned to deliver a methane source term from the Arctic Ocean to the atmosphere that varies spatially and temporally.

This page left blank.

2. A HYBRID MODELING FRAMEWORK FOR ESTIMATING MARINE SOURCES OF GREENHOUSE GASES FROM SHALLOW ARCTIC SHELVES

Newly developed modeling capability supported by the LDRD program now gives us the ability to probabilistically map gas distribution and quantity in the seabed by using a hybrid approach of geospatial machine learning, and predictive numerical thermodynamic ensemble modeling [2]. The novelty in this approach is its ability to produce maps of useful data in regions that are only sparsely sampled, a common challenge in the Arctic, and a major obstacle to progress in the past. By applying this model to the circum-Arctic continental shelves and integrating the flux of free gas and dissociating gas hydrates from the sediment column under climate forcing, we can provide the most reliable estimate of a time-varying source term for GHG flux that can be used by global oceanographic circulation, chemistry-climate, and Earth system models (such as DOE's E^3SM). This section describes the components of the workflow.

Our workflow consists of 3 main software packages: (1) the Global Predictive Seabed Model which provides us with machine-learned seabed parameters used in geophysical modeling, (2) Dakota which statistically samples on the seabed parameters provided by GPSM in order to create and drive ensemble simulations in the geophysical model, and (3) the geophysical numerical model, PFLOTRAN, which is a powerful subsurface flow and reactive transport simulator for porous media.

2.1. The Global Predictive Seabed Model (GPSM)

The objective of seafloor prediction is to obtain optimal estimates of any given quantity where it has not been directly measured. Because the seafloor is vast and very sparsely sampled in most quantities, we require a prediction almost everywhere. Conventional interpolation techniques (e.g. splines in tension), that rely only on geospatial proximity, ignore almost everything we know about the seabed are ill-suited for our purpose.

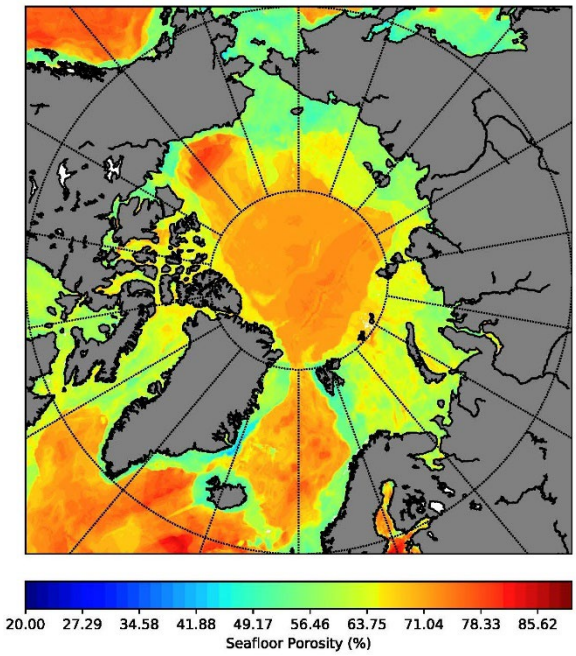

Figure 2. Seafloor porosity predicted by GPSM using geospatial machine learning. (Martin et al., 2015)

Geospatial Machine Learning (GML) predictions are based on the proximity in multi-dimensional geologic predictor space, rather than just geospatial proximity. With GML we predict, or interpolate intelligently, taking advantage of areas that may be geographically very distant, but geologically very similar. GML can use all the information we have about the seabed to predict what we do not know. Not relying strictly on geographical proximity allows prediction in geographical areas that are denied, as well as simply difficult-to-access, such as the Arctic.

GML uses predictors and a predictand. The quantity we wish to predict (the predictand) must also be observed at multiple locations (these observations are the sparse data). Increasing numbers of observations generally correspond to a denser sampling of predictor space, and more certain predictions.

The geologic predictors used in GML are quantities that are known both at the geospatial locations of the

observations, as well as the locations of sites at which we want to predict. These can be quantities that have been measured (e.g. bathymetry), calculated (e.g. distance from shore), or predicted from other GML applications (e.g. porosity). Spatial statistics of these parameters may also be used as predictors. One must clearly be careful to avoid circularity; e.g. using predicted porosity as a predictor to predict a quantity, then subsequently using that same quantity to upgrade the prediction of porosity.

The relationship between the predictors and the predictand need not be known a priori – this is a strength of the GML approach, but also means that for any given application we do not know which predictors will be the most useful. Bad predictors (those poorly correlated with the predictand), can degrade the prediction. For this reason, we typically employ several strategies of predictor (also called feature) selection – determining the best predictors for any given seafloor quantity.

Quantitatively determining the best predictors, as well as quantifying the accuracy of the final prediction, is done through validation. To validate any given group of predictors, we withhold a random fraction of the observed data (usually 10%, for 10-fold validation), make predictions at those locations, and then compare the predicted with the observed values. This is repeated with a different random fraction, until each observation has, at some point, been withheld and predicted. The error between observed and predicted is a reliable, quantitative measure of predictive skill of the prediction method. Validation proves quantitatively and decisively the superiority of machine learning interpolation to conventional, geospatial-only interpolation.

The Naval Research Laboratory's Global Predictive Seafloor Model (GPSM) is a practical implementation of GML designed to provide near real-time estimates of Navy-relevant quantities from continuous seafloor property fields generated by machine learning algorithms (K-Nearest Neighbor, Random Forests, etc.) given often sparse measurements or direct observations compiled from widely available sources.

GPSM has been in use and continuously improved since providing the first global seafloor porosity field, published in 2015 ([50]; see **Figure 2**). More recent publications include predictions of total organic carbon [51], seep probability [28], seafloor sediment accumulation rates [52], recent bathymetry change [53], sediment thickness vs. geologic age [54], density [55], and gas hydrate accumulation [56].

In this work, GPSM is a critical source of model input parameters. Because the seafloor is vast and very sparsely sampled in most quantities, it is impossible to use a measured value everywhere when modeling large regions, such as the Arctic continental shelves. GPSM provides needed model parameters that are spatially continuous and at a high resolution (5 arc minute x 5 arc minute). Because calculated quantities are obtained using machine learning techniques rather than interpolation based on spatial proximity, they provide us with the most reliable values in the absence of observations. Moreover, as a result of GPSM's validation methods, predicted parameter values provided at each seabed location have a standard deviation associated with them (used as a measure of uncertainty from the validation method). The standard deviation is used to construct a distribution for the seabed parameter, allowing us to sample across the distribution and create model ensemble members for geophysical modeling rather than being limited to deterministic simulations. Specifically, we use GPSM-derived seabed values for sedimentation rate (m yr^{-1}), total organic content (TOC) (%), heat flux (W m^{-2}), sediment porosity, seafloor depth (m), seafloor temperature (°C), among many other characteristics of interest.

Estimates for TOC and heat flux were made using the k-nearest neighbors (KNN) algorithm [54] based on datasets of TOC [57] and heat flux [58]. Preliminary predictions for sedimentation rate come from taking sedimentary thickness values from GlobSed [59] and dividing by their reported ages [60].

Seafloor temperature estimates are provided through the World Ocean Atlas [61] and depths were taken from SRTM15+ down-sampled to 5 minutes [62]. Porosity profiles were determined by the Random Forest method using data from the Deep Sea Drilling Project, Ocean Drilling Program, Integrated Ocean Drilling Program, and Pangaea data sets [63],[64]. Further detail on how GPSM is used in our simulation framework will be given in the following sections.

2.2. Dakota

We use the statistical software package, Dakota, to sample on the distribution associated with each uncertain seabed parameter at each simulation location within the computational domain used in geophysical numerical modeling. Dakota was developed to optimize simulation codes and provide uncertainty quantification of parameter studies [65] and has a wealth of capability that we do not use in this study but can be included for additional analysis of simulation results (see [2] for examples, such as determining correlation coefficients between input variables and output values). Values for the mean, μ, and standard deviation, σ, of each seafloor parameter from GPSM are written as input to Dakota to sample on for each simulation location. Dakota uses the Latin hypercube sampling method to produce a set of values for any uncertain variable used as input in the simulations by dividing the range of each variable into N distributions of probability 1/N and then selecting N values for each variable in order to accurately represent the variability of all parameters [66]. In this work, we assume the distribution is normal for all uncertain parameters and allow for the truncation of this distribution to prevent unphysical values from being chosen (i.e., negative values for parameters that can only be positive, etc.). Dakota is also used as a driver for the ensemble geophysical simulations it has partially defined through the statistical sampling method used.

2.3. PFLOTRAN HYDRATE Mode

The open source, massively parallel, multiphase flow and reactive transport finite volume simulator PFLOTRAN [105] is used as the geophysical numerical model in this workflow and was chosen both for its high-performance computing capabilities and its extensive in-house user and developer community at Sandia National Laboratories. Previous support by the LDRD program at Sandia National Laboratories allowed the development of gas hydrate modeling capability to model methane production along with associated free gas and/or gas hydrate formation in marine sediments (PFLOTRAN's HYDRATE Mode) [2]. This capability was verified through an international code comparison effort where results very closely matched those of simulators like TOUGH+HYDRATE and STOMP [74]. Moreover, it was applied to a well-studied gas hydrate province offshore North Carolina called Blake Ridge [56], and the results from this study showed strong agreement with previous modeling studies at this site and with data from Ocean Drilling Program expeditions [104].

Under the scope of the current work, further development was undertaken to fully treat the evolution of multiphase free gas, gas hydrate, ice, and liquid water systems in marine sediments under significant thermal and pressure perturbations and over geologic length- and time- scales. Specifically, the work presented here will discuss how ice fits into the governing equations solved by HYDRATE Mode, the 15 "phase states" of the simulator in HYDRATE Mode, capillary pressure function non-uniqueness when considering the presence of multiple non-wetting phases like ice, and an overview of all options available to a user of HYDRATE Mode in PFLOTRAN.

2.3.1. Governing Equations

PFLOTRAN's HYDRATE Mode solves a nonlinear system of partial differential equations describing transient conservation of water mass, component mass (e.g., methane), and energy. The system of

equations is tightly coupled and solved fully-implicitly using a two-point flux finite volume spatial discretization and backward Euler time discretization, ensuring unconditional stability of the solution. The system of equations is solved using a Newton-Raphson solution search technique. The code is fully parallelized and can run on structured or unstructured grids. The governing equations for mass and energy conservation are:

$$\frac{\partial}{\partial t}\phi\left(\sum_{\alpha=l,g,h,i} s_\alpha \rho_\alpha x_w^\alpha\right) + \nabla \cdot \left(q_l \rho_l x_w^l + q_g \rho_g x_w^g - \phi s_l D_l \rho_l \nabla x_w^l - \phi s_g D_g \rho_g \nabla x_w^g\right) = Q_w \quad \text{Equation 1}$$

$$\frac{\partial}{\partial t}\phi\left(\sum_{\alpha=l,g,h,i} s_\alpha \rho_\alpha x_m^\alpha\right) + \nabla \cdot \left(q_l \rho_l x_m^l + q_g \rho_g x_m^g - \phi s_l D_l \rho_l \nabla x_m^l - \phi s_g D_g \rho_g \nabla x_m^g\right) = Q_m \quad \text{Equation 2}$$

$$\sum_{\alpha=l,g,h,i}\left(\frac{\partial}{\partial t}(\phi s_\alpha \rho_\alpha U_\alpha) + \nabla \cdot (q_\alpha \rho_\alpha H_\alpha)\right) + \frac{\partial}{\partial t}\left((1-\phi)\rho_r C_p T\right) - \nabla \cdot (\kappa \nabla T) = Q \quad \text{Equation 3}$$

where ϕ is the porosity of the medium, s_α is the saturation of phase α, ρ_α is the density of phase α, x_w^α is the mass fraction of water in phase α, q_l and q_g are the respective advective liquid and gas fluxes, D_l and D_g are the respective liquid and gas diffusion coefficients, Q_w and Q_m are respective source/sink terms for water and the solute component, U_α is the specific internal energy of phase α, H_α is the specific enthalpy of phase α, C_p is the heat capacity of the rock, T is temperature, and κ is the composite thermal conductivity of all phases. $-\partial\partial t\phi\left(\sum_{\alpha=l,g,h,i} s_\alpha \rho_\alpha x_w^\alpha\right) + \nabla \cdot \left(q_l \rho_l x_w^l + q_g \rho_g x_w^g - \phi s_l D_l \rho_l \nabla x_w^l - \phi s_g D_g \rho_g \nabla x_w^g\right) = Q_w$ Equation 1 describes conservation of the water mass component (*w*) and $-\partial\partial t\phi\left(\sum_{\alpha=l,g,h,i} s_\alpha \rho_\alpha x_m^\alpha\right) + \nabla \cdot \left(q_l \rho_l x_m^l + q_g \rho_g x_m^g - \phi s_l D_l \rho_l \nabla x_m^l - \phi s_g D_g \rho_g \nabla x_m^g\right) = Q_m$ Equation 2 describes conservation of the solute component (*m*), which for the purpose of constitutive relationship development in this work is considered to be methane but which could be developed more generally in the future. $\alpha=l,g,h,i\left(\frac{\partial}{\partial t}(\phi s_\alpha \rho_\alpha U_\alpha) + \nabla \cdot (q_\alpha \rho_\alpha H_\alpha)\right) + \frac{\partial}{\partial t}\left((1-\phi)\rho_r C_p T\right) - \nabla \cdot (\kappa \nabla T) = Q$ Equation 3 describes conservation of energy across all phases, including the rock matrix and considering heat conduction through the composite material (rock matrix and pore constituents).

In this formulation, a given simulated porous medium can contain any combination of liquid (l), free gas (g), gas hydrate (h), and ice (i) phases. The gas hydrate and ice phases are considered immobile and can only move through the domain if the sedimentation feature is turned on, which is described in a later section. Therefore, the governing equations only contain advective flux terms for the liquid and gas phases. Similarly, diffusion is only modeled through the fluid phases and is neglected in the solids.

Advective fluxes are modeled using Darcy's Equation as follows:

$$q_\alpha = -\frac{k k_\alpha^r}{\mu_\alpha}\nabla(P_\alpha - \rho_\alpha g z) \quad \text{Equation 4}$$

where k is the intrinsic permeability of the porous medium, k_α^r is the relative permeability of mobile phase α, μ_α is the phase viscosity, and P_α is the phase pressure. In multiphase systems, the nonwetting phase pressure is constrained through a capillary pressure function relationship. HYDRATE Mode can access PFLOTRAN's standard capillary pressure relationships which include Van Genuchten and Brooks-Corey formulations, among others. Likewise, HYDRATE Mode also can use all of PFLOTRAN's standard relative permeability functions.

The Fourier heat conduction term uses a composite thermal conductivity term, κ, which includes all phases in the pore space and the solid rock phase. HYDRATE Mode can use any of the standard thermal conductivity options in PFLOTRAN, including temperature-dependent thermal conductivity, but because HYDRATE Mode models gas hydrate and ice it is recommended that the user use the default formulation for effective thermal conductivity, κ_{eff}:

$$\kappa_{eff} = \kappa_{dry} + \phi \sum_{\alpha=l,g,h,i} s_\alpha \kappa_\alpha \qquad \text{Equation 5}$$

where κ_{dry} is the dry thermal conductivity, an input parameter equivalent to $(1-\phi)k_{rock}$, κ_l= 0.59 W/m-K, κ_m=0.03 W/m-K, κ_h=0.58 W/m-K, and κ_i=2.2 W/m-K.

Furthermore, internal energy is related to enthalpy via phase pressure as follows:

$$U_\alpha = H_\alpha - \frac{P_\alpha}{\rho_\alpha} \qquad \text{Equation 6}$$

The internal energy of the ice phase is represented via the formulation of [67]:

$$U_i = L_w + 185T + 3.445(T^2 - 273.15^2), \quad T \geq 90K \qquad \text{Equation 7}$$
$$U_i = L_w + 4.475(T^2 - 273.15^2), \quad T < 90K$$

where L_w is the latent heat of fusion for water, set at -6017.1 J/mol.

The enthalpy of the hydrate phase is given by the following [68]:

$$H_h = C_{ph}\left(T - T_q\right) + \frac{H_{h0}}{N_{hyd}+1} \qquad \text{Equation 8}$$

where H_{h0} is the hydrate reference enthalpy, set to -54,734 J/mol, N_{hyd} is the hydration number (default is 6), T_q is the quadruple point (0C in the absence of salt), and C_{ph} is the heat capacity of hydrate, computed as follows:

$$C_{ph} = \frac{1620(M_w N_{hyd} + M_m)}{1000}$$ Equation 9

where M_w is the molecular weight of water and M_m is the molecular weight of methane.

To form a free gas phase from dissolved methane in an aqueous solution, methane must accumulate until its concentration exceeds its solubility in the aqueous phase. In the current equilibrium formulation, Henry's Law is used to describe the partitioning between the dissolved aqueous and free gas phases. The Henry's constant for methane is computed as follows [69]:

$$K_h = 1000e^{5.1345 + \frac{7837}{T} - \frac{1.509x10^6}{T^2} + \frac{2.06x10^7}{T^3}}$$ Equation 10

where K_h is the Henry's constant in Pa per dissolved mole fraction of methane. When the concentration of dissolved methane in aqueous solution surpasses its equilibrium concentration at a given pressure, the system transitions from the aqueous state to the two-phase gas-aqueous state. More information on phase state combinations in HYDRATE Mode can be found in the following sections.

Likewise, if enough methane is available in the dissolved phase and the pressure and temperature conditions are favorable for gas hydrate formation, excess methane will form a new methane hydrate phase. Formation of the methane hydrate phase consumes both water and methane in constant proportion, by default set to 0.1429 mol CH_4 per mol H_2O. There is also an associated exothermicity of hydrate formation, which is accounted for in the energy balance. Free gas, gas hydrate, and liquid can coexist at specific pressures and temperatures defined by the phase boundary. The default hydrate phase boundary is the representation from [70], and the user also has the option to use a more accurate (and more complex) Moridis (2003) formulation [71]. For this work, a simplified (and importantly, invertible) version of the Moridis (2003) equation was developed:

$$P_e = e^{0.0334940999T - 8.1938174346}, \quad T < T_q$$ Equation 11
$$P_e = e^{0.1100383278T - 29.1133440975}, \quad T \geq T_q$$

where P_e is the equilibrium pressure in MPa.

An ice phase forms whenever the temperature drops below T_q. If there is no salinity in the system, T_q is set to 0C. For this work, a salinity adjustment was added to shift the freezing temperature both of water and of gas hydrate. For gas hydrate, the equilibrium phase boundary is adjusted by a temperature correction as a function of salinity as follows in [72]:

$$dT = dT_0 \frac{\ln(1 - x_m^l)}{\ln(1 - x_{m,ref}^l)}$$ Equation 12

where dT_0 is the reference temperature correction, set to -0.37C, and $x^l_{m,ref}$ is the reference salt mole fraction, set to 0.03311.

For ice formation, T_q is adjusted as a function of and is computed as follows [73]:

$$dT = -57.5x^l_m + 112(x^l_m)^2 \quad \text{Equation 13}$$

where x^l_m is the dissolved salt mass fraction.

2.3.2. Representation of Ice and Hydrate Phase Behavior in HYDRATE Mode

When gas hydrate forms out of aqueous solution, its formation involves a density change, exothermic energy release, and consumption of the water and methane components. Therefore, further methane hydrate growth is constrained by several mechanisms, including pressure change, temperature change, and limited availability of the methane component to take from the aqueous phase.

In the case of ice formation, the ice phase only consumes the water component and not the methane component. If methane is dissolved in the pore space, the process of ice formation tends to concentrate methane in the remaining liquid water. As ice formation proceeds, the methane can supersaturate and eventually form a separate free gas or gas hydrate phase. Ice formation is typically only constrained by the resulting exothermic temperature change on freezing, meaning that if heat is sufficiently dissipated through the system over the timescales of interest it is very easy to completely fill the pore space with ice. This results in significant numerical challenges (especially in 1D) as the pore space becomes occluded with a solid and pressure in adjacent grid cells with fluid in them have no means of dissipating excess pressure buildup due to volume changes associated with ice formation. It is also physically unrealistic, as a liquid phase is known to exist in the small pores of sediments well below 0ºC. Therefore, in the current framework the option was included to treat both ice and gas hydrate formation in small pores as following a formulation of the Gibbs-Thomson equation that transforms pore radius to nonwetting phase capillary pressure vis-à-vis the Young-Laplace equation and all relevant assumptions as follows:

$$dT = -T_m \frac{P_c}{H_f \rho_\alpha \cdot 1000} \quad \text{Equation 14}$$

where dT is the freezing point depression of either ice or hydrate, T_m is the bulk melting temperature of a given phase (ice or hydrate), P_c is the phase capillary pressure, evaluated as a function of effective phase saturation (described in detail in a later section), H_f is the bulk enthalpy of fusion of ice (6033.54 J/mol) or hydrate (7161 J/mol), and ρ_α is the density of ice (920 kg/m^3) or hydrate (900 kg/m^3). The resulting effect is that for a solid ice or gas hydrate phase to precipitate in progressively smaller pores at a given pressure requires progressively lower temperatures. This ultimately adds an additional constraint to both hydrate and ice formation which can practically prevent full blockage of the pore space by a solid.

2.3.3. Capillary Pressure Function Non-Uniqueness

In the formulation developed here, liquid water is considered the only wetting phase. All other phases (free gas, gas hydrate, ice) are considered nonwetting phases. In order to apply a freezing point depression for ice phase or hydrate phase growth, the phase saturations are plugged into a capillary pressure function to obtain a phase capillary pressure and thus a freezing temperature offset. This is straightforward when transitioning from single phase liquid to two-phase (liquid-ice or liquid-hydrate). It is more complicated, however, when dealing with 3 or 4 phases coexisting in the pore space.

For instance, take the example scenario where dissolved methane exists in sediment pore water at high pressure, low temperature, and close to methane solubility in equilibrium with a gas hydrate phase. If the top of the sediment column were to begin to freeze, ice formation in the pore space would consume water but not methane. This would result in a concentration of the remaining methane in the pore water. As the ice phase grows, dissolved methane concentrations in the remaining pore water increase (methane mass stays constant and liquid water mass decreases). At some point, methane concentration exceeds its solubility, and a hydrate phase can form. But hydrate and ice cannot occupy the same pores at the same time, so using absolute phase saturations to compute their respective capillary pressures will result in underpredicting the extent of subcooling required to grow ice or hydrate. If, say, ice exists at 40% saturation and gas hydrate exists at 30% saturation. In this case, 70% of the pore space is occupied by non-wetting phases, so the wetting phase (water) will only be present in the smallest 30% of pores. If capillary pressure were evaluated independently for ice and for gas hydrate, the capillary pressure function would use an inconsistent value for wetting phase saturation (60% for the ice function and 70% for the gas hydrate function), and both values would be much greater than the actual amount. Thus, the capillary pressure function evaluation must consider all phases present.

If the behavior of the system is to be reversible, the resulting state of the system that includes gas hydrate and ice must be solely a function of phase saturations and not on the state of the system at some prior time. To achieve reversibility, the current approach assumes that the ice and hydrate phases partition the largest pore space in a consistent manner that is independent of simulation history. For simplicity, HYDRATE Mode assumes that all nonwetting phases partition the largest pore space in equal amounts. What this means is that for a 3-phase system with ice, gas hydrate, and water, the water remains in the small pores while the ice and gas hydrate partition the large pore space. If gas hydrate forms in pores occupied by ice, the ice must either melt or form in smaller pores to maintain its phase saturation. The resulting capillary pressure function evaluation proceeds as follows:

$$P_{c\alpha} = P_c(2s_\alpha), \qquad s_\alpha \le s_\beta$$
$$P_{c\alpha} = P_c(s_\alpha + s_\beta), \quad s_\alpha \ge s_\beta \qquad \text{Equation 15}$$

where $P_{c\alpha}$ is the capillary pressure of phase α, β denotes the other nonwetting phase in the system, and P_c denotes the function for capillary pressure evaluated at an arbitrary saturation, s.

Expanding this formulation, in the instance where four phases are present in the pore space (water, free gas, gas hydrate, and ice), assuming equal partitioning of the co-occupied pore space by the non-wetting phases, capillary pressure of each phase is computed as follows:

$$P_{c\alpha} = P_c(3s_\alpha), \qquad s_\alpha \le s_\beta \le s_\gamma$$
$$P_{c\alpha} = P_c(2s_\alpha + s_\beta), \quad s_\beta \le s_\alpha \le s_\gamma$$
$$P_{c\alpha} = P_c(2s_\alpha + s_\gamma), \quad s_\gamma \le s_\alpha \le s_\beta$$
$$P_{c\alpha} = P_c(2s_\alpha + s_\gamma), \quad s_\gamma \le s_\alpha \le s_\beta$$

Equation 16

2.3.4. Phase States and Primary Variables

Table 1. Primary Variables for Each Phase State in Hydrate Mode. P_l: liquid pressure, P_g: gas pressure, P_a: air pressure, RH: relative humidity x_m^a: mole fraction of methane in the aqueous phase, x_m^h: mole fraction of methane in the hydrate phase, x_m^i: mole fraction of methane in the ice phase, T: temperature, S_l: liquid saturation, S_g: gas saturation, S_h: hydrate saturation, S_i: ice saturation. In instances where P_g is solved but no gas phase exists, this is treated as the pressure of a gas phase were it to be present in the system (often also equal to the liquid pressure).

Phase State	Primary Variables
Aqueous (Liquid) State	P_l, x_m^a, T
Gas State	P_g, P_a (RH), T
Hydrate State	P_g, x_m^h, T
Ice State	P_g, x_m^i, T
Gas-Aqueous State	P_g, S_g, T
Hydrate-Gas State	P_g, S_g, T
Hydrate-Aqueous State	P_g, S_h, T
Hydrate-Ice State	P_g, S_h, T
Gas-Ice State	P_g, S_i, T
Aqueous-Ice State	P_l, x_m^a, S_l
Hydrate-Gas-Aqueous State	S_l, S_h, T
Hydrate-Aqueous-Ice State	P_g, S_l, S_i
Hydrate-Gas-Ice State	S_i, S_h, T
Gas-Aqueous-Ice State	P_g, S_l, S_i
Hydrate-Gas-Aqueous-Ice State	S_l, S_g, S_i

PFLOTRAN's HYDRATE Mode uses primary variable switching to evaluate state properties of the system in any given grid cell at a given simulation time. For example, if a given grid cell is in the liquid state, then that cell is fully saturated with liquid water and contains no other phases in the pore space. In this case, HYDRATE Mode solves for liquid pressure, mole fraction of dissolved methane, and

temperature as its primary variables. While the primary variable switching occurs internally when a phase transition occurs (e.g., from the liquid state to liquid-hydrate state), if a user intends to apply an initial or boundary condition to the model, the user must set such a condition with the primary variables that are appropriate for the intended state of the condition. For example, if the user initializes the system at hydrostatic pressure with only dissolved methane in the system, the initial condition of the simulation would be a liquid state condition with primary variables as described above. If the user were to then set a top boundary condition representing exposure to the air, then the boundary condition would be in the gas state and the primary variables would be total gas pressure, air partial pressure (or relative humidity), and temperature (see Table 1).

There are a few phase state combinations for which reading in primary variables by themselves does not immediately identify the phase state. Due to the structure of model initialization in the code, these phase states require the user to identify the intended state in the specification of the flow condition. Those states are Hydrate, Ice, Hydrate-Ice, and Hydrate-Aqueous-Ice.

In total, there are 15 combinations of phases that can be present in HYDRATE Mode. When considering the possibility of ice formation, there are 8 potential phase states in which ice could exist; these phase states were more robustly developed as part of this work. To check initialization for all phase states and internal phase state consistency, a suite of single-cell test problems was designed where each simulation is initialized and run to 1 day with no flux boundary conditions. By taking multiple timesteps, the simulator not only initializes the system at a given state with a given set of primary variables, it also must check whether the state changes given the set of primary variables. For a given material, **Table 2** describes the series of tests conducted to verify flow condition setting and internal consistency.

Table 2. Test Cases for Phase State Initialization and Internal Consistency. In bold are the primary variables used to define the state. Pure Hydrate and pure Ice states currently yield numerical convergence difficulties due to fixed methane and ice component mass fractions.

Phase State	T (C)	P_l (Pa)	P_g (Pa)	S_l	S_g	S_h	S_i	x_m^a	x_m^g
Liquid	**10**	**1E6**	--	1	0	0	0	**1E-4**	--
Gas	**25**	-9.9E7	**1E6**	0	1	0	0	--	**0.998**
Hydrate	--	--	--	--	--	--	--	--	--
Ice	--	--	--	--	--	--	--	--	--
Gas-Aq	**30**	9.682E5	**1E6**	0.5	**0.5**	0	0	2.24E-4	0.996
Hydrate-Gas	**18**	--	**1E8**	0	**0.7**	0.3	0	--	0.195
Gas-Ice	**-0.05**	--	**2E5**	0	0.8	0	**0.2**	--	0.997
Aq-Ice	-5.8E-3	**1E6**	--	**0.9**	0	0	0.1	**1E-5**	--
Hyd-Gas-Aq	**18**	1.948E7	1.949E7	**0.8**	0.14	**0.06**	0	5.47E-3	0.999
Hyd-Aq-Ice	-1.40E-2	**1E7**	--	**0.65**	0	0.05	**0.3**	1.18E-3	--

Phase State	T (C)	P_l (Pa)	P_g (Pa)	S_l	S_g	S_h	S_i	x_m^a	x_m^g
Hyd-Gas-Ice	**-1E-2**	--	2.62E6	0	0.65	**0.25**	**0.1**	--	0.999
Gas-Aq-Ice	-3.76E-3	1.91E5	**2E5**	**0.8**	0.15	0	**0.05**	8.99E-5	0.997
Hyd-Gas-Aq-Ice	-9.66E-3	2.59E6	2.62E6	**0.5**	**0.1**	0.2	**0.2**	1.18E-3	0.999

2.3.5. PFLOTRAN HYDRATE Mode Test Cases

Updated software capabilities were tested on a series of transient simulation test cases to as concept demonstration and to identify areas for performance improvement. The first test case is a modification of a 1D radial thermal stimulation test case that was part of the 2nd International Gas Hydrate Code Comparison Study (IGHCC2) to include capillarity, a simplified 3-phase equilibrium pressure formulation, and 3-phase effective saturation considerations following the formulation of $P_{c\alpha} = P_c(2s_\alpha), \quad s_\alpha \leq s_\beta$ Equation 15. The second test case tracks ice formation in a vertical water column which uses a new Dirichlet Seepage boundary condition and is designed to compare the effect of different pore size distributions on the freezing behavior of water in soils. The third test case is perhaps the most numerically complex and is an extension of the freezing test case which adds a gas source term and also uses a standard Dirichlet top boundary condition for comparison.

2.3.5.1. IGHCCS2 Thermal Test with Capillary Pressure

This test is a modification of the Benchmark Problem 3, Case 1 presented in [74] in which a 1D cylindrical model simulates the dissociation of gas hydrate by thermal stimulation. Benchmark Problem 3, Case 2, models gas hydrate dissociation by depressurization with similar sediment physical properties. The model is radially symmetric with a log-spaced discretization starting with $\Delta r = 0.02$ m and ending with a max $\Delta r = 12.6$ m for a total domain radius of 1 km. The model starts with a hydrate saturation of 50%, a uniform pressure of 4.6 MPa, uniform temperature of 3ºC, and applies a heat source at the center of 150 W. In the initial formulation, the thermal stimulation problem does not consider capillary pressure.

For this test, we incorporated the capillary pressure function from the depressurization benchmark problem as well as a simplified version of the Moridis (2003) phase boundary, Gibbs Thomson effects on hydrate growth due to capillarity, and scaling of the mobile phase saturations to send the relative permeability functions values for phase saturations expressed as fractions of only the mobile pore phases (excluding solid phases like hydrate; this would result in, e.g., an effective water saturation of 1 if the system had only gas hydrate and water in the pore space).

In the original problem, all teams showed numerical oscillations in the hydrate and gas saturation solutions. This is seemingly an unavoidable component to these kinds of problems, which involve solving numerically challenging problems related to coupled thermodynamics and phase behavior. Interestingly, incorporating capillary pressure appears to dampen this effect. It also results in lower gas saturations even though total mass in the system should be constant, which is likely due to gas compressibility effects. This also verifies that the simplified phase boundary produces similar results; small differences in the leading edge of the gas hydrate propagation front could be due to the changes to relative permeability computation and small differences in the phase boundary computation. Both simulations run in comparable times (roughly 1.5 min). Results are shown in **Figure 3**.

2.3.5.2. Freezing with Seepage Boundary Condition, P_c smoothing

In this test problem, ice formation was modeled in a 1D vertical column for 2 different pore systems. The column is 1 km thick with 1-m grid spacing in the vertical dimension. It is initialized at hydrostatic, water-saturated conditions at 20 MPa at the bottom of the domain. The initial temperature everywhere is 2ºC, and a small concentration of methane is initialized in the system (1E-04 mol CH4/mol total). The bottom boundary is a Dirichlet BC set to the same conditions as the initial condition, and the top boundary is set to a gas state with a temperature below freezing. The simulation is run for 10 kyrs.

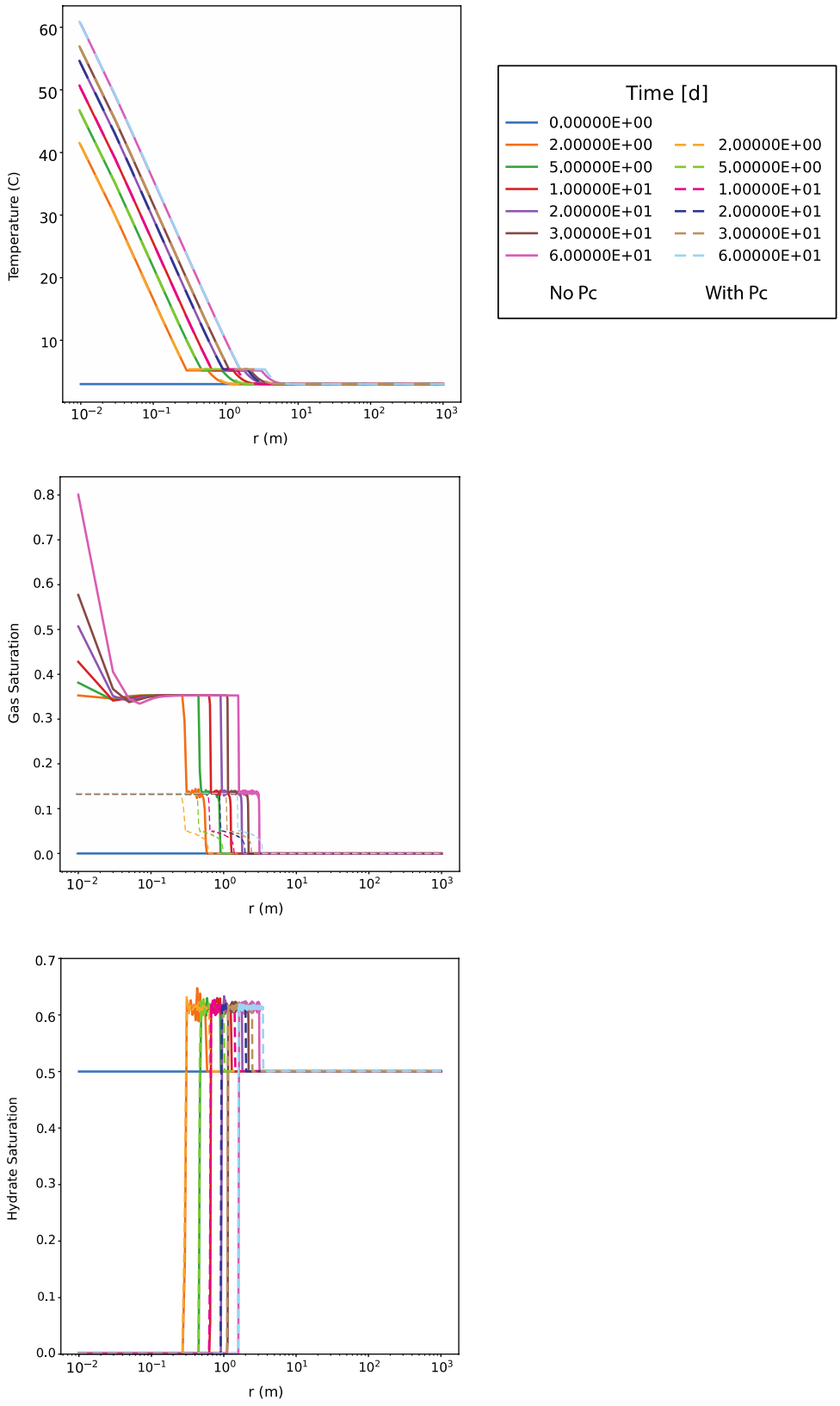

Figure 3. Thermal stimulation benchmark problem including updated HYDRATE mode features in dashed lines (labeled “no Pc”) compared to the original in solid lines (labeled “with Pc”).

This simulation is meant to model exposure of the water-saturated soil to air temperatures below freezing and thus prompt freezing of the soil from top to bottom. The test also demonstrates that freezing is inhibited as ice enters progressively smaller pores, requiring greater and greater subcooling below the bulk freezing temperature of water. The test makes use of a new boundary condition called DIRICHLET_SEEPAGE (modeled after a similar style boundary condition available to RICHARDS mode in PFLOTRAN), in which the simulator only allows flux of gas into the domain if the pressure across the boundary is greater than a BC_REFERENCE_PRESSURE. This is useful for a situation where the modeled gas component, in this case methane, is not the same as the gas that would be represented by a gas phase boundary and thus no significant influx of that component would be expected, such as if the boundary were a standard atmospheric air composition. Finally, a new feature of PFLOTRAN is invoked in this example whereby the unsaturated end of the capillary pressure curve is smoothed (instead of capped), which can allow for better numerical convergence (see **Figure 4**). The capillary pressure functions used here generally represent a pore system with bigger pores (generally lower capillary pressures) and a lower capillary entry pressure ("larger pores" in **Figure 4**) as compared to a system with smaller pores (larger capillary pressures) and a higher capillary entry pressure ("smaller pores" in **Figure 4**). The Van Genuchten parameters used to describe these two pore systems are described in **Table 3**.

Table 3. Van Genuchten parameters for each test for the freezing example.

	Larger Pores	Smaller Pores
Alpha (Pa^{-1})	5.8E-04	1E-04
m	0.5	0.2
S_{rl}	0.1	0.1
Max P_c (Pa)	1E+08	1E+08

The influence of the pore network on ice phase formation is apparent in **Figure 5**. In the system with larger pores, ice is less inhibited from forming and it therefore can accumulate in higher saturations at higher temperatures. The system with smaller pores requires a greater degree of subcooling to precipitate ice in the pore space, resulting in overall lower ice saturations. The ice front penetrates deeper at 10 kyrs in the simulation with smaller pores though, and correspondingly the smaller pore simulation sees slightly more subcooling at depth at 10 kyrs than the large pore simulation. This could be because less ice has formed in total in the simulation with smaller pores and therefore there is less heat released due to the phase change, which could allow the temperature pulse to propagate faster. Finally, in both simulations there is an increase in dissolved methane concentration in the liquid pore water upon ice formation because ice formation only consumes the water component and excludes the methane component. The degree to which methane becomes concentrated is a function of the ice saturation.

2.3.5.3. Freezing with Gas Production

In this test, the same domain as described above is simulated with a source term of methane turned on for the first 1,000 years of the simulation and is distributed between 200- and 300-meters sediment depth. The top boundary is a standard Dirichlet boundary condition where gas flux is allowed across the top boundary. This leads to accumulation of dissolved methane in the upper part of the column, some of which is likely erroneously generated by influx from the top. In addition, the initial and

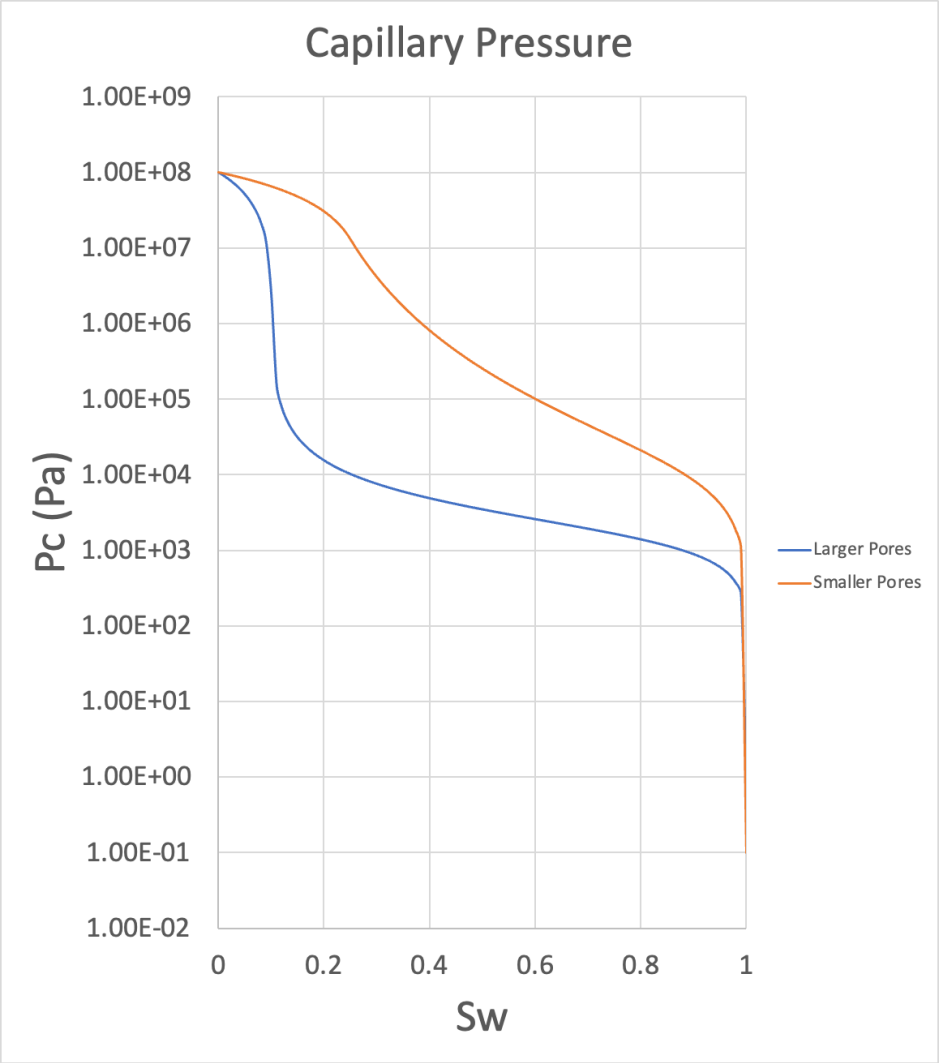

Figure 4. Capillary pressure (a proxy for pore size distribution) as a function of liquid water saturation (wetting phase), for 2 different pore systems.

bottom boundary dissolved methane mole fraction is set to 5E-04 instead of 1E-04 in this simulation in order to speed up hydrate formation. The initial conditions and boundary conditions are otherwise the same as the previous simulation. The sediment capillary pressure function is slightly different and is summarized in **Figure 6** and **Table 1**.

This test is significantly more numerically challenging than the previous example because it involves two solid phases forming in the pore space at the same time. The ice phase forms downward from the top, and the hydrate phase forms in place over the course of the simulation. After about 3,000 years, the ice front meets the hydrate front and **Figure 7** demonstrates the importance of including accurate phase partitioning vis-à-vis $P_{c\alpha} = P_c(2s_\alpha), \quad s_\alpha \leq s_\beta$

Equation 15. At 1,000 years, ice saturations are at around 40% of the pore space as the ice front reaches 200 m depth while hydrate saturations at 200 m exceed 60% saturation. If ice were to keep forming as if no hydrate existed in the pore space at 200 m, the simulator would end up with

over 100% saturation of solid ice + hydrate in the pore space. Not only is greater than 100% saturation physically impossible, but it is also numerically challenging in 1D to have grid

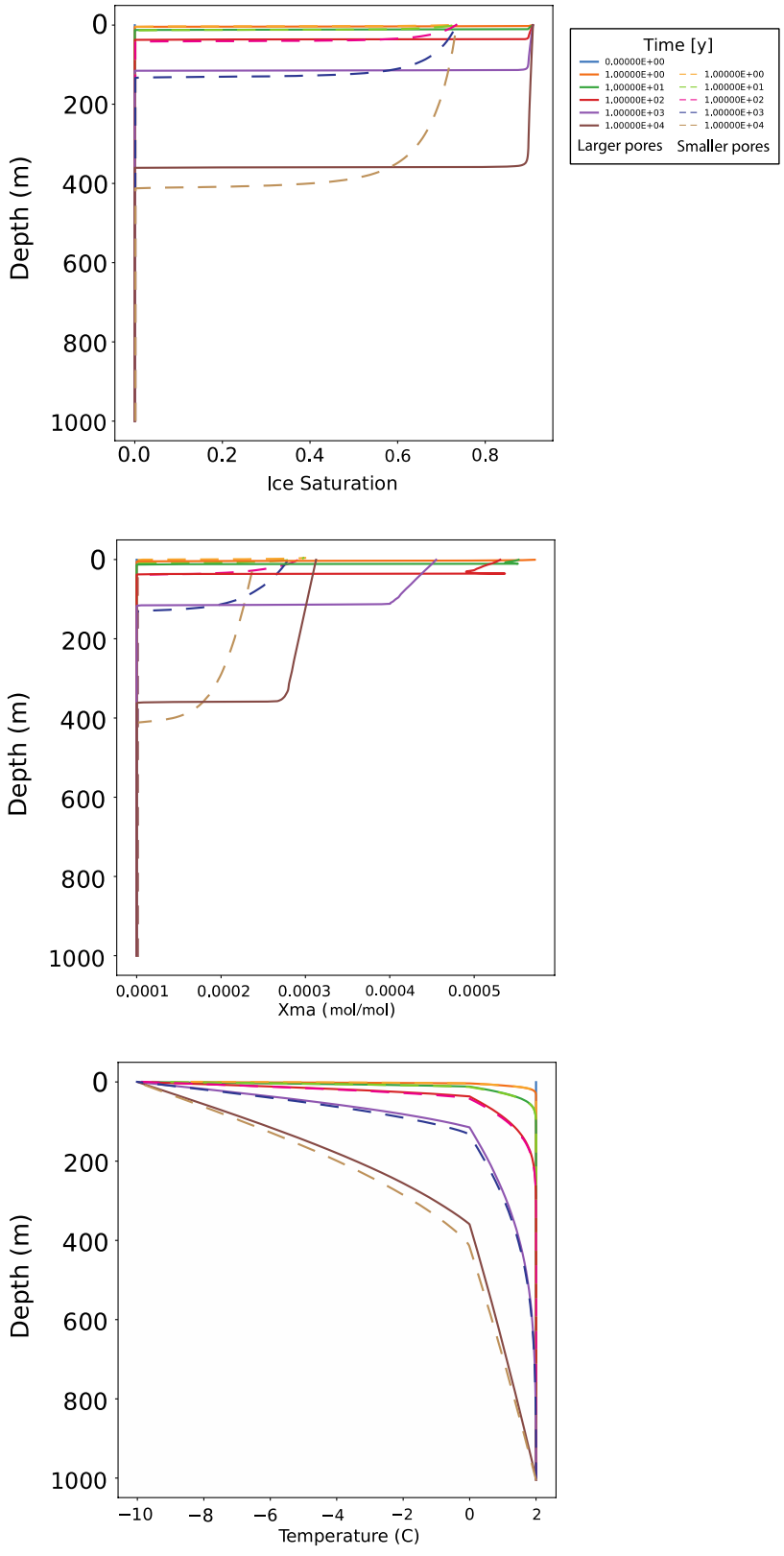

Figure 5. Ice saturation, methane mole fraction, and temperature profiles over time for simulations using 2 different soils.

cells that are completely occupied by solid phases as there is no way to diffuse pressure buildup and the primary variables governing the phase state of the system have less of an influence on the system Jacobian. When considering co-occupancy of the large pore space by both hydrate and ice, there is a noticeable drop in ice saturation in the region already containing hydrate. In this region, the sum of ice and hydrate saturations does not exceed 100%. There are some numerical oscillations apparent in the hydrate saturation profile (and some in the ice saturation profile), which are likely because the combined ice + hydrate saturation is approaching the residual liquid saturation and water is starting to become immobile. This can be problematic because it takes away response of the system to pressure perturbations via invoking fluid flow, which can make the problem significantly more difficult to solve. This suggests that an area for future investigation could be into different mechanisms for scaling the inputs to the relative permeability functions. Also, significant assumptions were made in the model about how the nonwetting phases partition the large pore space and in how both the ice phase and hydrate phase are inhibited from forming in small pores. If the inhibiting force were stronger than the functions currently implemented, for a given simulation we might expect to see less hydrate and ice formation. At lower hydrate and ice saturations, the simulator would likely have a much easier time converging since an appreciable amount of the liquid phase would still exist in the pore space.

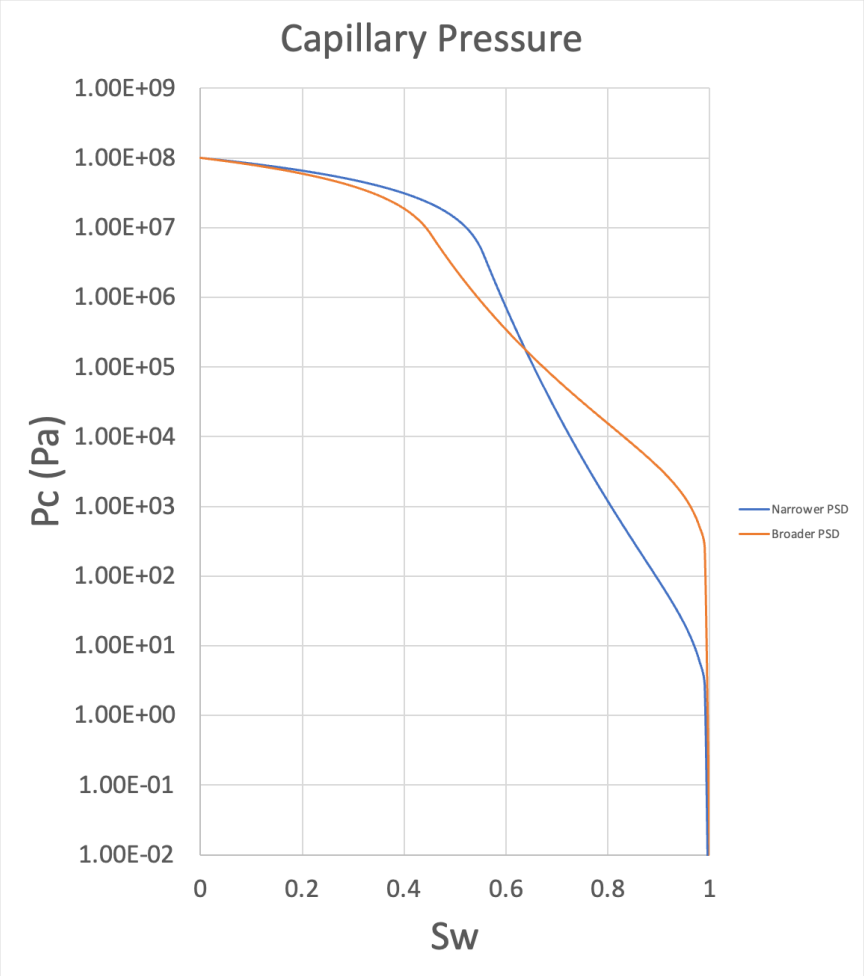

Figure 6. Capillary pressure function for the "narrower" and "broader" pore size distribution (PSD) used in the test of freezing with an internal methane source.

Table 4. Van Genuchten parameters for the "narrower" and "broader" pore size distribution cases of the test of freezing with an internal methane source.

	Narrower PSD	Broader PSD
Alpha (Pa^{-1})	0.1	5.8E-04
m	0.05	0.1
S_{rl}	0.1	0.1
Max P_c (Pa)	1E+08	1E+08

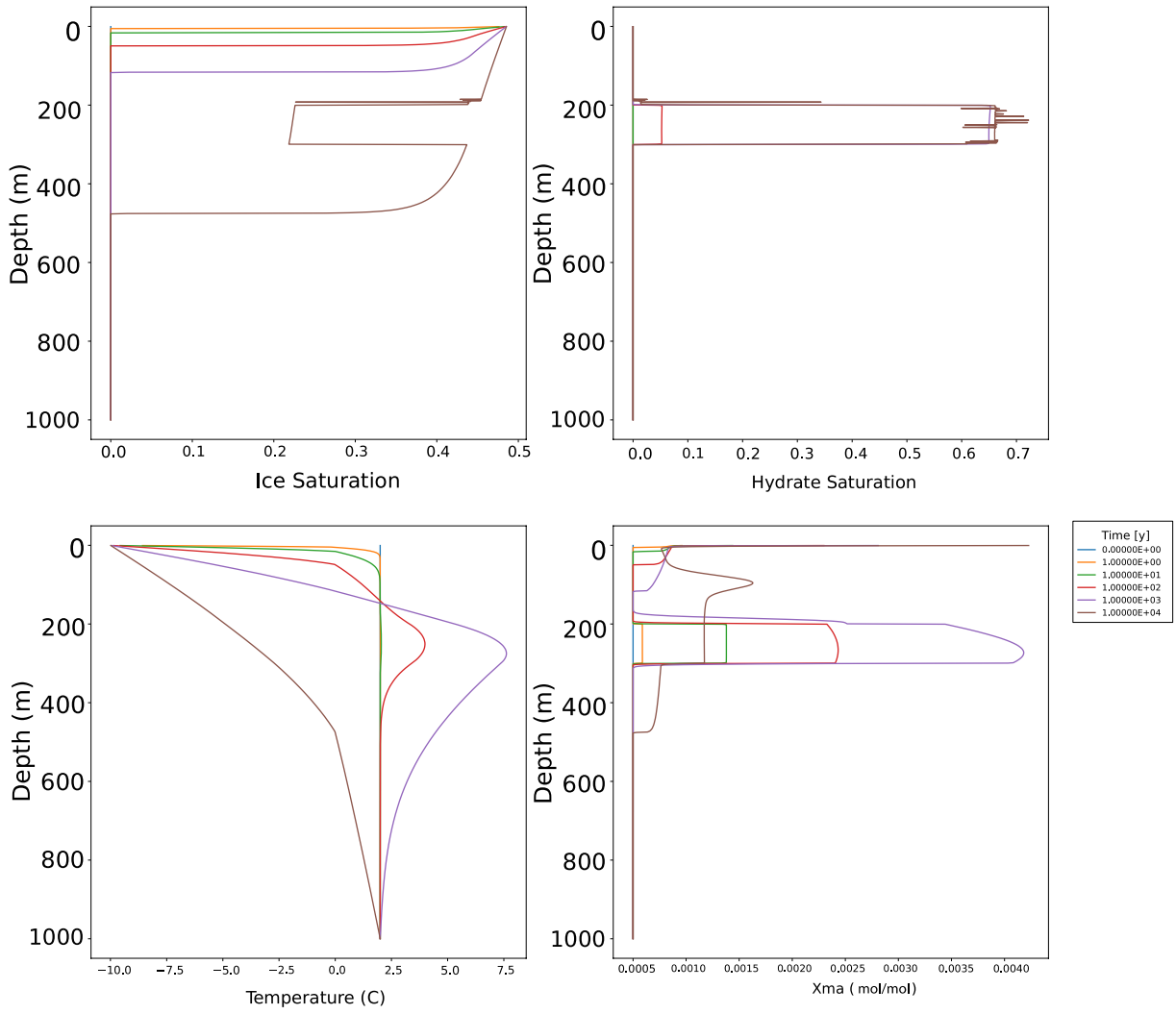

Figure 7. Ice saturation, hydrate saturation, temperature, and aqueous methane mole fraction evolution over time for a test involving freezing from the top and methane production within the model domain.

In addition to the saturation distribution, the interaction between hydrate and ice formation influences the thermal state of the system in this simulation. While the temperature distribution at 10 kyrs is very

similar to the simulation example with only freezing, in earlier years while hydrate is forming there is a noticeable increase in temperature associated with exothermic hydrate formation over that period. Correspondingly, the methane mole fraction profile reflects concentration due to the downward propagation of the ice front as well as changes in methane solubility due to changes in temperature within the zone containing gas hydrate.

Like the simulations with only ice formation, these simulations were also run with two different pore size distributions expressed via the capillary pressure function (**Figure 6**). However, to achieve simulation convergence both pore systems had to be characterized by higher capillary pressures than in the previous example. This indicates that the conditions imposed on the model for this example, which result in significant formation of both ice and hydrate, require significant inhibition of ice and hydrate growth in order to keep enough of the pore space saturated with liquid to achieve convergence. A future area of investigation should be into whether this issue is resolved by running in 2D and 3D, if phase growth inhibition needs to be expressed in a more advanced way, or if more advanced numerical techniques need to be developed to overcome this hurdle.

Results of these simulations confirm the phenomenon that was observed in the previous test. In this test, the broader pore size distribution is associated with lower capillary pressures at ~50% phase saturation. It is in this range where we see separation in ice saturations in **Figure 8**, where the broader pore size distribution example exhibits higher ice saturations than the narrower pore size distribution. At total nonwetting phase saturations above 60%, however, the capillary pressures for both curves become similar, which is why the hydrate saturation profiles at the same time for both examples look similar.

The simulations presented in this section illustrate the need to constrain the growth of hydrate and ice in porous media as a function of pore size distribution. Without significant capillary inhibition to nonwetting phase growth, these solids can completely occlude the pore space and cause significant numerical challenges. These challenges can be addressed through manipulation of pore size distributions and through scaling the liquid and gas phase saturations as fractions of the mobile phases instead of as fractions of total pore space, but as the total hydrate + ice saturations approach 100%, there is clearly still work to be done to address numerical challenges. Future work will explore new numerical techniques to address this issue and also to potentially more realistically represent phase growth inhibition at high nonwetting phase saturations.

2.3.5.4. HYDRATE Mode Options

The following is a recap of some of the new options that are available in HYDRATE Mode that were discussed in previous sections and how to invoke them in PFLOTRAN. For examples of their usage, see the Appendix. The keywords available in HYDRATE Mode along with a brief description of their usage is included in **Table 5**.

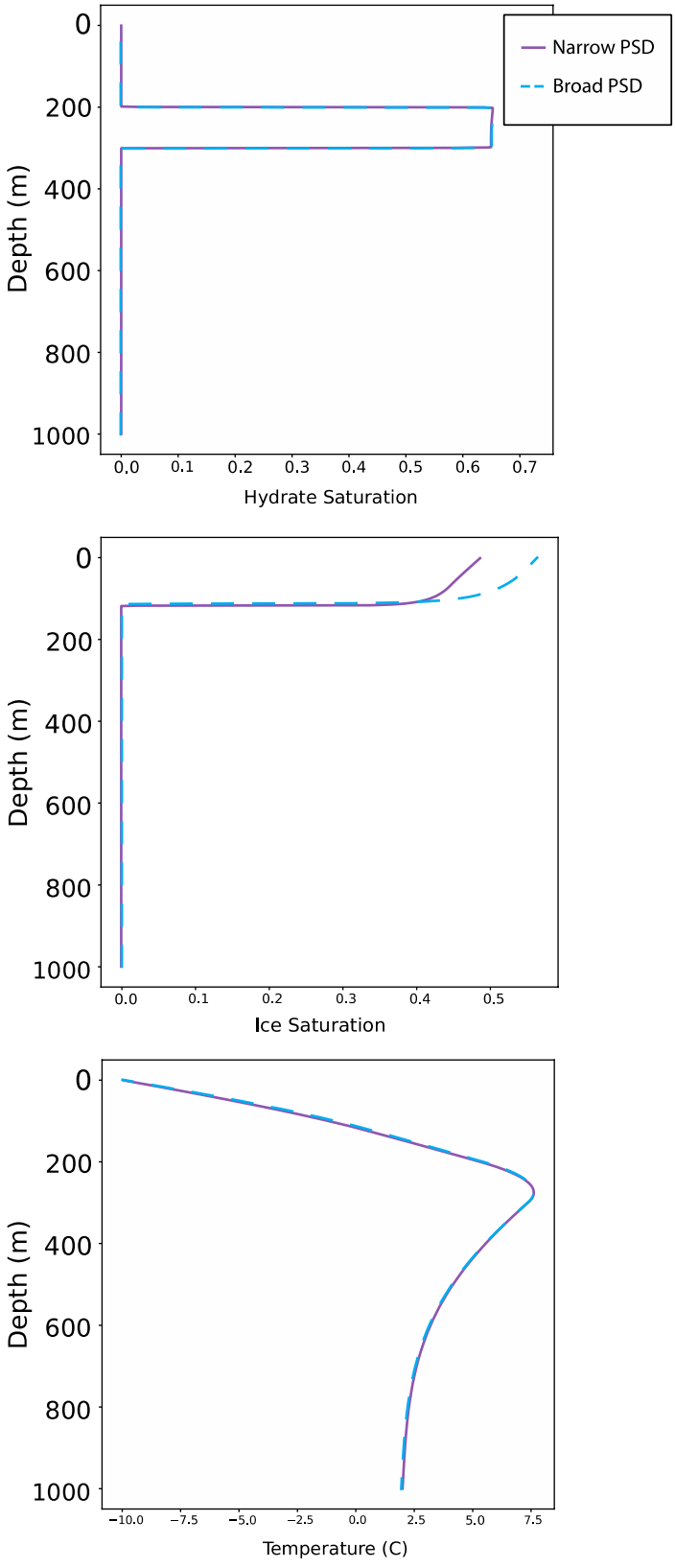

Figure 8. Hydrate saturation, ice saturation, and temperature at 1,000 years simulation time for the "narrower" and "broader" pore size distribution examples.

Table 5. Keywords available in HYDRATE mode and their usage.

Keyword	Usage
HYDRATE_PHASE_BOUNDARY	Set the equation for the phase boundary. Available options are MORIDIS, MORIDIS_SIMPLE, and KAMATH
WITH_GIBBS_THOMSON	Turns on the Gibbs-Thomson effect
GT_3PHASE	Turns on Gibbs-Thomson effect for 3 (or more) phases
SCALE_PERM_BY_HYD_SAT	Scales the permeability by hydrate saturation using the [75] formulation
EFFECTIVE_SAT_SCALING	Scales the liquid and gas phase fractions by the total saturation of mobile phases for input to relative permeability functions
ADJUST_SOLUBILITY_WITHIN_GHSZ	Adjusts the solubility of methane within the gas hydrate stability zone according to [77] formulation
BC_REFERENCE_PRESSURE	Sets the reference pressure for the DIRICHLET_SEEPAGE flow condition
SALINITY	Sets a constant salinity (mass fraction) to shift freezing point and hydrate phase boundary
WITH_SEDIMENTATION	Turns on sedimentation flux
METHANOGENESIS	Opens the METHANOGENESIS block, which currently sets a source term following [76]
ALPHA	Within the METHANOGENESIS block, sets the organic carbon mass fraction
K_ALPHA	Within the METHANOGENESIS block, sets the conversion factor from organic carbon to methane (should be set to 2241)
LAMBDA	Within the METHANOGENESIS block, sets the microbial reaction rate
V_SED	Within the METHANOGENESIS block, sets the sedimentation rate
SMT_DEPTH	Within the METHANOGENESIS block, sets the depth of the SMT (m), above which no methanogenesis occurs

3. PALEOCEANOGRAPHIC CONDITIONS OF THE ARCTIC OCEAN

Although the field of paleoceanography traces its origins to the 1950s [78], quantitative understanding of the late Pleistocene near-surface temperature history of the Arctic Ocean remains rudimentary [79]. Several factors contribute to this state of affairs, including: an overall paucity of sediment cores compared to other ocean basins, due in part to the difficulty of ship operations in sea ice; low sedimentation rates, commonly with hiatuses during glacial maxima (particularly in the western Arctic [79]); and small anticipated temperature signals relative to proxy noise, given that Holocene sea surface temperatures are already close to freezing. More paleotemperature work has been done in the high latitude North Atlantic south of Fram Strait (e.g. [80][81][82]), but here we treat that region as heavily influenced by the Atlantic Ocean and outside of the Arctic Ocean proper.

The oxygen isotopic composition ($\delta^{18}O$) of planktic foraminifera (cosmopolitan protozoans that secrete calcium carbonate shells) can serve as a paleotemperature proxy if the $\delta^{18}O$ of past seawater can be constrained. There are at least 20 existing Pleistocene-Holocene $\delta^{18}O$ records of varying quality and temporal scale in the Arctic [83], and about 40 Last Glacial Maximum (LGM, ~19-23 kilo annum (kA)) observations [84][85]. Seawater $\delta^{18}O$ is affected by global ice volume, which is relatively easy to correct for, and the local hydrologic cycle. Unfortunately, the large dynamic range of salinity and hence seawater $\delta^{18}O$ in the Arctic makes foraminiferal $\delta^{18}O$ very difficult to interpret in terms of temperature. Instead, Arctic $\delta^{18}O$ records are best interpreted as qualitative salinity histories (e.g., [84][86]).

Aside from $\delta^{18}O$, the most commonly applied sea surface temperature proxies in paleoceanography are based on: biotic assemblages (foraminifera, radiolaria, diatoms, dinoflagellates); the magnesium content (Mg/Ca) of planktic foraminifera; and the saturation index of algal lipids (alkenone $U^{k'}_{37}$). In the MARGO LGM compilation, the Arctic Ocean contains only foraminiferal assemblage data, which extend to 84°N in the North Atlantic sector and imply a warming of roughly 1°C [87]. We are not aware of any Late Pleistocene-Holocene Mg/Ca or alkenone sea surface temperature records from the Arctic Ocean proper.

Our best insights into Arctic Ocean near-surface temperatures come from Mg/Ca in benthic foraminifera and in ostracods, which are microscopic benthic crustaceans. While we would like to have benthic records from continental shelf depths, the published data are from deeper waters. In the Canadian Basin, [88] presented an 8 kA Holocene ostracod Mg/Ca record from 203 m water depth, and two 7 kA Holocene benthic foraminiferal Mg/Ca records from 369 m. Together these records vary between about -1 and 1.5°C, but with no clear trends over the Holocene. [89] compiled 50 kA of ostracod Mg/Ca data from 31 Arctic cores from a range of water depths and latitudes. During Marine Isotope Stage 3 (MIS 3, ~25-50 kA), water depths of between 1 and 3 km warmed by ~2°C, while the sole core from shallower depths (~250 m) was close to freezing. This pattern was interpreted as a warming and downward expansion of the Atlantic Layer, which is today found below the colder and fresher Polar Mixed Layer and Pacific Water and centered around 500 m water depth. Informed by numerical modeling, the cause of the intermediate depth warming was inferred to be a deepening of the glacial halocline in response to reduced runoff, preventing the Atlantic Layer (now dubbed Glacial Arctic Intermediate Water) from losing heat to the surface. Although [89] had fewer intermediate depth observations from the LGM, that interval appears to have warmed even more than MIS 3. These observations make some predictions for the glacial-interglacial history of the shallow subsurface, but data are sorely lacking.

3.1. Research Strategy

Conversations with Arctic paleoceanographers Tom Cronin (USGS, Reston) and Jesse Farmer (Princeton University) suggested that on the one-year timescale of this project, it would be very difficult to find shelf-depth cores with benthic foraminifera or ostracods. We therefore decided to target Mg/Ca in the ubiquitous planktic foraminifer *Neogloboquadrina pachyderma*, rendering the water depth of cores mostly irrelevant. In the modern Arctic, *N. pachyderma* calcifies mainly below the mixed layer, with larger (ontogenetically older) specimens calcifiying deeper [90]. We selected the smallest size fraction that could be reliably handled, 150-212 μm, which is estimated to occupy water depths around 150 m on average. This habitat is in the upper half of the Arctic pycnocline, and it is possible that these organisms would migrate vertically if the pycnocline depth changed over time. However, the fact that *N. pachyderma* $\delta^{18}O$ and Mg/Ca do record past climate variations implies that these foraminifera don't simply track an isopycnal surface. Nevertheless, habitat uncertainty is an unavoidable complication when using planktic foraminifera.

N. pachyderma was one of the first planktic foraminifera to be calibrated for the Mg/Ca paleotemperature proxy [91]. Several subsequent *N. pachyderma* calibration studies consistently show exponential Mg/Ca sensitivities of 8 to 9% per °C, with estimated pre-exponential constants ranging from ~0.4 to 0.6 [92]. In cold waters, the pre-exponential constant has a strong influence on reconstructed temperatures. Here we use the following approximation, which yields realistic Holocene temperatures for our measurements to date:

$$\frac{Mg}{Ca} = 0.7e^{0.09T} \qquad \text{Equation 17}$$

Additional (underway) Mg/Ca measurements will help us determine whether this equation is broadly appropriate for Arctic Ocean *N. pachyderma*.

Mg/Ca-based paleotemperatures can theoretically be combined with *N. pachyderma* $\delta^{18}O$ to remove the temperature signal from the $\delta^{18}O$ of calcite, leaving an estimate of seawater $\delta^{18}O$. Although it is not straightforward to convert seawater $\delta^{18}O$ into a quantitative salinity history (due to uncertain $\delta^{18}O$:salinity relationships in the past, and the effect of brine rejection during sea ice formation), it should give us a better constraint on paleosalinity than foraminiferal $\delta^{18}O$ alone. We therefore leverage our Mg/Ca measurements by also analyzing $\delta^{18}O$ (and $\delta^{13}C$) on splits of the same samples.

3.2. Core Selection

Suitable sediment cores were identified with the help of Tom Cronin, who maintains a large collection of Arctic sediment samples. We surveyed 29 cores on the basis of their coordinates, temporal span, sedimentation rates, and evidence of hiatuses. Nearly all of the cores have radiocarbon-based age models. We selected four cores that provide a good balance between desirable temporal characteristics and broad spatial coverage. PS2163-1 is located in the Barents/Kara sector on the flank of Gakkel Ridge (86°N, 59°E, 3040 m water depth). It is 27 cm long and spans from ~3 to 43 kA with no apparent LGM hiatus, and sedimentation rates of ~0.6-0.8 cm/kA. It therefore provides a low-resolution continuous record from MIS 3 until the late Holocene. 96-12-P1 is close to the North Pole in the Laptev Sea sector on the Lomonosov Ridge (87°N, 145°E, 1003 m water depth). We sampled the core to 240 cm which corresponds to ~160 kA. 96-12-P1 has a mean sedimentation rate of ~1.5

cm/kA and no apparent LGM hiatus, so it provides a relatively high-resolution record of the entire past glacial-interglacial cycle (MIS 6 to Holocene). AOS94-B8 is close to the East Siberian and Chukchi Seas on the Mendeleev Ridge (78°N, 177°W, 1031 m water depth). It spans from ~4 to 52 kA but with a 14 kA hiatus across the LGM. Sedimentation rates are relatively high at ~1-2 cm/ky, so this core provides a relatively high-resolution look at MIS 3 and the Holocene. Finally, P1-92-AR25 sits on Northwind Ridge in Canada Basin (75°N, 157°W, 1625 m water depth). Although this core is missing the Holocene, it has an average sedimentation rate close to 5 cm/kA and no apparent LGM hiatus. It therefore provides a high-resolution record of MIS 3 (from ~42 kA) through the deglaciation.

3.3. Analytical Methods

Previously washed and sieved (sand fraction) sediment samples were dry-sieved to isolate the 150-212 μm particle sizes. *N. pachyderma* specimens were then individually picked using a wetted paintbrush under a binocular microscope. There are at least five recognized morphotypes of *N. pachyderma* [93],[94], and we targeted the quadrate Nps-2. From each sample we picked 50 specimens for trace metal analysis (~300 μg $CaCO_3$) and 25 specimens for stable isotope analysis (~150 μg). Given a total of 200 sediment samples across the four cores, this amounted to 15,000 foraminifera picked.

Prior to trace metal analysis, the foraminifera must be cleaned of contaminants. The first step in this process is to crush the shells between two glass slides under a binocular microscope, to expose interior chambers to the chemical cleaning process. Crushed samples are then transferred to polypropylene microcentrifuge tubes to undergo a three-stage cleaning process [95][96]. The first stage removes fine-grained extraneous material (clays) through repeated sonication and siphoning of supernatant. This is followed by reductive cleaning in a buffered anhydrous hydrazine solution, to remove iron/manganese oxide coatings. Finally, organic matter is oxidized using a buffered hydrogen peroxide solution. Once samples are crushed, 30 samples can be cleaned in about six hours. Cleaned samples are then dissolved in nitric acid and analyzed on a ThermoFinnigan Element2 sector field inductively-coupled plasma mass spectrometer (ICP-MS) at the University of Colorado Boulder Trace Metal Lab [97]. A total of 11 elemental ratios are measured against liquid standards, with our focus here on Mg/Ca. Analytical precision (1σ RSD) is ±0.5% for Mg/Ca.

Foraminifera do not need to be chemically cleaned for $\delta^{18}O$ analysis, only weighed on a microbalance. $\delta^{18}O$ and $\delta^{13}C$ are measured on a Thermo Delta V continuous-flow stable isotope ratio mass spectrometer attached to a GasBench II gas preparation device, at the University of Colorado Boulder Earth Systems Stable Isotope Laboratory. Repeated measurements of in-house standards yield precisions of ±0.1 ‰ or better for both $\delta^{18}O$ and $\delta^{13}C$.

3.4. Results

As of this writing, only core PS2163-1 has a complete Mg/Ca record. For the other three cores, sample preparation for trace metals (picking, crushing, and cleaning) is about 85% complete, but analysis by ICP-MS awaits. Sample weighing for stable isotopes is also substantially complete, but analysis cannot occur until October because the global helium shortage prevents operation of the mass spectrometer until then.

At the core site of PS2163-1 (86°N, 59°E), *N. pachyderma* Mg/Ca documents subsurface (150 m) temperatures of ~1°C during the mid-Holocene, warming to ~2°C during the early Holocene and deglaciation, and peaking at ~3°C during the LGM (**Figure 9**). Coldest temperatures, close to the

freezing point of seawater, occurred during late MIS 3. Earlier in MIS 3, temperatures were around 0°C.

The MIS 3 cooling is consistent with a thickening of the polar surface/mixed layer as hypothesized by [89]. The LGM temperatures suggest that the maximum intermediate depth warming documented by [89] at that time extended close to the sea surface, implying a shallow halocline, perhaps due to extensive ice cover. During deglaciation, excessive runoff from ice sheet melting likely maintained a shallow mixed layer and halocline [86], but by then the intermediate water was cooler [89].

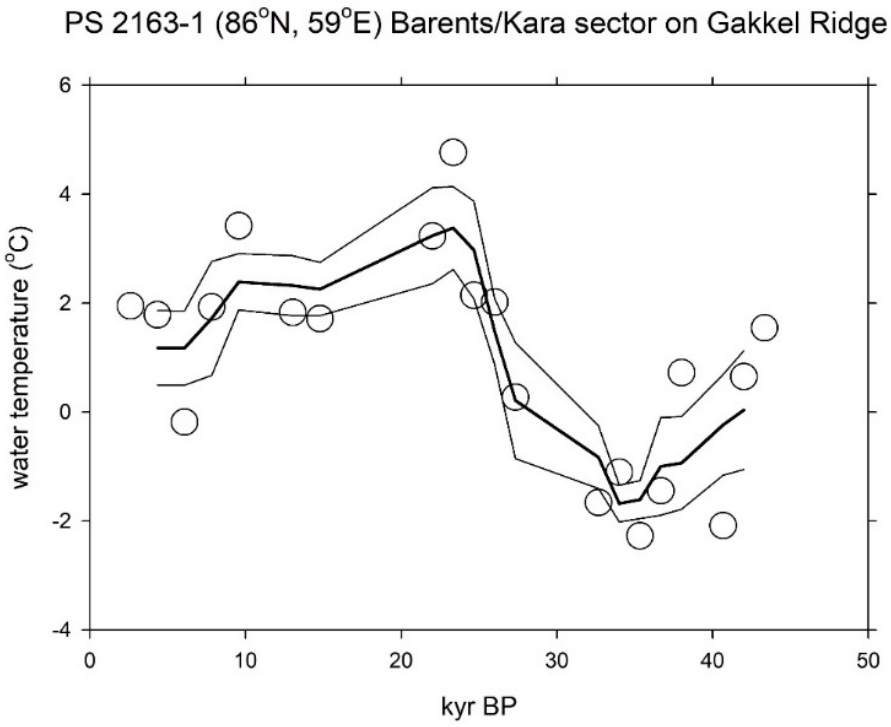

Figure 9. Subsurface (~150 m) paleo-temperatures recorded by *N. pachyderma* Mg/Ca in core PS2163-1. Heavy line is a three-point running mean and light lines are ±1 standard error uncertainty.

We use the Mg/Ca record from core PS2163-1 to generate a preliminary scenario for the temperature history of the Arctic near surface (**Figure 10**). This scenario is informed by prior work and the paleoceanographic interpretation described above, but is currently quite speculative until the other three cores are analyzed. Reconstructed Late Holocene temperatures of 1°C are assigned to the last interglacial (MIS 5), except for the early portion of the peak interglacial MIS 5e. The early Holocene and deglacial temperature of 2°C is assigned to early MIS 5e and the penultimate deglaciation, as well as (more speculatively) the mini-deglaciation following MIS 4 at ~53-62 kA [86]. The glacial peaks of the LGM, MIS 4, and MIS 6 are assigned the LGM temperature of 3°C. Finally, MIS 3 currently stands alone as the coldest interval. To apply this history in the numerical model, we propose adding the temperature anomaly (red line in **Figure 10**) to the 150 m modern temperature in each grid cell. For simplicity, sea surface temperatures can be held constant at the modern values, since they are typically close to freezing already. Then anomalies can be interpolated with water depth, from the assigned value at 150 m to zero at the sea surface.

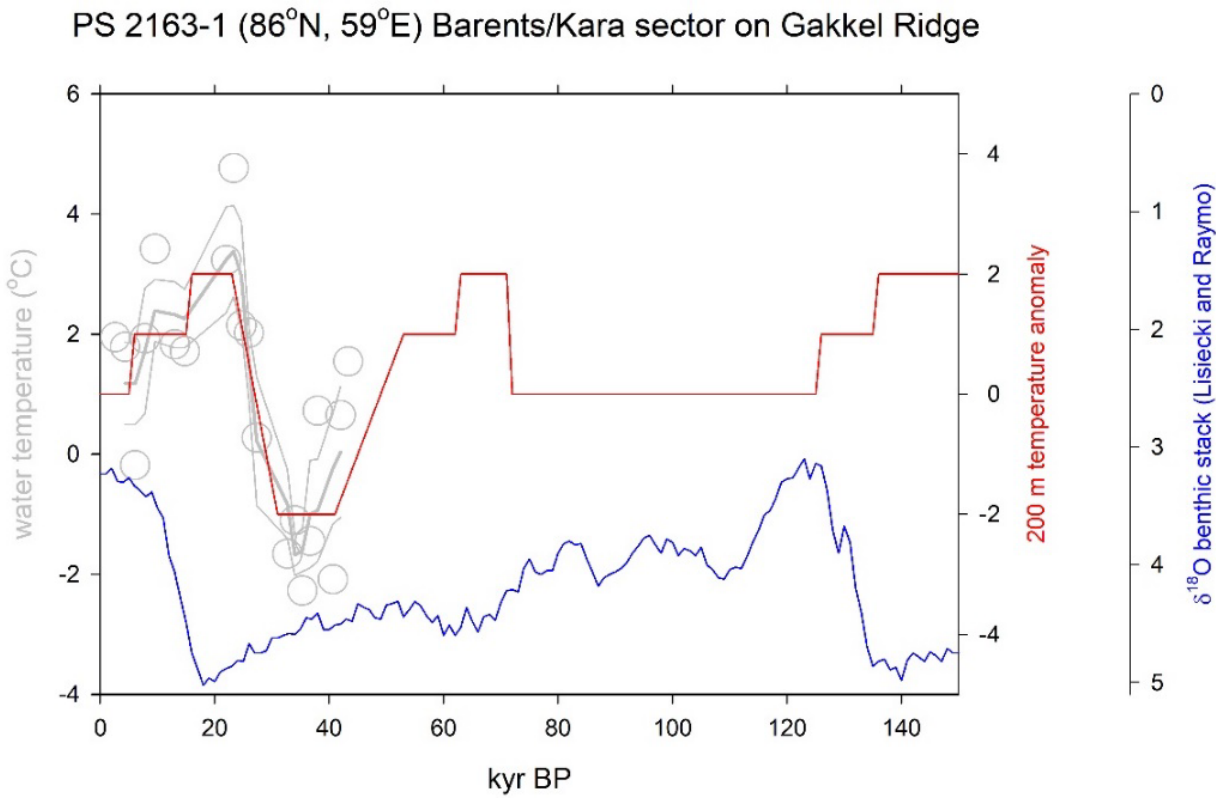

Figure 10. Mg/Ca paleotemperatures as shown in Figure 9 (gray), with the addition of our preliminary scenario for temperature anomalies through time (red). The global benthic $\delta^{18}O$ stack of Lisiecki and Raymo (2005) is shown for reference (blue).

This page left blank.

4. DEMONSTRATION OF THE HYBRID MODELING FRAMEWORK ON THE ALASKA DOMAIN

In this section, we present a demonstration of the developed framework that applies a hybrid modeling technique using geospatial machine learning and geophysical numerical modeling to produce probabilistic predictions of methane emissions from the Arctic seabed. Because the majority of *dissolved* methane flux is thought to be taken up by the anaerobic oxidation of methane (AOM) [23], mediated by a consortium of methane-oxidizing Archaea and sulfate-reducing bacteria (as described in **Section 1.2**), we focus instead on *ebullition*, or gas phase methane flux from the seabed to the water column. Because methane in gaseous form is not directly accessible to the AOM community [27], it is assumed that the entire amount of methane transported within the gas phase can reach the water column. Furthermore, to estimate how much of the modeled ebullitive flux may reach the atmosphere, simple yet highly predictive 1D models of free and dissolved gas transport in the shallow water column toward the atmosphere [31],[32] can be adopted. In general, these models show that bubbles released only from shallow water depths (e.g., ~ 100 m or less) may have appreciable amounts of methane left inside of them by the time they reach the ocean surface. Therefore, we have reduced the simulation domain to treat seabed areas with a present-day water depth less than 175 m. This limits the simulation domain to the Arctic continental shelf. Finally, for the demonstration presented here, we further limit the computational domain to the region surrounding Alaska (with further details given in the following subsections).

We note that the modeling workflow demonstration presented in this section is still a work in progress, but at the time of this writing, has been developed to an advanced stage capable of being exercised through its entire workflow – from model set-up to model prediction. Here we present the details of this workflow in their current advanced stage and point out sections of the framework's needed improvements where applicable. As such, the results presented here are not meant to be interpreted as new scientific evidence, but rather, a demonstration of how new scientific modeling predictions using this framework can be made and used to better understand marine sources of methane emissions under climate warming and how this framework can be used to provide a source term to global climate models over space and time.

4.1. Geographic Location

The modeling demonstration site was chosen surrounding Alaska's modern-day shoreline. This region experienced large variations in sea level across past glacial cycles as did the entire Arctic coastline (as described in **Section 1.1**). As shown in **Figure 11** (in red), the relative sea level (RSL) for the Beaufort Sea varied from ~ 30 m above present day sea level 120 kA BP to ~ 100 m below present day sea level at the LGM [98],[99]. In blue, **Figure 11** shows the mean annual air temperature (MAAT) over the last glacial cycle, which was at times ~ 10ºC colder than modern temperatures [100],[101]. As a consequence, vast regions of the presently submerged Alaskan continental shelf would have been exposed during portions of the last glacial cycle. In North America, Alaska is unique because the state encompasses the largest contiguous land area at high latitude that was never glaciated over its lower elevations [102], therefore, it is understood that the entire exposed seabed would have formed permafrost (where MAAT was cold enough, such as in the northern portions of the state). After the LGM, as the environment warmed, sea level began to rise back up again. This marine transgression changed the thermal conditions of inundated permafrost, initiating warming and thawing of submarine permafrost that continues today.

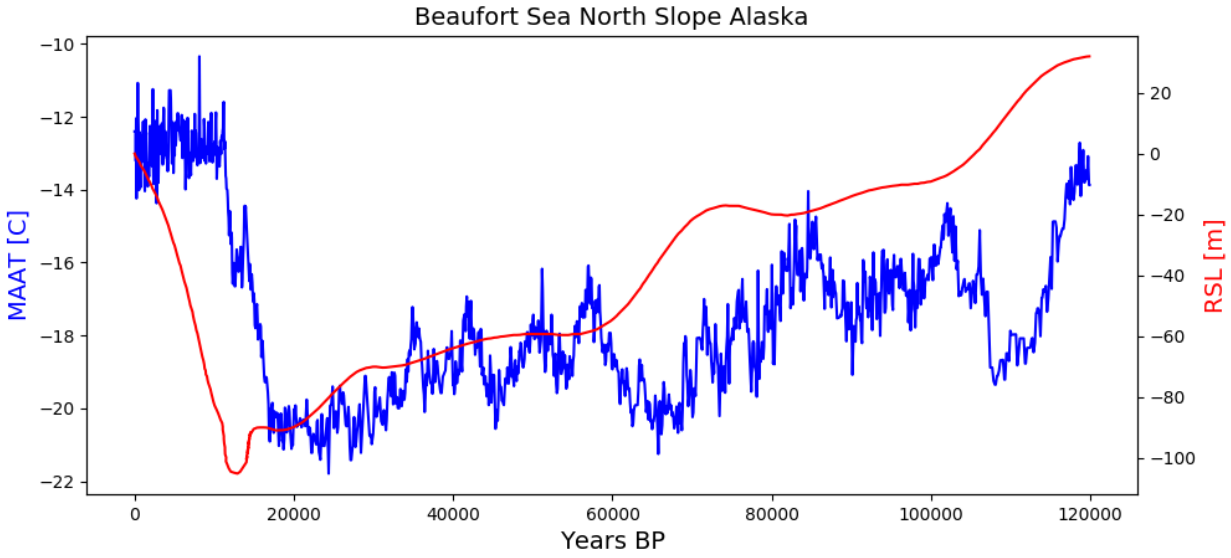

Figure 11. Evolution of the mean annual air temperature (MAAT – blue, left axis) and relative sea level (RSL – red, right axis) over the last glacial cycle. RSL records were made based on [98][99] and personal communication with J. X. Mitrovica. MAAT records were made based on the temperature anomaly from [100] applied to modern-day temperatures [101].

To demonstrate the current capabilities of the hybrid modeling framework developed in this study, we modeled probabilistic submarine permafrost and methane gas distribution and gas flux in the seabed off the coast of Alaska in response to environmental forcing. The simulations were set up using a flexible version of the Dakota-PFLOTRAN workflow that runs on Sandia's Common Engineering Environment's (CEE) High Performance Compute Servers. The computational domain is situated between 170°W & 140°W and 60°N & 74°N and includes only the locations where present-day water depths are less than 175 m within these coordinates. Furthermore, we down-selected 2,009 locations within this area to run 1D simulations at an approximate spatial resolution of 5 arc minutes in longitude and 10 arc minutes in latitude, resulting in a computational domain that covers the majority of the shallow continental shelf of Alaska (Error! Reference source not found.). 1D simulation locations are shown as black dots.

4.2. Model Setup and Methods

GPSM parameters within the geographic boundaries (170°W & 140°W and 60°N & 74°N) were obtained at a resolution of 5 arc minutes. The available parameters included seafloor depth (**Figure 13A**), seafloor temperature (**Figure 13B**), heat flux (**Figure 13C**), sedimentation rate (**Figure 13D**), and total organic carbon (**Figure 13E**). Of these parameters, the latter four were applied as conditions/constraints at the top of the down-selected 1D simulated sediment columns (also referred to as "profiles"). Seafloor depth was used to calculate evolving top boundary conditions for pressure and temperature.

The RSL history accounts for changes in sea level due to glaciation (**Figure 11**). RSL history is used to calculate the overburden pressure at each simulation location over time associated with changing water depth relative to the present-day depth. In addition, it is also used to calculate the temperature at the top of the 1D sediment column according to when the profile would be exposed to atmospheric conditions as opposed to submerged oceanic conditions. When profiles are exposed to the

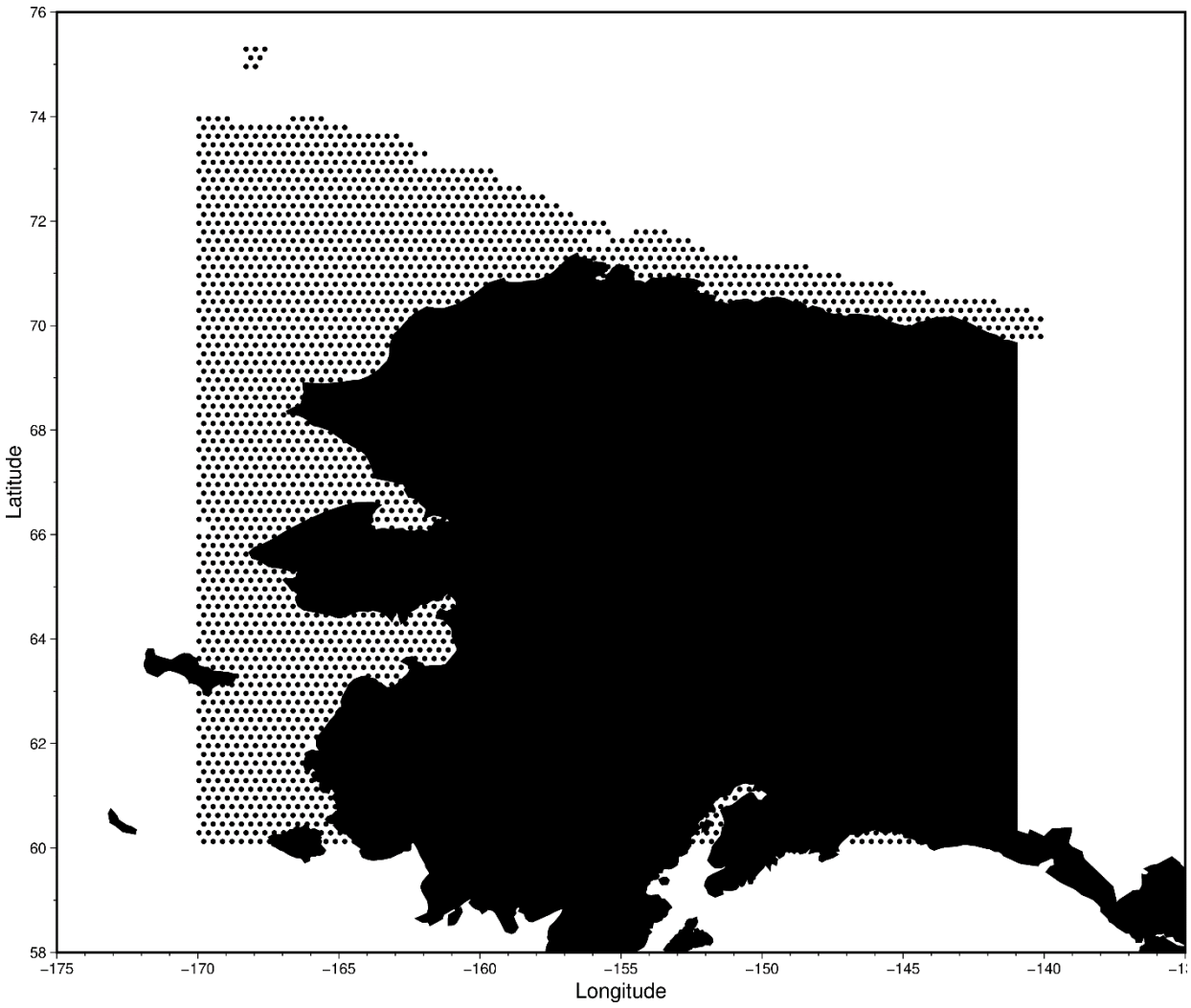

Figure 12. Geographic location of study site and 1D simulation profile locations.

atmosphere, the MAAT value from **Figure 11** is applied. When profiles are submerged by the ocean, the modern-day seabed temperature is applied.

The method to determine boundary conditions used here employs two simplifications that should be improved with future use. First, the RSL curve used is site-specific to the nearshore Beaufort Sea along the North Slope, yet we applied it to the entire computational domain. This is a simplification we made because this was the only RSL curve available to us at the time of this writing. However, results can be improved by using many site-specific RSL curves and applying them in their respective regions within the larger computational domain. Similarly, this should be done for MAAT also. Second, when the profiles are submerged by the ocean, the modern-day seabed temperature is applied. This is another simplification we made because we did not have a historic record of the bottom water temperature, which should be applied instead. However, as informed by prior work and the paleoceanographic interpretation described in **Section 3** of this study, we used the Mg/Ca record from core PS2163-1 to generate a preliminary scenario for the temperature history of the Arctic near surface (**Figure 10**). To apply this history in the numerical model, we propose adding the temperature anomaly (red line in **Figure 10**) to the 150 m modern temperature in each grid cell. For simplicity, sea

surface temperatures can be held constant at the modern values, since they are typically close to freezing already. Then anomalies can be interpolated with water depth, from the assigned value at 150 m to zero at the sea surface. This work in planned for FY23 by the authors.

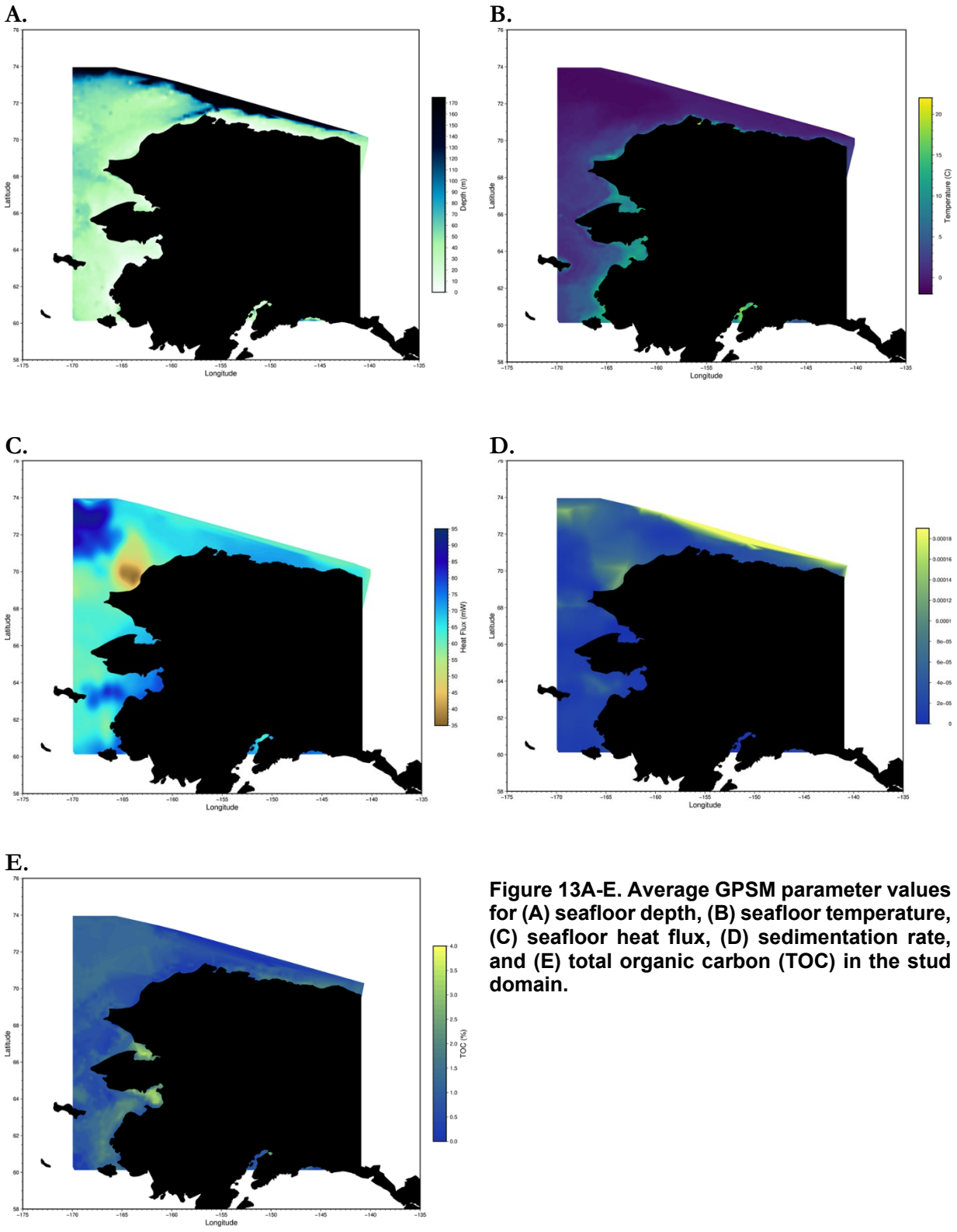

Figure 13A-E. Average GPSM parameter values for (A) seafloor depth, (B) seafloor temperature, (C) seafloor heat flux, (D) sedimentation rate, and (E) total organic carbon (TOC) in the stud domain.

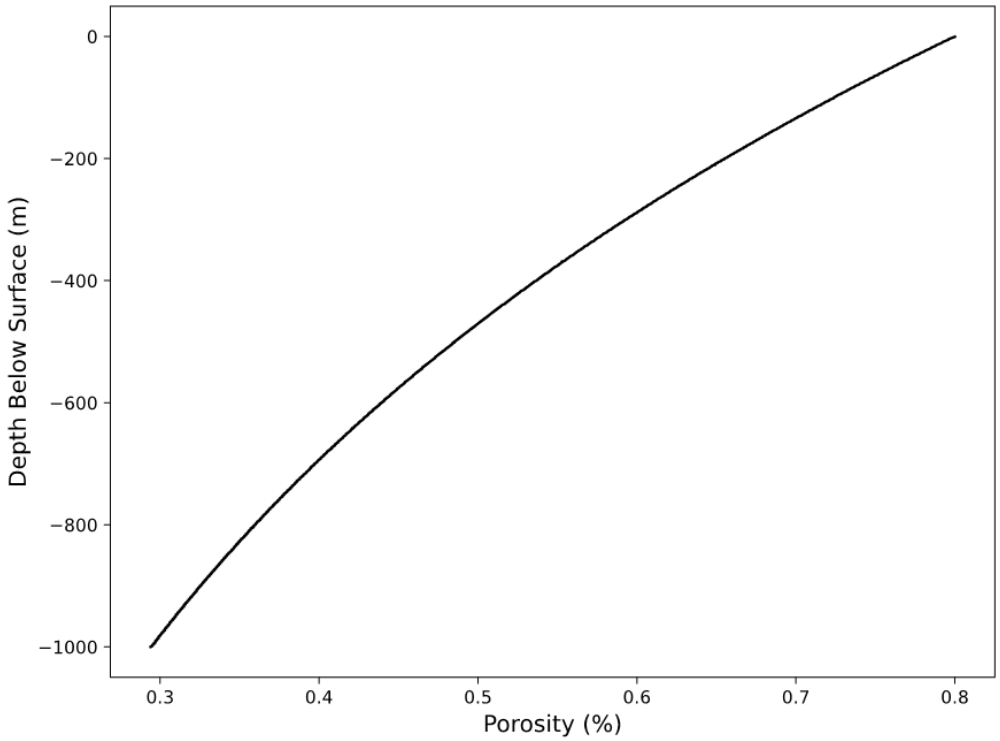

Figure 14. The porosity (%) profile as a function of depth (m). The same profile is used for both ice and gas simulations.

Porosity at each 1D simulation profile location decreases with depth accounting for compaction and is shown in **Figure 14**.

Simulations for each 1D profile location occur in two phases – the first phase simulates submarine formation (dubbed "ice simulations") while the second phase simulates both permafrost and methanogenesis (dubbed "gas simulations"). All input decks and associated external text files are included in the Appendix, **Sections A.4, A.5, and A.6**.

4.2.1. Ice Simulations

Each 1D profile location begins with an ice simulation to estimate submarine permafrost distribution. For each ice simulation, Dakota takes the average value of the seafloor depth, seafloor temperature, and heat flux from the provided GPSM dataset. The sedimentation rate and total organic carbon from GPSM are not used for the ice simulations. In addition, the methanogenesis model within PFLOTRAN Hydrate Mode is turned off, and as a result, no gas is simulated during this phase.

All ice runs simulate 405 kA of time, representing three full glacial cycles which begin 525 kA BP. Each glacial cycle is a repeat of the most recent glacial cycle (which occurred 0 – 120 kA BP in reality) and is shown in **Figure 11**. Three glacial cycles were simulated so as to give the model "spin-up time," allowing the evolving permafrost depth to come to a quasi-steady state before gas simulations were started. Due to numerical issues associated with the sharp discontinuity in RSL between cycles, the discontinuity is smoothed by extending the 120 kA cycle duration to a duration of 135 kA, and a smooth connection is made between the end of one cycle and the beginning of the next. This was done purely for numerical reasons. A better approach would be to use historical records for each past glacial cycle so that the data is naturally continuous. Because we only had information on RSL for the

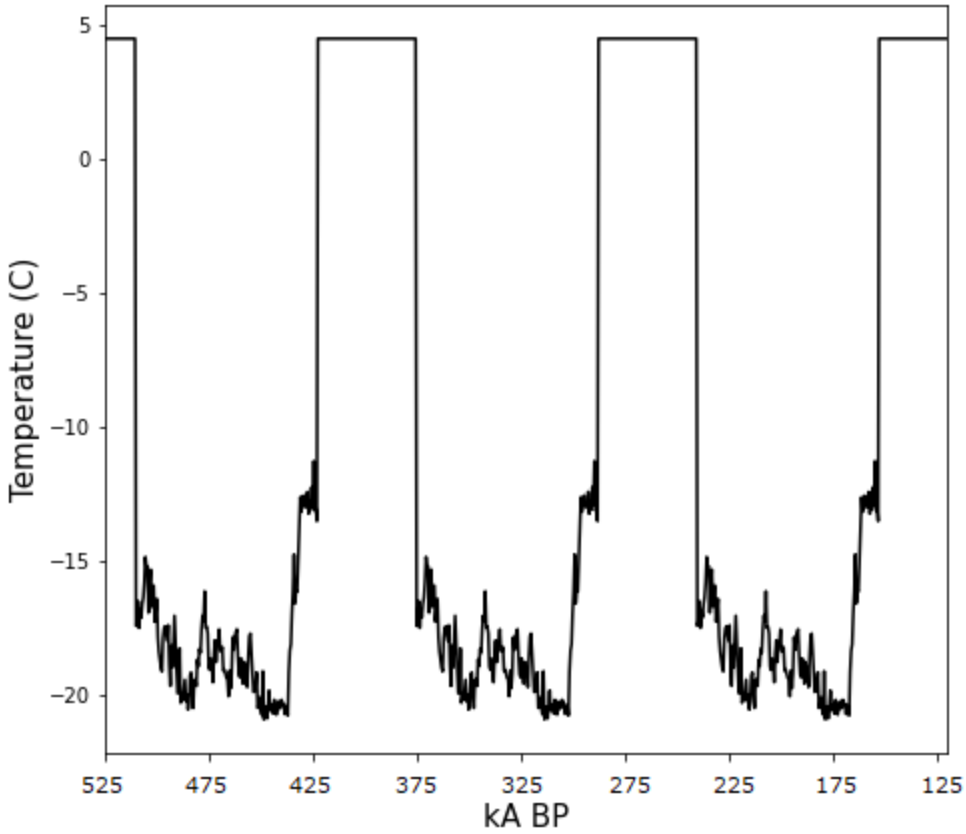

Figure 15. Top temperature boundary condition for an example ice simulation, Profile 332811, located at 165.792ºW and 66.4583ºN, where present day water depth is 14 m.

most resent glacial cycle (0 – 120 kA BP), we used the information we had and repeated it three times in lieu of actual records.

The simulation is driven by the evolving boundary conditions for temperature and pressure over the span of the 3 back-to-back glacial cycles. **Figure 15** and Figure 16 show the top temperature and pressure boundary condition for one of the 1D simulations, Profile 332811, located at 165.792ºW and 66.4583ºN, where present day water depth is 14 m. Temperature alternates between the seabed temperature (~ 3ºC) and the MAAT as applied from **Figure 11**. Similarly, the pressure alternates between the hydrostatic pressure and atmospheric pressure. This evolving boundary condition is specified in PFLOTRAN HYDRATE Mode via the LIST feature in an external file called from the main input deck (see Appendix **Section A.6**). Initial conditions are made physically consistent with the boundary conditions applied at 525 kA BP. An example PFLOTRAN HYDRATE Mode input deck for an ice simulation is provided in the Appendix **Section A.4**.

Model output is given every 5 kA, and includes variables of interest such as ice saturation, liquid pressure, temperature, etc. The particular output frequency and variable list is adjustable by the user. Additionally, a checkpoint/restart file is requested at the end of the ice simulation run, at a simulation time of 405 kA, equivalent to 120 kA BP. In this checkpoint/restart file, all of the variables PFLOTRAN needs to restart the simulation again are saved. The restart file is used to begin the last glacial cycle of the simulation, which includes methanogenesis (described in next section).

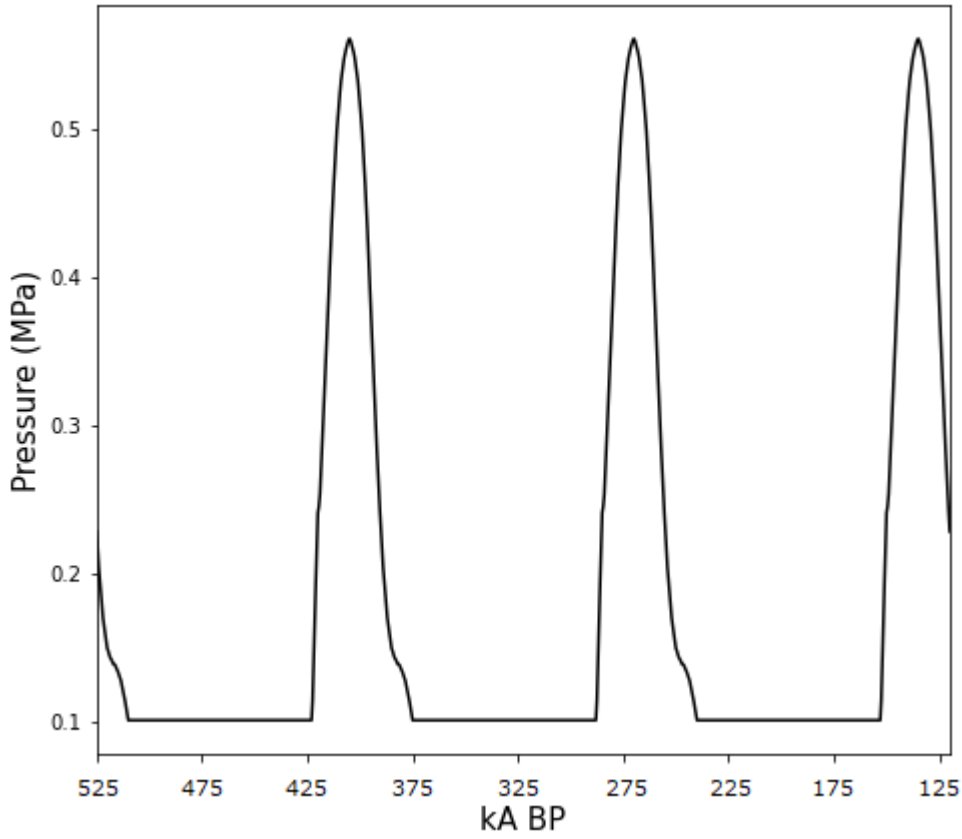

Figure 16. Top pressure boundary condition for an example ice simulation, Profile 332811, located at 165.792ºW and 66.4583ºN, where present day water depth is 14 m.

4.2.2. Gas Simulations

The ice simulations are followed by gas simulations designed to model methanogenesis and methane flux from the seabed to the water column at each location. Each gas simulation begins by utilizing the restart file generated by the ice simulation at 405 kA of simulated time (equivalent to 120 kA BP). This allows the overall workflow to pick up exactly where it left off. Each gas simulation runs for 150 kA, which includes an additional (4^{th}) glacial cycle plus 30 kA into the future, putting the end point of each simulation at 555 kA of simulation time. Present day is represented at 525 kA of simulation time, or 0 kA BP, while the LGM is represented at 507 kA of simulation time, or 18 kA BP. Example pressure and temperature data for the gas simulation at the same location represented in **Figure 15** and **Figure 16** are show in red in **Figure 17**. In addition, the gas simulations also utilize the same external flow conditions file (**Section A.6**) as the ice simulations.

We note that the 30 kA future years from the present day have not been designed to represent projected warming scenarios, as ideally should be the case. Instead, we simply used the extended portion of the glacial cycle that was designed to smooth the RSL curve. In effect, this extends the present-day conditions for temperature while simulating a small sea level rise. Future work will create more physically meaningful future scenarios for the modeling workflow. We include modeling results for 10 kA in the future as an example of the workflow capability, but these results should not be considered or interpreted as new scientific evidence.

Previously, the ice simulations used GPSM average parameter values for seafloor depth, seafloor temperature, and heat flux. The methane simulations also rely on these data, but in addition, sample on sedimentation rate and total organic carbon (TOC). For each 1D simulation profile, Dakota selects 25 samples among combinations of sedimentation rate and TOC Latin applying Hypercube methodology. These samples make up 25 ensemble members (or alternatively, "realizations") at each profile location

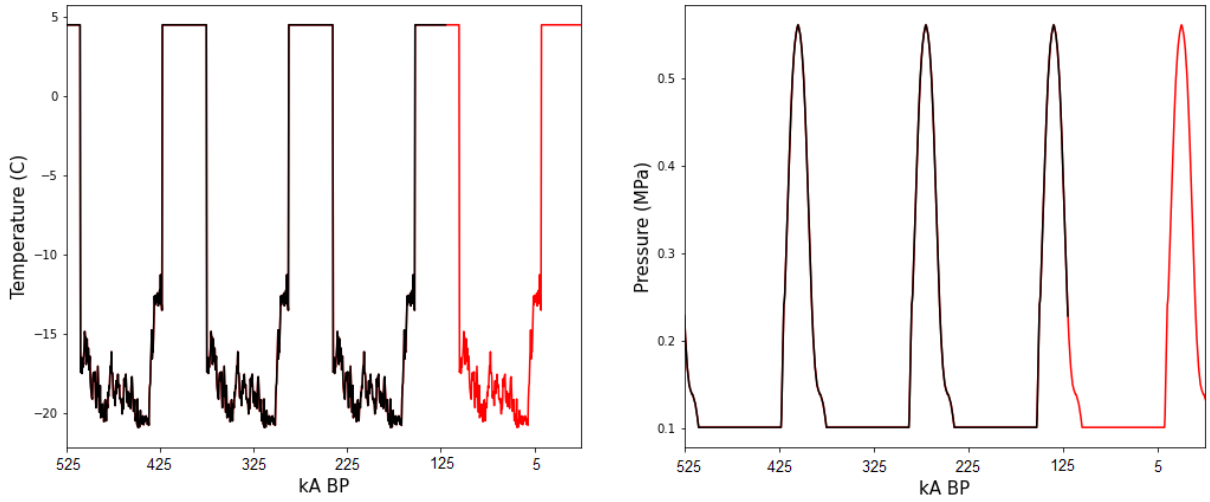

Figure 17. Top pressure (left) and pressure (right) boundary conditions for an example simulation, Profile 332811, located at 165.792ºW and 66.4583ºN, where present day water depth is 14 m. In black, the ice simulation portion of the simulation is shown, while in red the gas simulation portion is shown.

and enable probabilistic modeling results for methane gas flux. Additionally, both sedimentation and methanogenesis are turned on within the PFLOTRAN simulation. This allows methane gas to form and migrate throughout the shallow offshore sediments. We note that the TOC has been multiplied by a factor of 50 in these demonstration simulations in order to increase the methanogenesis over the short time frame of simulation (150 kA). The reasoning behind this was purely for visualization purposes in the demonstration. In reality, such geologic systems have evolved over several millions of years, allowing gas and gas hydrate to form and deposit, yet we only simulate a fraction of this time. When we set the TOC to realistic values, very little gas accumulated within the short time span of the simulation. Rather than initialize the simulations with gas and methane hydrate, we simply increased the rate of methanogenesis so that we could demonstrate the capabilities of this workflow.

We note that the number of samples (25) should ideally be much larger to allow for proper statistical analysis of the probabilistic results. We limited our sampling to 25 due to computational resource limitations and the computation time available to us. With 25 samples, one should capture the average of a particular quantity in the ensemble results fairly well; however, in order to get meaningful statistics for the true possible range in model predictions (e.g., the tails of a distribution), at least 100 samples should be run.

An important value to note within the PFLOTRAN input deck is GAS_RESIDUAL_SATURATION. This value indicates the minimum gas saturation required for free gas mobility throughout the sediment column. When gas saturation is lower than the residual gas saturation (set to 0.10 in these demonstration simulations), only dissolved gas is mobile and ebullition will not be possible. The residual gas saturation is a poorly constrained quantity in geophysical

modeling. Therefore, it is recommended that future modeling set-ups sample on this quantity, in addition to sedimentation rate and TOC. In general, we expect that smaller values of residual gas saturation will increase methane fluxes and may shift the onset of emissions to earlier times after permafrost thaw.

4.3. Modeling Results

We note, again, that the modeling workflow demonstration presented in this section is still a work in progress, but at the time of this writing, has been developed to an advanced stage capable of being exercised through its entire workflow – from model set-up to model prediction. As the capabilities of the PFLOTRAN HYDRATE Mode model are still being debugged and fine-tuned, the following results should be observed more as a proof of capabilities rather than as reliable, predictive science results. Given this expectation, we present the results of the ensemble simulations next.

4.3.1. Simulation Performance Statistics

A single ice simulation utilizing GPSM average parameter values was initialized for each of the 2,009 Alaskan domain locations (previously shown in **Figure 12**) and run for a total of 405 kA of simulation time. Of the 2,009 simulations, 1,973 were successful, while the remaining 36 PFLOTRAN HYDRATE Mode simulations failed. This equates to an ice simulation success rate of approximately 98%. Locations where the ice simulations failed to produce results are left blank on the figures.

Upon completion of successful ice simulations, gas simulations applying 25 Dakota-sampled GPSM parameters for combinations of sedimentation rate and TOC were initialized. They ran for 150 kA of simulation time. Of the 1,973 locations modeled to include methanogenesis, 1,493 were successful, while the remaining 480 PFLOTRAN HYDRATE Mode simulations failed to complete. This equates to a gas simulation success rate of approximately 75% - much lower than that of the ice simulations. In **Figure 18**, we present a map of all failed simulations for visual reference.

The main reason for failed simulations was numerical difficulty, especially when methanogenesis was included (e.g., the gas simulations). As described in **Section 2.3**, in the formulation developed here, liquid water is considered the only wetting phase. All other phases (free gas, gas hydrate, ice) are considered nonwetting phases. In order to apply a freezing point depression for ice phase or hydrate phase growth, the phase saturations are plugged into a capillary pressure function to obtain a phase capillary pressure and thus a freezing temperature offset. This is straightforward when transitioning from single phase liquid to two-phase (liquid-ice or liquid-hydrate). It is more complicated, however, when dealing with 3 or 4 phases coexisting in the pore space. In addition, PFLOTRAN's HYDRATE Mode uses primary variable switching to evaluate state properties of the system in any given grid cell at a given simulation time. There are 15 possible combinations for phase state, each corresponding to a set of primary variables. We have found that the numerical stability is most sensitive to the phase states and capillary pressure curve formulation. The majority of the failing simulations experienced trouble during phase transitions, such as when a freezing front passes through a region with mobile gas, for example. As seen in **Figure 18**, many of the failing gas simulations coincide with an area of anomalously low heat flow (**Figure 13C**), which would promote freezing. We note that PFLOTRAN HYDRATE Mode still requires development work to improve its robustness in this respect.

4.3.2. Submarine Permafrost Distribution

The average permafrost distribution for the LGM (18 ka BP), present day, and 10 kA in the future are presented in **Figure 19**, **Figure 20**, and **Figure 21**. These figures show the depth to the bottom of the submarine permafrost layer and were calculated as the deepest depth where ice saturation was

non-zero. How deep the frozen layer reaches at the LGM depends on several factors, namely the timing of exposure (which is primarily determined by the bathymetry), bottom water temperature prior to atmospheric exposure, and the heat flux (which determine the temperature profile in the sediment column at the time of atmospheric exposure). The depth of the submarine permafrost at the present day depends most heavily on the rate of thaw after submergence. The most important players are bottom water temperature, heat flux, and timing of submergence. Permafrost along the shelf edges has been submerged the longest and thus is expected to be the most degraded. However, regions where heat flux is high or bottom water temperatures are warm due to river discharge may create regions which support accelerated thaw unrelated to the timing of submergence. Regions where permafrost thaw is substantial is hypothesized to promote methanogenesis, due to an increased availability of organic matter, and increased sediment permeability for fluid flow.

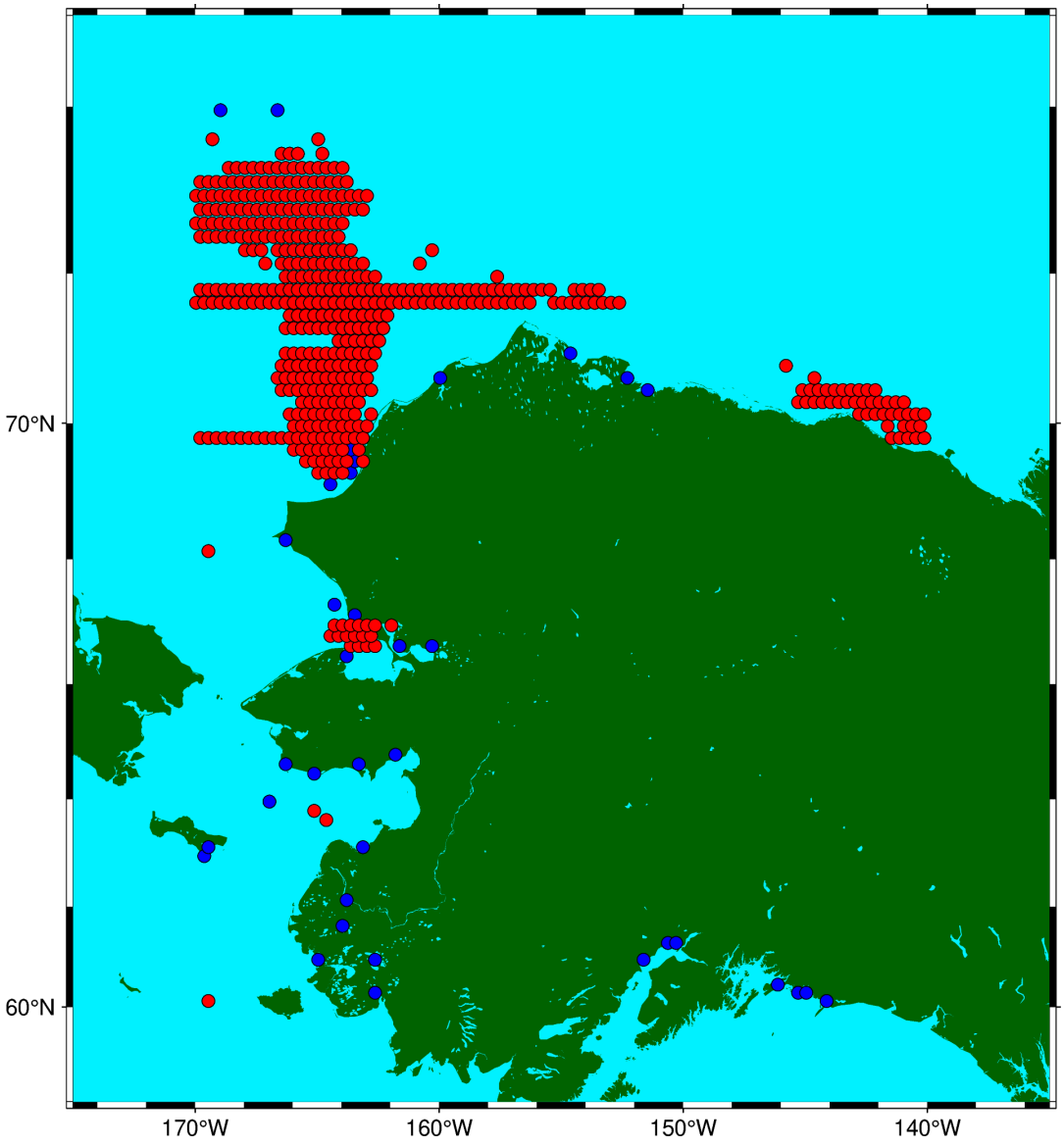

Figure 18. Map of failed PFLOTRAN HYDRATE Mode simulations where no data was available as a result. Blue show failed ice simulations (~ 2% of all simulations) and red show failed gas simulations (~ 25% of all simulations).

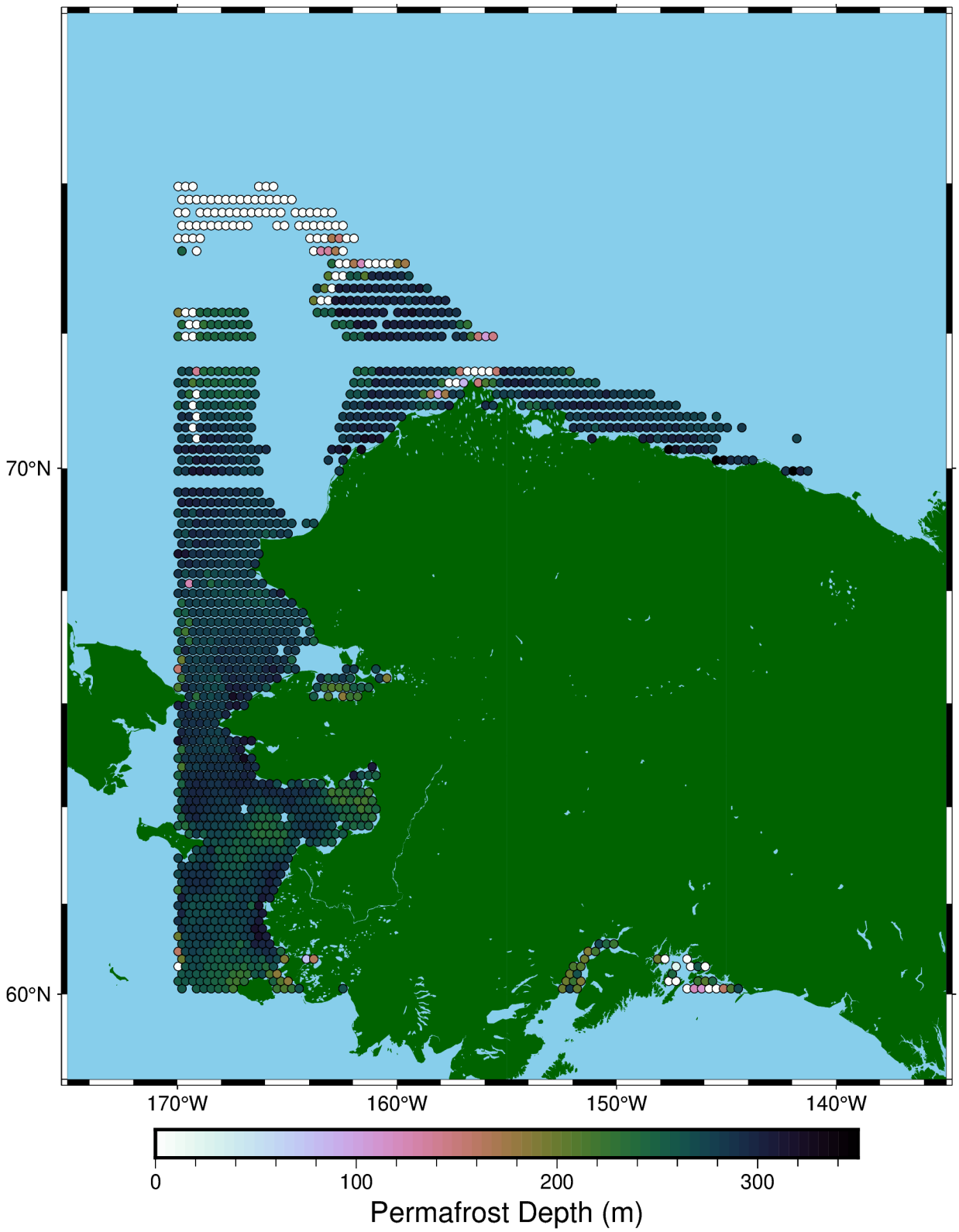

Figure 19. Permafrost depth (distance to the bottom of the permafrost layer) at the Last Glacial Maximum (LGM, 18 kA BP). Locations within the computational domain that are missing data did not complete (simulations failed).

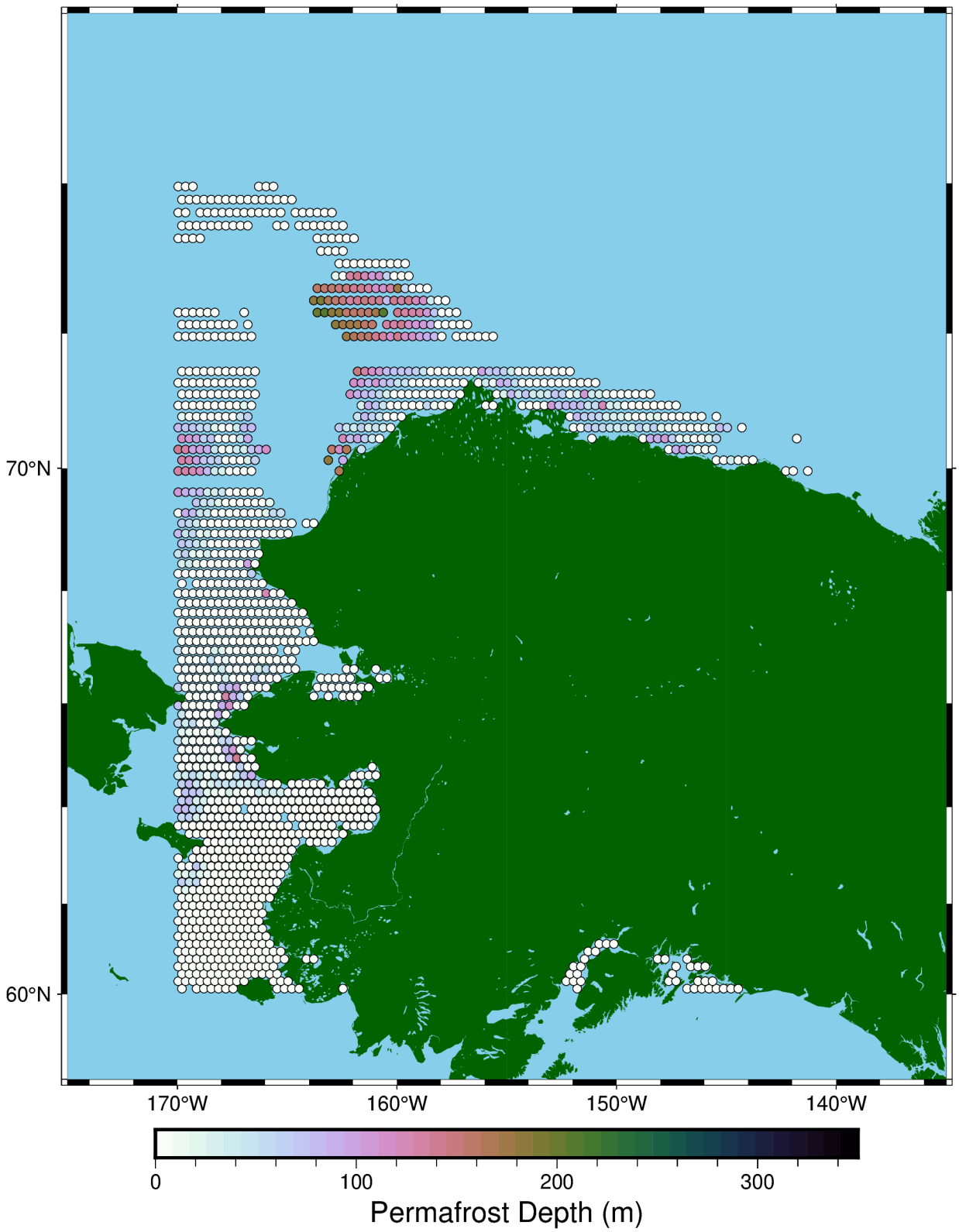

Figure 20. Permafrost depth (distance to the bottom of the permafrost layer) at the present day (0 kA BP). Locations within the computational domain that are missing data did not complete (simulations failed).

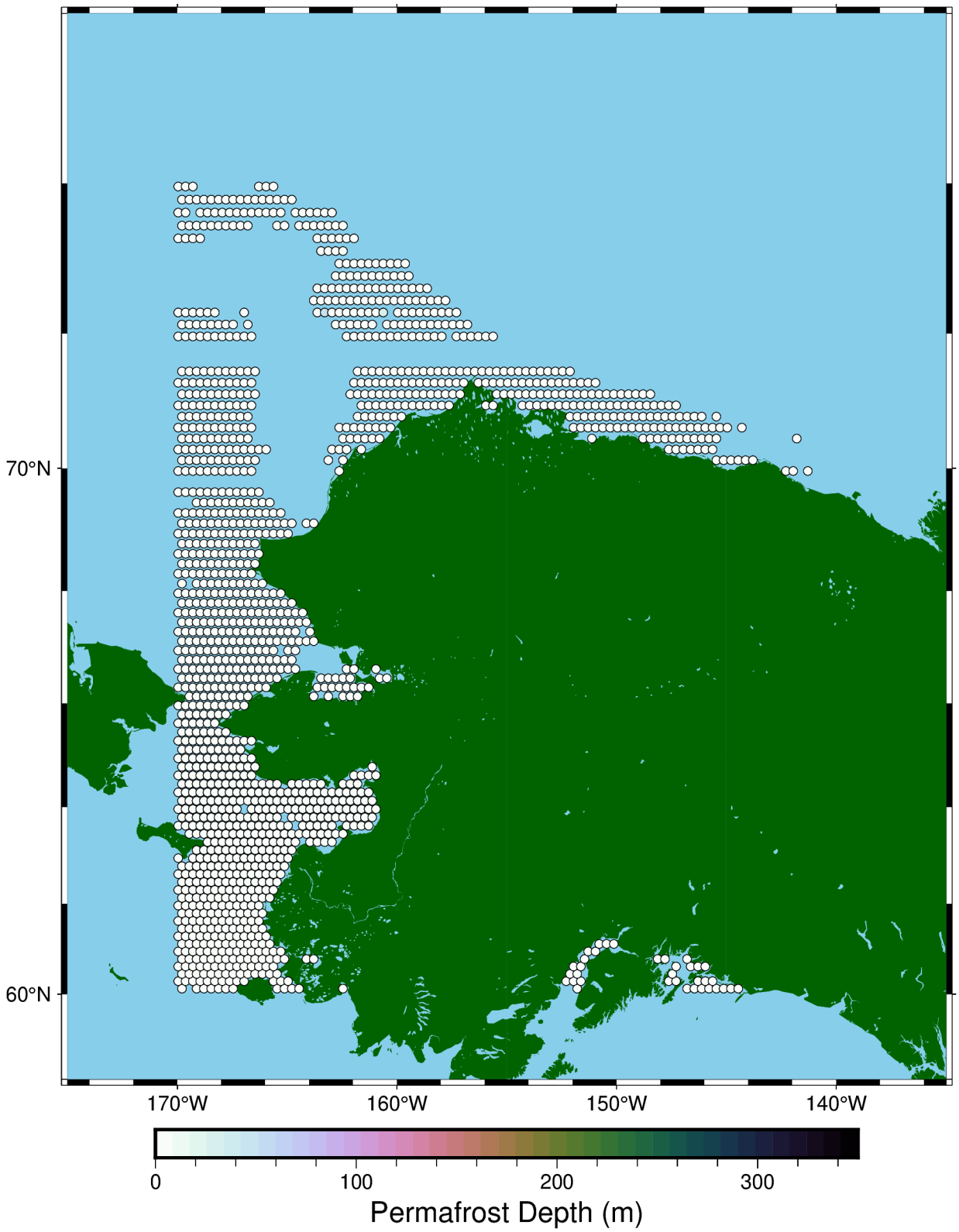

Figure 21. Permafrost depth (distance to the bottom of the permafrost layer) at 10 kA in the future. Locations within the computational domain that are missing data did not complete (simulations failed).

4.3.3. Methane Gas Distribution and Seabed-Water Flux

The average gas flux (kg yr^{-1}) at the 1 m^2 sediment-water column boundary, representing methane gas emissions from the sediments into the water column, for the LGM, present day, and 10 kA in the future are shown in **Figure 22**, **Figure 23**, and **Figure 24**. In these figures, bubble size and color are indicative of the magnitude of gas flux. We note that some simulation locations do not appear as their flux is either negligible, or the simulations failed to complete. A comparison against **Figure 18** is necessary to determine which of the two reasons for missing data applies, as presented. Once the numerical challenges are sorted out, failing simulations should no longer be an issue. For more detail, in **Figure 25**, **Figure 26**, and **Figure 27**, we also present the minimum and maximum values of gas flux at the LGM, present day, and 10 kA in the future.

While we must emphasize that these results are only notional and should not be interpreted as scientific evidence, certain trends can be identified. Little to no gas emissions from the seabed are predicted at the LGM, when the majority of the computational domain was exposed to the atmosphere. However, appreciable gas flux is seen in the northwest portion of the domain, where the seabed is deep enough that it is still submerged. At the present day, a significant increase in gas phase methane emissions is predicted. Emission rate magnitude is expected to increase with increasing TOC and sedimentation rate, as well as the state of permafrost degradation and the increase in sediment permeability associated with thaw. Interestingly, the model predicts a decrease in gas emissions 10 kA in the future relative to the present day. Although the methanogenesis parameters were held constant throughout the simulation period and gas mass increased over time, increasing sea level increases the pressure, and drives gaseous methane into solution, limiting gas phase saturation and thus mobility.

In Figure 28, the methane gas flux at three profile locations is shown at several depths within the 1D sediment columns, highlighting the capability of the modeling workflow to track and quantify gas movement within the simulations. The locations for each profile are as follows - Profile 220481: 166°W & 64°N, Profile 324121: 169°W & 66°N, and Profile 592139: 155°W & 71°N. It is immediately noticeable that the majority of mobile gas exists near the sediment surface, and not at depth. This is a result of the short time span of the simulations when methanogenesis occurred. Because the source of gas is highest near the top of the sediment column and decays towards depth, the top of the sediment column is expected to form gas before the rest of it does. If these simulations were allowed to run for time spans more representative of the geologic record, gas formation would also be expected at deeper depths.

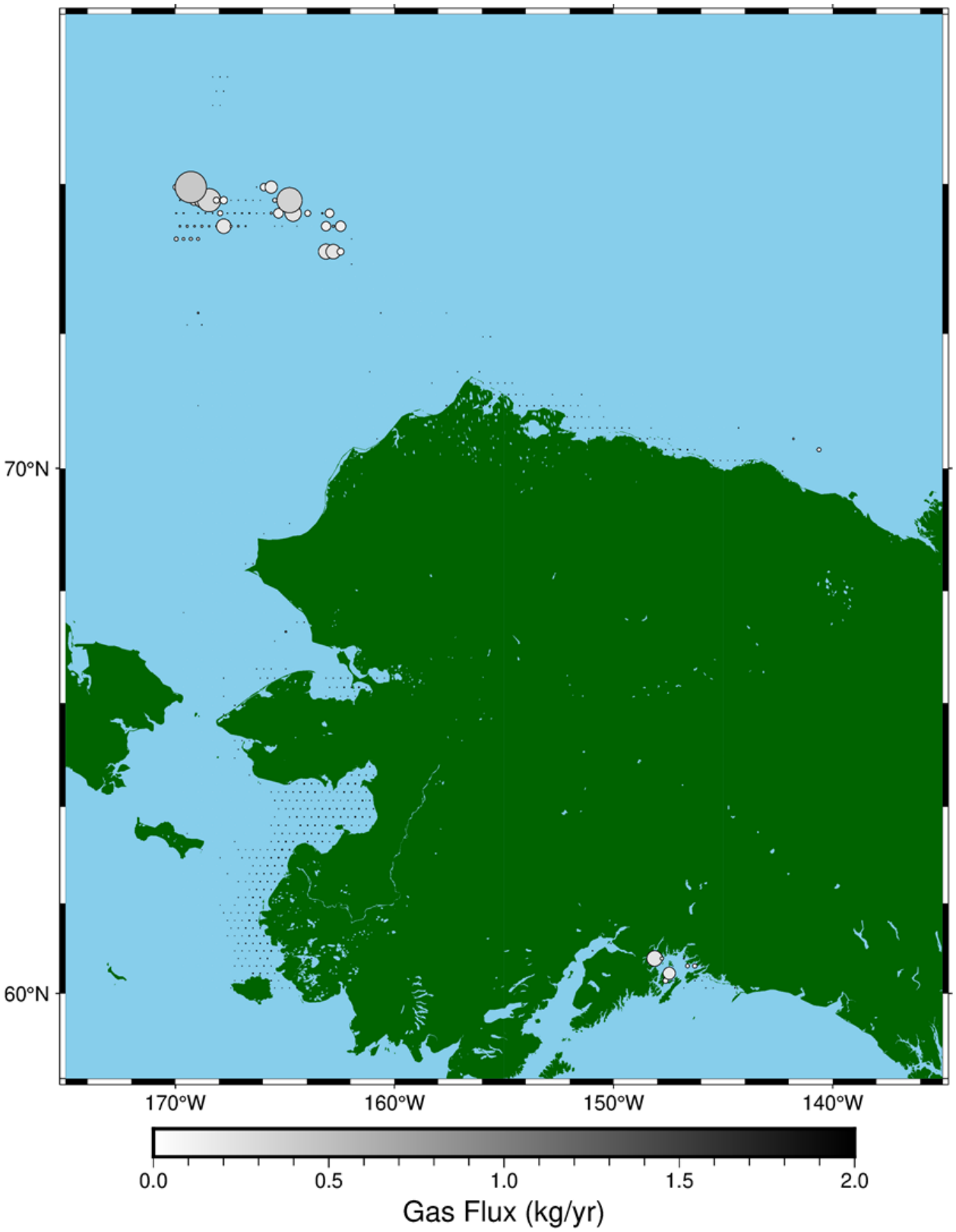

Figure 22. Average methane gas flux at the 1 m^2 sediment surface at the LGM (18 kA BP). Bubble size & color are indicative of magnitude. Some locations do not appear as their flux is negligible or the simulations failed.

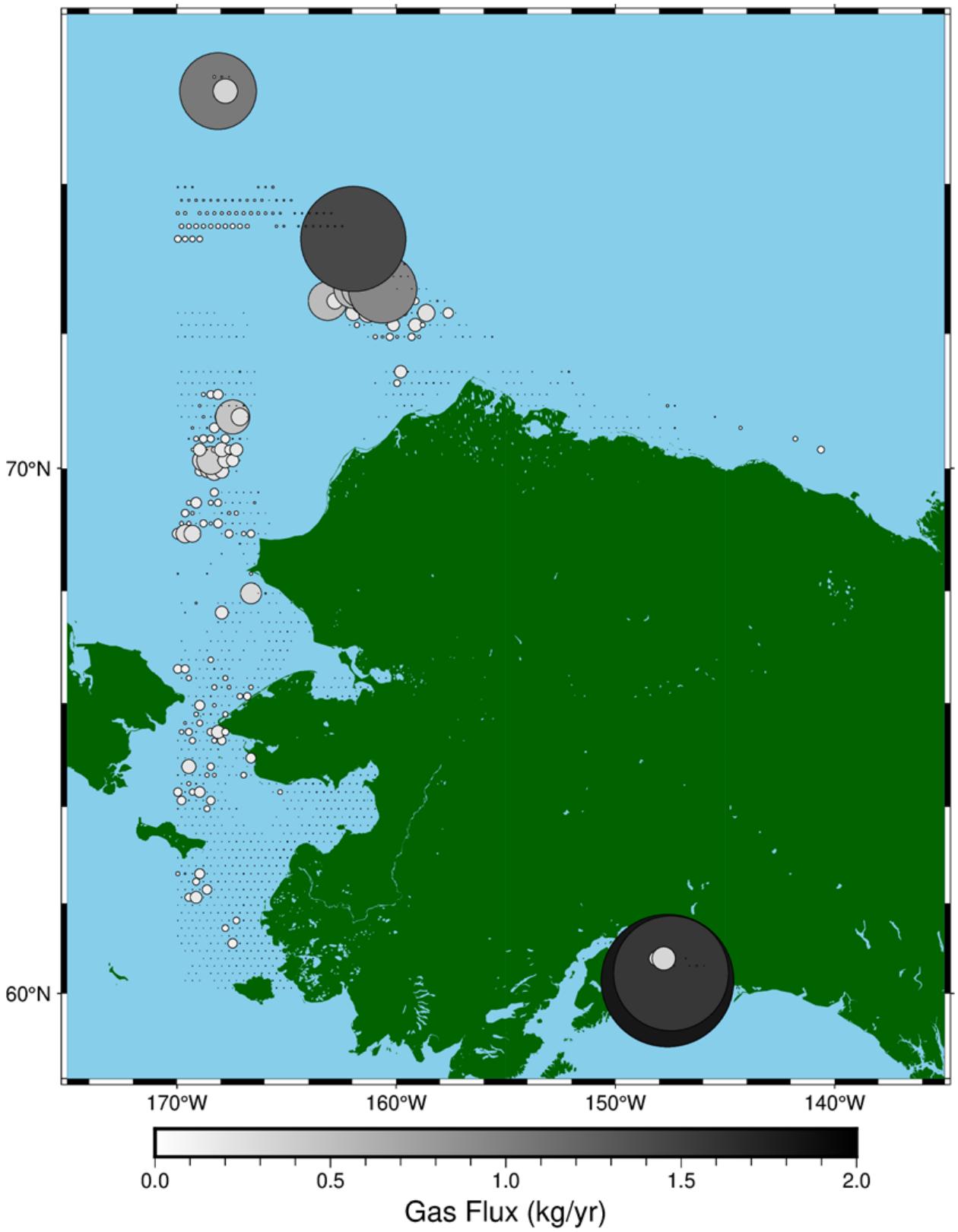

Figure 23. Average methane gas flux at the 1 m^2 sediment surface at the present day (0 kA BP). Bubble size & color are indicative of magnitude. Some locations do not appear as their flux is negligible or the simulations failed.

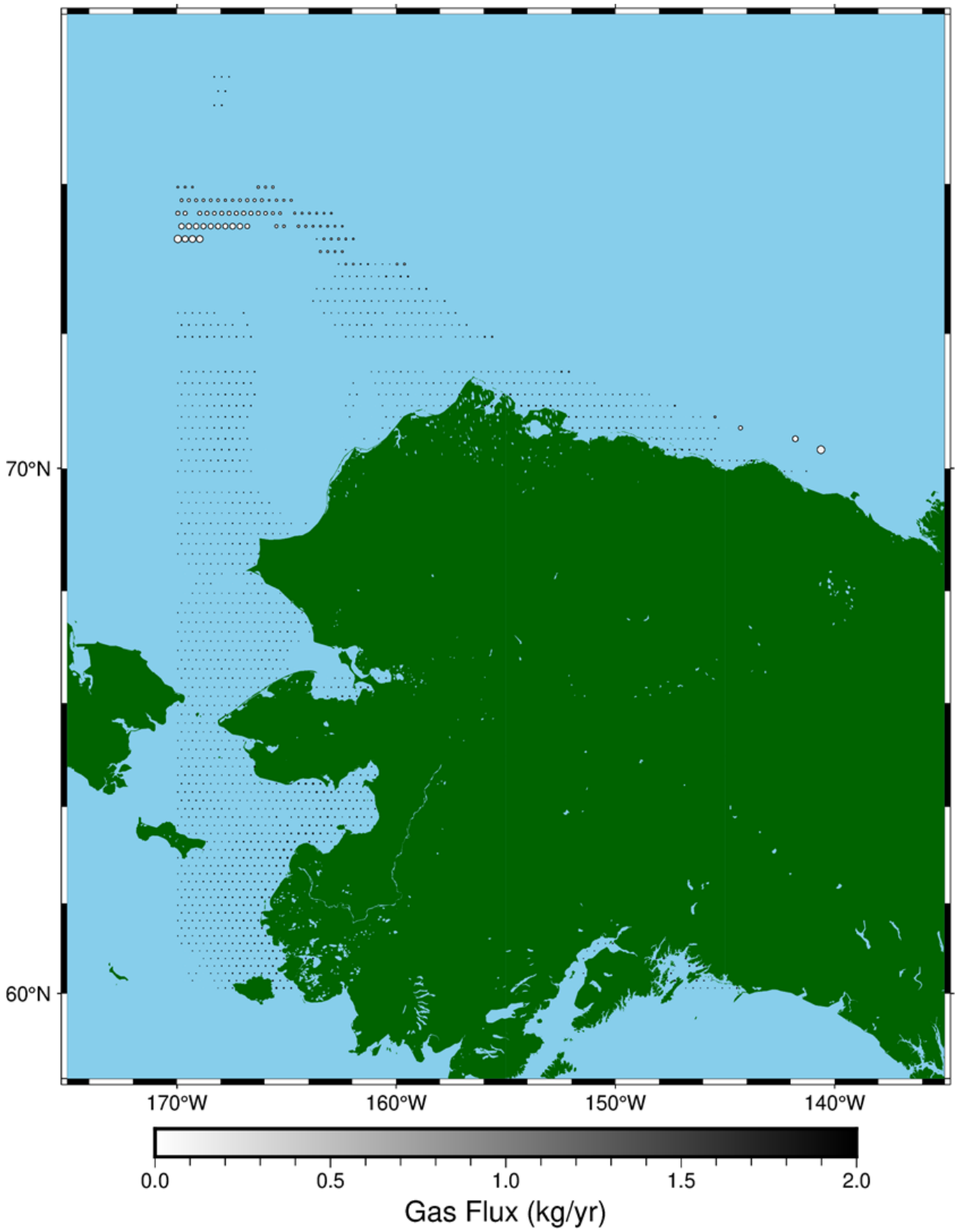

Figure 24. Average methane gas flux at the 1 m^2 sediment surface 10 kA in the future. Bubble size & color are indicative of magnitude. Some locations do not appear as their flux is negligible or the simulations failed.

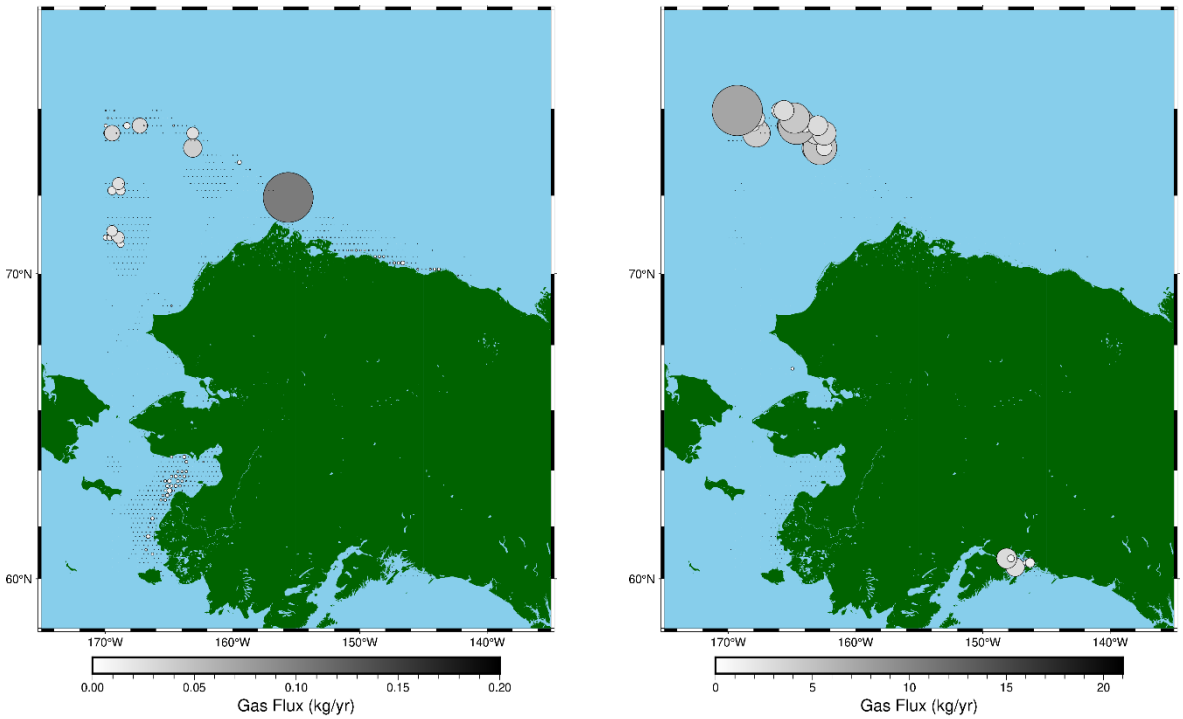

Figure 25. Minimum (left) and maximum (right) methane gas flux at the 1 m^2 sediment surface at the LGM (18 kA BP). Bubble size & color are indicative of magnitude. Some locations do not appear as their flux is negligible or the simulations failed.

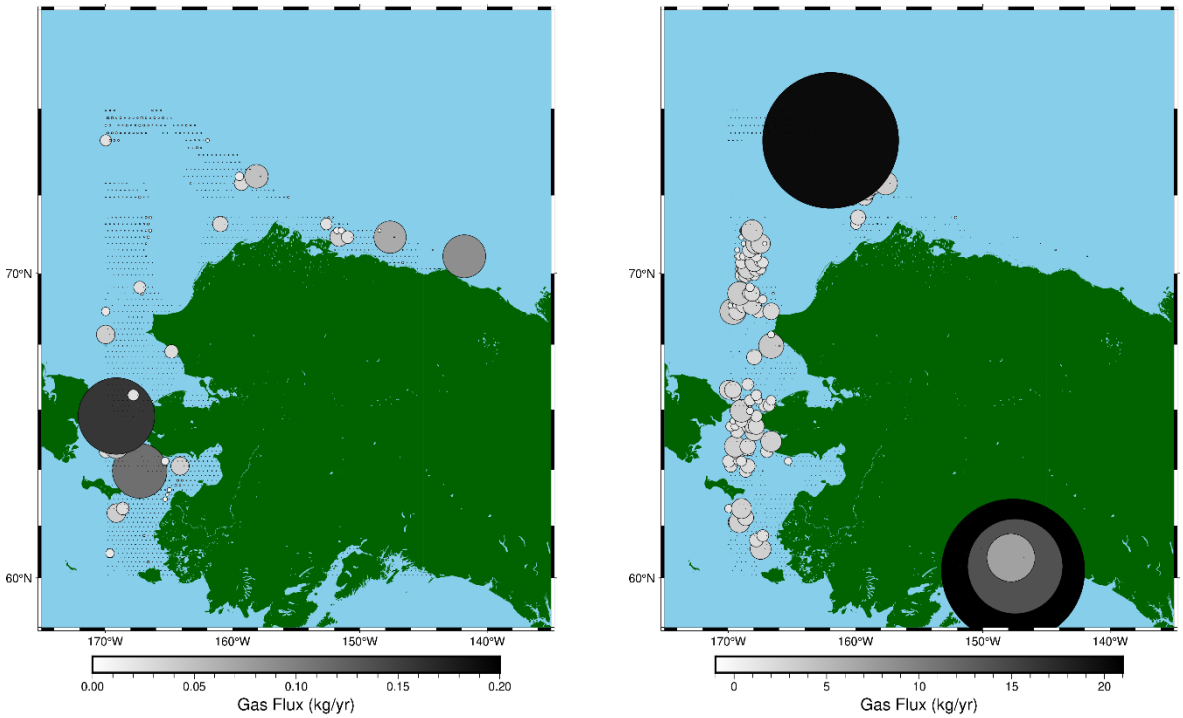

Figure 26. Minimum (left) and maximum (right) methane gas flux at the 1 m^2 sediment surface at the present day (0 kA BP). Bubble size & color are indicative of magnitude. Some locations do not appear as their flux is negligible or the simulations failed.

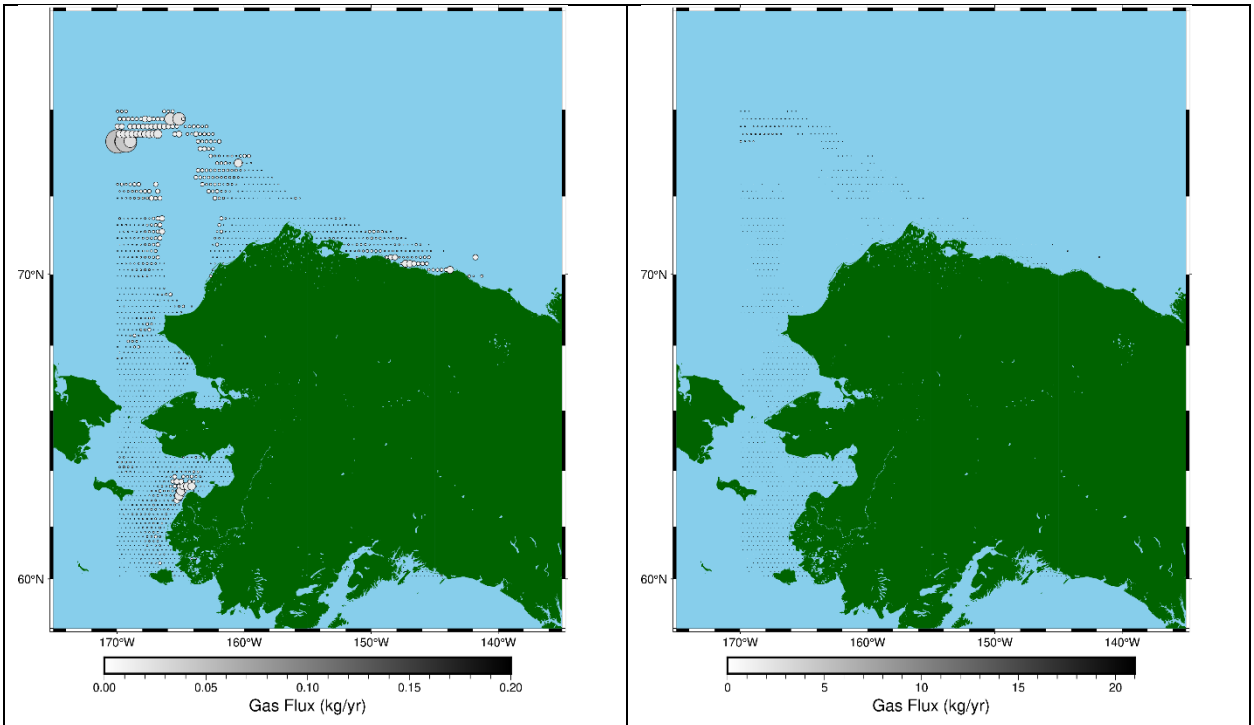

Figure 27. Minimum (left) and maximum (right) methane gas flux at the 1 m^2 sediment surface 10 kA in the future. Bubble size & color are indicative of magnitude. Some locations do not appear as their flux is negligible or the simulations failed.

In this section, we have presented the capability that this hybrid workflow can provide for ensemble modeling of the thermodynamics and methanogenesis on the Arctic continental shelf, resulting in probabilistic predictions for methane gas emissions from the seabed to the sediment column. We must emphasize, again, that the demonstration presented here should not be interpreted as scientific evidence, but rather, a proof of concept of the workflow capability. Much more improvements are necessary in the PFLOTRAN HYDRATE Mode process model, and the selection of model input parameters, before results can be used for scientific purposes.

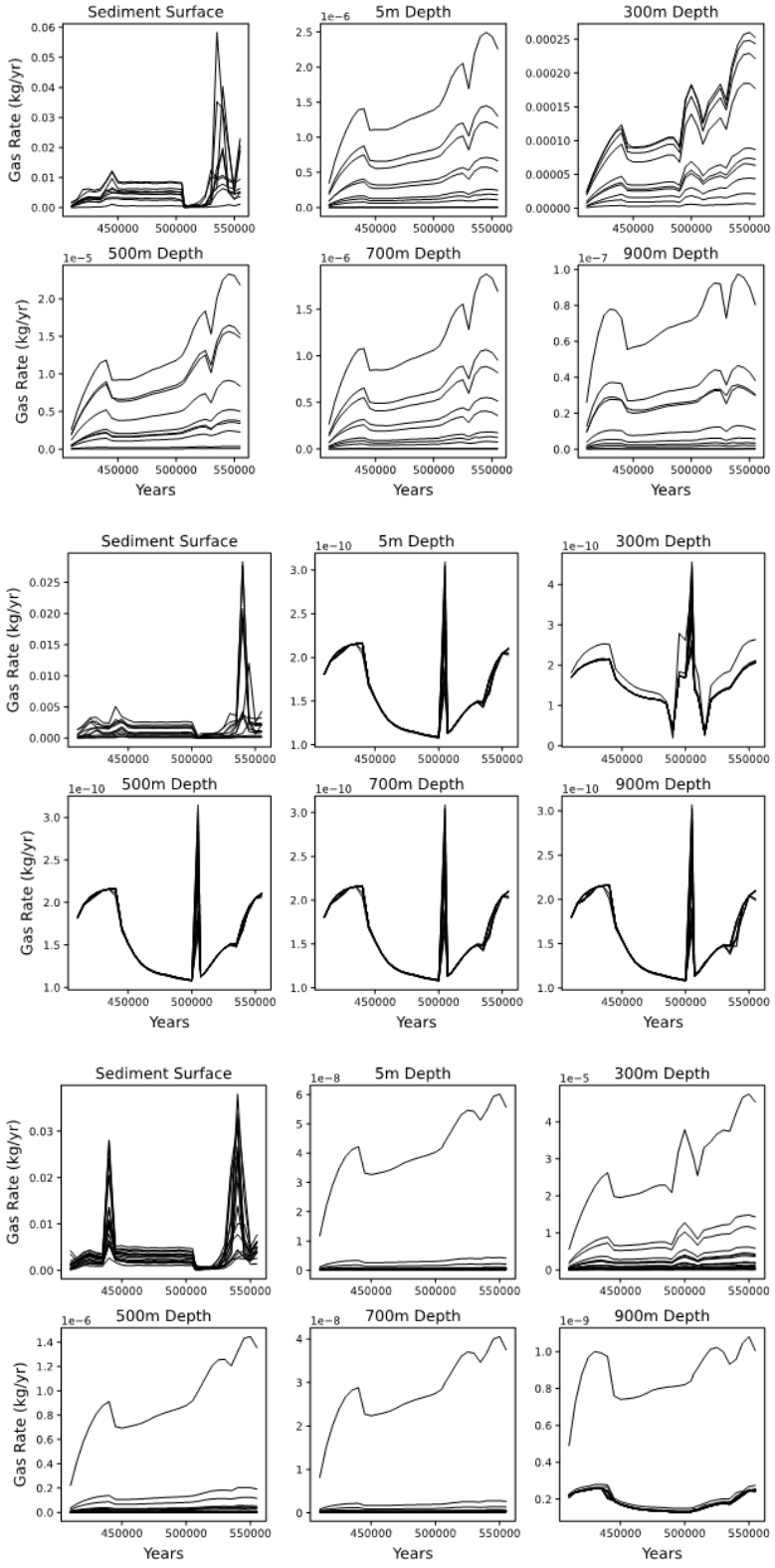

Figure 28. Methane gas flux (per 1 m^2) over simulation time at different depths for Profiles 220481, 324121, and 592139. The LGM corresponds to 507 kA.

5. APPLICATION TO GLOBAL CLIMATE MODELING

Global climate models allow us to better understand how the Earth's climate will evolve as an interconnected, complex system. Models such as the DOE's E^{3}SM, an advanced Earth system model, do this through the coupled simulation of land, ocean, and atmospheric physics, and require the world's most powerful supercomputers to run. One of the stated goals of this work is to use the developed hybrid modeling workflow to provide a reliable estimate of a time-varying source term for marine GHG flux to global oceanographic circulation and Earth system models. In this section, we briefly explore the history and current status of DOE's E^{3}SM, and what it may require before E^{3}SM can utilize such a source term.

E^{3}SM Version 1 (E^{3}SMv1) was released to the broader scientific community in April 2018, and E^{3}SM Version 2 (E^{3}SMv2) was tagged in September 2021. At the time of this writing, E^{3}SM is still in its second version. E^{3}SM Science is organized around three science drivers with simulation campaigns focused on water cycle, biogeochemistry, and cryosphere research. Each campaign employs unique model configurations optimized to address the associated research challenges by varying their choice of biogeochemical species. Marine GHG flux most closely fits into E^{3}SM's biogeochemistry science campaign.

In the current E3SMv2, the model prescribes a global methane mole fraction in the atmosphere. For historical runs the methane input data are from years 0 to 2014 and are obtained from [103], which provides consolidated data sets of historical atmospheric (volume) 31 mixing ratios of 43 greenhouse gases specifically for the purpose of climate model runs (see **Figure 29**). The future runs (2014-2500) use data from the same group, but the methane data are modeled with MAGICC7.0 (see **Figure 30**). MAGICC stands for 'Model for the Assessment of Greenhouse Gas Induced Climate Change'. It is a prime reduced-complexity model, often used by IPCC, for key scientific publications and by a number of Integrated Assessment Models, according to the MAGICC website.

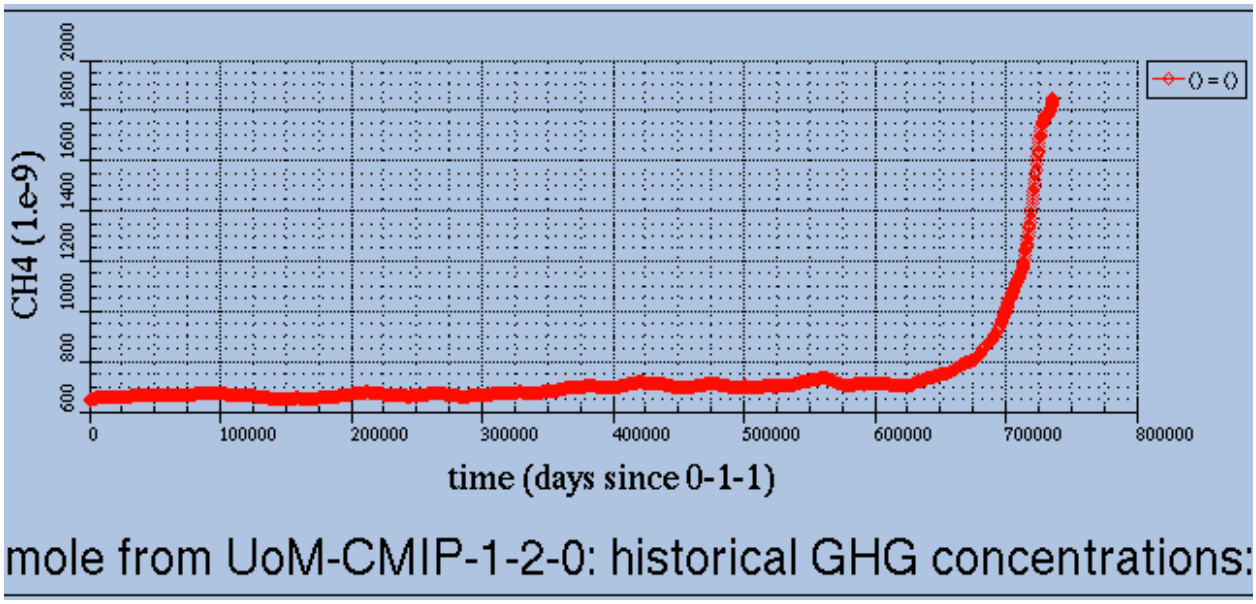

Figure 29. Atmospheric methane mole fraction prescribed for historical runs in E^{3}SMv2.

Of particular emphasis is the current version of E^{3}SM *prescribes* a methane mole fraction in the atmosphere, rather than allowing interaction between the atmosphere and land or marine sources of methane. Furthermore, the methane mole fraction in the atmosphere is applied homogenously, meaning the amount of methane does not vary in space, only in time.

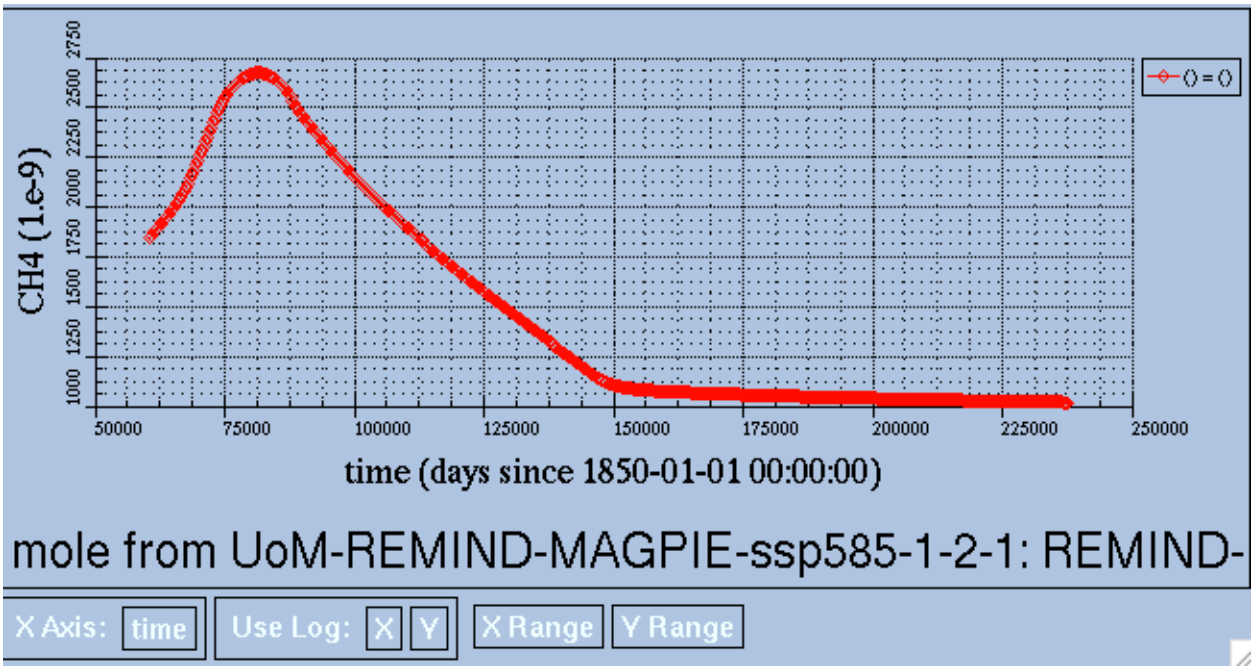

Figure 30. Atmospheric methane mole fraction prescribed for future runs in E3SMv2.

Until now, biogeochemistry configurations of E^{3}SM have only included CO_2 as an interactively modeled GHG in the atmosphere. However, development is underway on E^{3}SM Version 3 (E^{3}SMv3), in which researchers have proposed to work on several critical improvements for the next phase, focusing on methane. These include the capability to: (i) simulate methane based on surface emissions and climate feedbacks, and (ii) simulate methane gas in the stratosphere, which is critical to simulating the climate impact of its evolving emissions. This work is projected to occur under Phase III of the project, which will start in FY23 and go through FY25. Only after this work is completed, will E^{3}SM be configured such that a spatially and temporally varying source of marine GHG (particularly methane) can be of use to climate projects.

6. CONCLUSIONS AND FUTURE WORK

This report summarizes our group's effort at developing a numerical modeling framework designed to produce a first-of-its-kind estimate of Arctic methane gas releases from the marine sediments to the water column, and potentially to the atmosphere, where positive climate feedback may occur.

Newly developed modeling capability supported by the Laboratory Directed Research and Development (LDRD) program at Sandia National Laboratories now gives us the ability to probabilistically map gas distribution and quantity in the seabed by using a hybrid approach of geospatial machine learning, and predictive numerical thermodynamic ensemble modeling. The novelty in this approach is its ability to produce maps of useful data in regions that are only sparsely sampled, a common challenge in the Arctic, and a major obstacle to progress in the past. We have summarized the workflow developed in this study, and provided details on each software component: GPSM, Dakota, and PFLOTRAN HYDRATE Mode.

By applying this model to the circum-Arctic continental shelves and integrating the flux of free gas from *in situ* methanogenesis and dissociating gas hydrates from the sediment column under climate forcing, we can provide the most reliable estimate of a spatially and temporally varying source term for greenhouse gas flux that can be used by global oceanographic circulation and Earth system models (such as DOE's E^3SM). We have presented a demonstration of this workflow for a site which considers Alaska's continental shelf. In this demonstration, we've made several simplifications to the input parameters, highlighting where improvements should be made in future work. We also note that debugging and fine-tuning PFLOTRAN HYDRATE Mode performance is ongoing. Nevertheless, we have demonstrated the capabilities of the hybrid modeling workflow, including its ability to probabilistically map submarine permafrost, methane hydrate, and methane gas distribution and flux over historical time periods through the future.

This page left blank.

REFERENCES

[1] Sayedi, S. S., B. Abbott, B. Thornton, J. M. Frederick, J. Vonk, P. Overduin, C. Schadel, E. Schuur, A. Bourbonnais, A. Gavrilov, S. He, G. Hugelius, M. Jakobsson, M. Jones, D. Joung, G. Kraev, R. Macdonald, A. D. McGuire, C. Mu, M. O'Regan, K. Schreiner, C. Stranne, E. Pizhankova, A. Vasiliev, S. Westermann, J. P. Zarnetske, T. Zhang, M. Ghandehari, S. Baeumler, B. Brown, R. Frei, and A. Maslakov (2020), Subsea permafrost carbon stocks and climate change sensitivity estimated by expert assessment, Environmental Research Letters, Vol. 15, No. 12, doi:10.1088/1748-9326/abcc29.

[2] Frederick, J. M., William K. Eymold, Michael A. Nole, Benjamin J. Phrampus, Taylor R. Lee, Warren T. Wood, David Fukuyama, Olin Carty, Hugh Daigle, Hongkyu Yoon, and Ethan Conley (2021), Forecasting Marine Sediment Properties with Geospatial Machine Learning, SAND2021-10675, Sandia National Laboratories, Albuquerque, NM.

[3] Osterkamp, T. E., G. C. Baker, W. D. Harrison and T. Matava (1989), Characteristics of the active layer and shallow subsea permafrost, Journal of Geophysical Research Oceans, Vol. 94, 16227–36.

[4] Lindgren, A., G. Hugelius, P. Kuhry, T. R. Christensen and J. Vandenberghe (2016), GIS-based maps and area estimates of Northern Hemisphere permafrost extent during the last glacial maximum: LGM permafrost, Permafrost and Periglacial Processes, Vol. 27, pg. 6–16.

[5] Clark, P. U., A. S. Dyke, J. D. Shakun, A. E. Carlson, J. Clark, et al. (2009), The last glacial maximum, Science, Vol. 325, 710–4.

[6] Tesi, T. et al. (2016), Massive remobilization of permafrost carbon during post-glacial warming, Nature Communications, Vol. 7, 13653.

[7] Lindgren, A., G. Hugelius and P. Kuhry (2018), Extensive loss of past permafrost carbon but a net accumulation into present-day soils, Nature, Vol. 560, 219.

[8] Frederick, J. M. and B. A. Buffett (2014), Taliks in relict submarine permafrost and methane hydrate deposits: pathways for gas escape under present and future conditions, Journal of Geophysical Research Earth Surface, Vol. 119, 106–22.

[9] Thornton, B. F. and P. Crill (2015), Arctic permafrost: microbial lid on subsea methane, Nature Climate Change, 5, 723.

[10] Ruppel, C. D. and J. D. Kessler (2017) The interaction of climate change and methane hydrates, Reviews in Geophysics, Vol. 55, 126–68.

[11] Lambeck, K., H. Rouby, A. Purcell, Y. Sun and M. Sambridge (2014), Sea level and global ice volumes from the last glacial maximum to the Holocene, Proceedings of the National Acadademies of Sciences, Vol. 111, 15296–303.

[12] Overduin, P. P., S. von T. Deimling, F. Miesner, M. N. Grigoriev, C. Ruppel et al. (2019), Submarine permafrost map in the Arctic modeled using 1-D transient heat flux (SuPerMAP), Journal of Geophysical Research Oceans, Vol. 124, 3490–507.

[13] Hugelius, G. et al. (2014), Estimated stocks of circumpolar permafrost carbon with quantified uncertainty ranges and identified data gaps, Biogeosciences, Vol. 11, 6573–93.

[14] Schuur, E. A. G. et al. (2015), Climate change and the permafrost carbon feedback, Nature, Vol. 520, 171–9.

[15] Hubberten, H-W. and N. N. Romanovskii (2001), Terrestrial and offshore permafrost evolution of the Laptev Sea region during the last Pleistocene-Holocene glacial-eustatic cycle, Permafrost

Response on Economic Development, Environmental Security and Natural Resources (Berlin: Springer), pp 43–60.

[16] Shakhova, N. E., D. Y. Nicolsky and I. P. Semiletov (2009), Current state of subsea permafrost on the East Siberian Shelf: tests of modeling results based on field observations, Doklady Earth Science, Vol. 429, 1518–21.

[17] Ruppel, C. D., B. M. Herman, L. L. Brothers and P. E. Hart (2016), Subsea ice-bearing permafrost on the U.S. Beaufort Margin: 2. borehole constraints, Geochemistry, Geophysics, Geosystems, Vol. 17, 4333–53.

[18] Vonk, J. E. et al. (2012), Activation of old carbon by erosion of coastal and subsea permafrost in Arctic Siberia, Nature, Vol. 489, 137–40.

[19] Hoehler, T. M., M. J. Alperin, D. B. Albert and C. S. Martens (1994), Field and laboratory studies of methane oxidation in an anoxic marine sediment—evidence for a methanogen–sulfate reducer consortium, Global Biogeochemical Cycles, Vol. 8, 451–463.

[20] Borowski, W.S., C. K. Paull and W. Ussler III (1996), Marine pore-water sulfate profiles indicate in situ methane flux from underlying gas hydrate, Geology, Vol. 24, 655–658.

[21] Boetius, A., K. Ravenschlag, C. J. Schubert, D. Rickert, F. Widdel et al. (2000), A marine microbial consortium apparently mediating anaerobic oxidation of methane, Nature, Vol. 407, 623–626.

[22] Reeburgh, W.S. (2007), Oceanic methane biogeochemistry, Chemical Reviews, Vol. 107, 486–513.

[23] Regnier, P., A. W. Dale, S. Arndt, D. E. LaRowe, J. Mogollon, and P. Van Cappellen (2011), Quantitative analysis of anaerobic oxidation of methane (AOM) in marine sediments: A modeling perspective, Earth-Science Reviews, Vol. 106, 105-30.

[24] Bayon, G., G. M. Henderson and M. Bohn (2009), U–Th stratigraphy of a cold seep carbonate crust, Chemical Geology, Vol. 260, 47–56.

[25] Overduin, P. P., S. Liebner, C. Knoblauch, F. Günther, S. Wetterich, et al. (2015), Methane oxidation following submarine permafrost degradation: measurements from a central Laptev Sea shelf borehole, Journal of Geophysical Research Biogeosciences, Vol. 120, 2014JG002862.

[26] Alperin, M. and T. Hoehler (2010), The ongoing mystery of sea-floor methane, Science, Vol. 329, 288-9.

[27] Puglini, M., V. Brovkin, P. Regnier, and S. Arndt (2020), Assessing the potential for non-turbulent methane escape from the East Siberian Arctic Shelf, Biogeosciences, 17, 3247–3275, doi:10.5194/bg-17-3247-2020.

[28] Phrampus, B. J., T. R. Lee and W. T. Wood (2019), A global probabilistic prediction of cold seeps and associated seafloor fluid expulsion anomalies (SEAFLEAs), Geochemistry, Geophysics, Geosystems, Vol. 21, doi:10.1029/2019GC008747.

[29] Adams, D. D. (2005), Diffusive flux of greenhouse gases—methane and carbon dioxide—at the sediment-water interface of some lakes and reservoirs of the world, in Greenhouse Gas Emissions: Fluxes and Processes, Hydroelectric Reservoirs and Natural Environments, edited by A. Tremblay et al., pp. 129–153, Springer, New York.

[30] Joyce, J., and P. W. Jewell (2003), Physical controls on methane ebullition from reservoirs and lakes, Environmental and Engineering Geoscience, Vol. 9, 167–178.

[31] Jansson, P., B. Ferre, A. Silyakova, K. O. Dolven, and A. Omstedt (2019), A new numerical model for understanding free and dissolved gas progression toward the atmosphere in aquatic methane seepage systems, Limnology and Oceanography: Methods, doi:10.1002/lom3.10307.

[32] McGinnis, D. F., J. Greinert, Y. Artemov, S. E. Beaubien and A. Wuest (2006), Fate of rising methane bubbles in stratified waters: How much methane reaches the atmosphere?, Journal of Geophysical Research, Vol. 111, C09007.

[33] Myhre, C. L., et al. (2016), Extensive release of methane from Arctic seabed west of Svalbard during summer 2014 does not influence the atmosphere, Geophys. Res. Lett., 43, 4624–4631, doi:10.1002/2016GL068999.

[34] Shakhova, N., et al. (2014), Ebullition and storm-induced methane release from the East Siberian Arctic Shelf, Nature Geoscience., 7, 64–70, doi:10.1038/NGEO2007.

[35] Weber, T., N. A. Wiseman and A. Kock (2019), Global ocean methane emissions dominated by shallow coastal waters, Nature Communications, Vol. 10, 4584, doi:10.1038/s41467-019-12541-7.

[36] Mcguire, A. D., L. G. Anderson, T. R. Christensen, S. Dallimore, L. Guo, D. J. Hayes, M. Heimann, T. D. Lorenson, R. W. Macdonald, and N. Roulet (2009), Sensitivity of the carbon cycle in the Arctic to climate change, Ecological Monographs, Vol. 79, 523–55.

[37] Shakhova, N., Semiletov, I., Gustafsson, O., Sergienko, V., Lobkovsky, L., Dudarev, O., Tumskoy, V., Grigoriev, M., Mazurov, A., Salyuk, A., Ananiev, R., Koshurnikov, A., Kosmach, D., Charkin, A., Dmitrevsky, N., Karnaukh, V., Gunar, A., Meluzov, A., and Chernykh, D. (2016), Current rates and mechanisms of subsea permafrost degradation in the East Siberian Arctic Shelf, Nat. Commun., 8, 15872, doi:10.1038/ncomms15872.

[38] Shakhova, N., Semiletov, I., and Chuvilin, E. (2019), Understanding the permafrost–hydrate system and associated methane releases in the East Siberian Arctic Shelf, Geosciences, 9, 251, doi:10.3390/geosciences9060251.

[39] Berchet, A. et al. (2016), Atmospheric constraints on the methane emissions from the East Siberian Shelf, Atmos. Chem. Phys., 16, 4147–4157, doi: 10.5194/acp-16-4147-2016.

[40] Steinbach, J., et al. (2021), Source apportionment of methane escaping the subsea permafrost system in the outer Eurasian Arctic Shelf, Proceedings of the National Academy of Sciences, 118(10), e2019672118, doi:10.1073/pnas.2019672118.

[41] Thornton, B. F., Geibel, M. C., Crill, P. M., Humborg, C., and Mörth, C.-M. (2016), Methane fluxes from the sea to the atmosphere across the Siberian shelf seas, Geophys. Res. Lett., 43, 5869–5877.

[42] Overduin, P. P., Liebner, S., Knoblauch, C., Günther, F., Wetterich, S., Schirrmeister, L., Hubberten, H.-W., and Grigoriev, M. N. (2015), Methane oxidation following submarine permafrost degradation: Measurements from a central Laptev Sea shelf borehole, J. Geophys. Res.-Biogeo., 120, 965–978.

[43] Sparrow, K.J., Kessler, J.D., Southon, J.R., Garcia-Tigreros, F., Schreiner, K.M., Ruppel, C.D., Miller, J.B., Lehman, S.J. and Xu, X. (2018). Limited contribution of ancient methane to surface waters of the US Beaufort Sea shelf. Science advances, 4(1), eaao4842.

[44] Sapart, C. J., Shakhova, N., Semiletov, I., Jansen, J., Szidat, S., Kosmach, D., Dudarev, O., van der Veen, C., Egger, M., Sergienko, V., Salyuk, A., Tumskoy, V., Tison, J.-L., and Röckmann, T. (2017), The origin of methane in the East Siberian Arctic Shelf unraveled with triple isotope analysis, Biogeosciences, 14, 2283–2292, doi:10.5194/bg-14-2283-2017.

[45] James, R. H., et al. (2016), Effects of climate change on methane emissions from seafloor sediments in the Arctic Ocean: A review, Limnol. Oceanogr., 61, S283–S299.

[46] Saunois, M., et al. (2016), The global methane budget 2000–2012, Earth Syst. Sci. Data, 8, 697–751, doi:10.5194/essd-8-697-2016.

[47] Yurganov, L., D. Carroll, A. Pnyushkov, I. Polyakov, and H. Zhang (2021), Ocean stratification and sea-ice cover in Barents and Kara seas modulate sea-air methane flux: satellite data, Advances in Polar Science, 32(2), 118-140, doi: 10.13679/j.advps.2021.0006.

[48] Rutgers van der Loeff, M. M., N. Cassar, M. Nicolaus, B. Rabe and I. Stimac (2014), The influence of sea ice cover on air-sea gas exchange estimated with radon-222 profiles, Journal of Geophysical Research Oceans, Vol. 119(5), 2735-51.

[49] Malakhova, V., and E. Golubeva (2022), Model Study of the Effects of Climate Change on the Methane Emissions on the Arctic Shelves, Atmosphere, 13, 274, doi:10.3390/atmos13020274.

[50] Martin, K. M., Wood, W. T., & Becker, J. J. (2015). A global prediction of seafloor sediment porosity using machine learning. Geophysical Research Letters, 42(24).

[51] Lee, T. R., Wood, W. T., and Phrampus, B. J. (2019). A Machine Learning (kNN) Approach to Predicting Global Seafloor Total Organic Carbon. Global Biogeochemical Cycles, 33(1):37–46.

[52] Restreppo, G. A., Wood, W. T., and Phrampus, B. J. (2020). Oceanic sediment accumulation rates predicted via machine learning algorithm: towards sediment characterization on a global scale. Geo-Marine Letters, 40(5):755–763.

[53] Obelcz, J., W. T. Wood, B. J. Phrampus, T. R. Lee (2020), Machine learning augmented time-lapse bathymetric surveys: A case study from the Mississippi river delta front, Geophysical Research Letters, 47 (10), e2020GL087857.

[54] Lee, T. R., B. J. Phrampus, J. Obelcz, W. T. Wood, A. Skarke (2020), Global marine isochore estimates using machine learning, Geophysical Research Letters, 47 (18), e2020GL088726.

[55] Graw, J. H., W. T. Wood, B. J. Phrampus (2021), Predicting global marine sediment density using the random forest regressor machine learning algorithm, Journal of Geophysical Research: Solid Earth, 126 (1), e2020JB020135.

[56] Eymold, W. K., Frederick, J. M., Nole, M., Phrampus, B. J., and Wood, W. T. (2021). Prediction of Gas Hydrate Formation at Blake Ridge Using Machine Learning and Probabilistic Reservoir Simulation. Geochemistry, Geophysics, Geosystems, 22(4).

[57] Seiter, K., Hensen, C., Schröter, J., and Zabel, M. (2004). Organic carbon content in surface sediments—defining regional provinces. Deep Sea Research Part I: Oceanographic Research Papers, 51(12):2001–2026.

[58] Goutorbe, B., J. Poort, F. Lucazeau, and S. Raillard (2011), Global heat flow trends resolved from multiple geological and geophysical proxies, Geophysical Journal International, 187(3), 1405-1419, doi:10.1111/j.1365-246X.2011.05228.x.

[59] Straume, E., Gaina, C., Medvedev, S., Hochmuth, K., Gohl, K., Whittaker, J. M., Abdul Fattah, R., Doornenbal, J. C., & Hopper, J. R. (2019). GlobSed: Updated total sediment thickness in the world's oceans. Geochemistry, Geophysics, Geosystems, 20(4), 1756-1772.

[60] Muller, R. D., Seton, M., Zahirovic, S., Williams, S. E., Matthews, K. J., Wright, N. M.,... Hosseinpour, M. (2016). Ocean basin evolution and global-scale plate reorganization events since Pangea breakup. Annual Review of Earth and Planetary Sciences,44, 107–138, doi:10.1146/annurev-earth-060115-012211.

[61] Locarnini, R. A., A. V. Mishonov, O. K. Baranova, T. P. Boyer, M. M. Zweng, H. E. Garcia, J. R. Reagan, D. Seidov, K. W. Weathers, C. R. Paver, I. V. Smolyar, 2019: World Ocean Atlas 2018, Volume 1: Temperature. A. V. Mishonov, Technical Ed., NOAA Atlas NESDIS 81.

[62] Tozer, B., D. T. Sandwell, W. H. F. Smith, C. Olson, J. R. Beale, P. Wessel (2019), Global Bathymetry and Topography at 15 Arc Sec: SRTM15+, Earth and Space Science, 6(10), 1847-1864, doi:10.1029/2019EA000658.

[63] Martin, K. M., Wood, W. T., & Becker, J. J. (2015). A global prediction of seafloor sediment porosity using machine learning. Geophysical Research Letters, 42(24).

[64] Martin, K., & Wood, W. (2017). A new model of marine sediment compression. Earth and Planetary Science Letters, 477, 21–26, doi:10.1016/j.epsl.2017.08.008.

[65] Adams, B.M., Bohnhoff, W.J., Dalbey, K.R., Ebeida, M.S., Eddy, J.P., Eldred, M.S., Hooper, R.W., Hough, P.D., Hu, K.T., Jakeman, J.D., Khalil, M., Maupin, K.A., Monschke, J.A., Ridgway, E.M., Rushdi, A.A., Seidl, D.T., Stephens, J.A., Swiler, L.P., and Winokur, J.G., "Dakota, A Multilevel Parallel Object-Oriented Framework for Design Optimization, Parameter Estimation, Uncertainty Quantification, and Sensitivity Analysis: Version 6.12 User's Manual," Sandia Technical Report SAND2020-12495, November 2020.

[66] McKay, M. D., Beckman, R. J., & Conover, W. J. (1979). Comparison of three methods for selecting values of input variables in the analysis of output from a computer code. Technometrics, 21(2), 239-245.

[67] Fukusako, S., and Yamada, M. (1993), Recent Advances in Research on Water-Freezing and Ice-Melting Problems, Experimental Thermal and Fluid Science, 6, 90-105.

[68] Handa, Y. P. (1988), A calorimetric study of naturally occurring gas hydrates. Industrial & engineering chemistry research, 27(5), 872-874.

[69] Carroll, J. J., and Mather, A. E. (1997), A Model for the Solubility of Light Hydrocarbons in Water and Aqueous Solutions of Alkanolamines, Chem. Engng. Sci., 52, 545-552.

[70] Kamath, V. A. (1984), Study of heat transfer characteristics during dissociation of gas hydrates in porous media. University of Pittsburgh.

[71] Moridis, G. J. (2003), Numerical studies of gas production from methane hydrates, SPE J., 8 (4), 359-370.

[72] Dickens, G. R., & Quinby-Hunt, M. S. (1997), Methane hydrate stability in pore water: a simple theoretical approach for geophysical applications. Journal of Geophysical Research: Solid Earth, 102(B1), 773-783.

[73] Fujino, K., Lewis, E. L., & Perkin, R. G. (1974), The freezing point of seawater at pressures up to 100 bars. Journal of Geophysical research, 79(12), 1792-1797.

[74] White, M. D., Kneafsey, T. J., Seol, Y., Waite, W. F., Uchida, S., Lin, J. S., ... & Zyrianova, M. (2020), An international code comparison study on coupled thermal, hydrologic and geomechanical processes of natural gas hydrate-bearing sediments. Marine and Petroleum Geology, 120, 104566.

[75] Dai, S. and Y. Seol (2014), Water permeability in hydrate-bearing sediments A pore-scale study. Geophysical Research Letters, 41, p. 4176-84.

[76] Malinverno, A. (2010), Marine gas hydrates in thin sand layers that soak up microbial methane. Earth and Planetary Science Letters, 292(3):399–408.

[77] Davie, M. K., Zatsepina, O. Y., & Buffett, B. A. (2004). Methane solubility in marine hydrate environments. Marine geology, 203(1-2), 177-184.

[78] Emiliani, C. (1955), Pleistocene temperatures, Journal of Geology, 63, 538-578.

[79] Jakobsson, M., et al. (2014), Arctic Ocean glacial history, Quaternary Science Reviews, 92, 40-67, doi:10.1016/j.quascirev.2013.07.033.

[80] Aagaard-Sørensen, S., K. Husum, M. Hald, T. Marchitto, and F. Godtliebsen (2014), Sub sea surface temperatures in the Polar North Atlantic during the Holocene: Planktic foraminiferal Mg/Ca temperature reconstructions, The Holocene, 24(1), 93-103, doi: 10.1177/0959683613515730.

[81] Aagaard-Sørensen, S., K. Husum, K. Werner, R. F. Spielhagen, M. Hald, and T. M. Marchitto (2014), A Late Glacial–Early Holocene multiproxy record from the eastern Fram Strait, Polar North Atlantic, Marine Geology, 355, 15-26, doi:10.1016/j.margeo.2014.05.009.

[82] Łącka, M., M. Cao, A. Rosell-Melé, J. Pawłowska, M. Kucharska, M. Forwick, and M. Zajączkowski (2019), Postglacial paleoceanography of the western Barents Sea: Implications for alkenone-based sea surface temperatures and primary productivity, Quaternary Science Reviews, 224, 105973, doi:10.1016/j.quascirev.2019.105973.

[83] Langner, M., and S. Mulitza (2019), Technical note: PaleoDataView – a software toolbox for the collection, homogenization and visualization of marine proxy data, Clim. Past, 15(6), 2067-2072, doi: 10.5194/cp-15-2067-2019.

[84] Nørgaard-Pedersen, N., R. F. Spielhagen, H. Erlenkeuser, P. M. Grootes, J. Heinemeier, and J. Knies (2003), Arctic Ocean during the Last Glacial Maximum: Atlantic and polar domains of surface water mass distribution and ice cover, Paleoceanography, 18(3), 8-1 - 8-19.

[85] Tierney, J. E., J. Zhu, J. King, S. B. Malevich, G. J. Hakim, and C. J. Poulsen (2020), Glacial cooling and climate sensitivity revisited, Nature, 584(7822), 569-573, doi: 10.1038/s41586-020-2617-x.

[86] Nørgaard-Pedersen, N., R. Spielhagen, J. Thiede, and H. Kassens (1998), Central Arctic Surface Ocean Environment During the Past 80,000 Years, Paleoceanography, 13(2), 193-204.

[87] Waelbroeck, C., et al. (2009), Constraints on the magnitude and patterns of ocean cooling at the Last Glacial Maximum, Nature Geoscience, 2(2), 127-132, doi: 10.1038/ngeo411.

[88] Farmer, J. R., T. M. Cronin, A. de Vernal, G. S. Dwyer, L. D. Keigwin, and R. C. Thunell (2011), Western Arctic Ocean temperature variability during the last 8000 years, Geophysical Research Letters, 38(24), doi:10.1029/2011GL049714.

[89] Cronin, T. M., G. S. Dwyer, J. Farmer, H. A. Bauch, R. F. Spielhagen, M. Jakobsson, J. Nilsson, W. M. Briggs, and A. Stepanova (2012), Deep Arctic Ocean warming during the last glacial cycle, Nature Geoscience, 5(9), 631-634, doi: 10.1038/ngeo1557.

[90] Hillaire-Marcel, C., A. de Vernal, L. Polyak, and D. Darby (2004), Size-dependent isotopic composition of planktic foraminifers from Chukchi Sea vs. NW Atlantic sediments—implications for the Holocene paleoceanography of the western Arctic, Quaternary Science Reviews, 23(3), 245-260, doi:10.1016/j.quascirev.2003.08.006.

[91] Nürnberg, D. (1995), Magnesium in tests of Neogloboquadrina pachyderma sinistral from high northern and southern latitudes, The Journal of Foraminiferal Research, 25(4), 350-368, doi: 10.2113/gsjfr.25.4.350.

[92] Livsey, C. M., R. Kozdon, D. Bauch, G.-J. A. Brummer, L. Jonkers, I. Orland, T. M. Hill, and H. J. Spero (2020), High-Resolution Mg/Ca and δ18O Patterns in Modern Neogloboquadrina pachyderma From the Fram Strait and Irminger Sea, Paleoceanography and Paleoclimatology, 35(9), e2020PA003969, doi:10.1029/2020PA003969.

[93] Eynaud, F., T. M. Cronin, S. A. Smith, S. Zaragosi, J. Mavel, Y. Mary, V. Mas, and C. Pujol (2009), Morphological variability of the planktonic foraminifer Neogloboquadrina pachyderma from ACEX cores: Implications for Late Pleistocene circulation in the Arctic Ocean, Micropaleontology, 55(2/3), 101-116.

[94] El Bani Altuna, N., A. J. Pieńkowski, F. Eynaud, and R. Thiessen (2018), The morphotypes of Neogloboquadrina pachyderma: Isotopic signature and distribution patterns in the Canadian Arctic Archipelago and adjacent regions, Marine Micropaleontology, 142, 13-24, doi: https://doi.org/10.1016/j.marmicro.2018.05.004.

[95] Boyle, E. A., and L. D. Keigwin (1985), Comparison of Atlantic and Pacific peleochemical records for the last 215,000 years: changes in deep ocean circulation and chemical inventories, Earth and Planetary Science Letters, 76, 135-150.

[96] Boyle, E. A., and Y. Rosenthal (1996), Chemical hydrography of the South Atlantic during the last glacial maximum: Cd vs. d13C, in The South Atlantic: Present and Past Circulation, edited by G. Wefer and e. al., pp. 423-443, Springer-Verlag, Berlin.

[97] Marchitto, T. M. (2006), Precise multi-elemental ratios in small foraminiferal samples determined by sector field ICP-MS, Geochemistry, Geophysics, Geosystems, 7, Q05P13, doi:10.1029/2005GC001018.

[98] Peltier, W. R. (2004), Global glacial isostasy and the surface of the ice-age Earth: The ICE-5G (VM2) Model and GRACE, Annu. Rev. Earth Planet. Sci., 32, 111–149.

[99] Kendall, R. A., J. X. Mitrovica, and G. A. Milne (2005), On post-glacial sea level—II. Numerical formulation and comparative results on spherically symmetric models, Geophys. J. Int., 161, 679–706.

[100] Petit, J. R., et al. (1999), Climate and atmospheric history of the past 420,000 years from the Vostok Ice Core, Antarctica, Nature, 399, 429–436.

[101] Zhang, T., T. E. Osterkamp, and K. Stamnes (1996), Some characteristics of the climate in Northern Alaska, U.S.A., Arctic Alpine Res., 28(4), 509–518.

[102] Kaufman, D.S., and Manley, W.F., (2004), Pleistocene Maximum and Late Wisconsin glacier extents across Alaska, U.S.A., in Ehlers, J., and Gibbard, P.L., eds., Quaternary Glaciations - Extent and Chronology, Part II, North America: Developments in Quaternary Science, 2b, Elsevier, 9-27.

[103] Meinshausen, M. et al. (2016), Historical greenhouse gas concentrations, Geosci. Model Dev. Disc., doi:10.5194/gmd-2016-169.

[104] Bhatnagar, G., Chapman, W. G., Dickens, G. R., Dugan, B., & Hirasaki, G. J. (2007). Generalization of gas hydrate distribution and saturation in marine sediments by scaling of thermodynamic and transport processes. American Journal of Science, 307(6), 861-900.

[105] Lichtner, P., et al. (2022), PFLOTRAN User Manual, http://documentation.pflotran.org

This page left blank.

APPENDIX A. PFLOTRAN HYDRATE MODE INPUT DECKS

A.1. hydrate_thermal.in (Section 2.3.5.1)

Note this input deck is displayed in two-column format for space efficiency.

```
#Description: Gas hydrate example: 1D Radial Thermal
Dissociation
SIMULATION
  SIMULATION_TYPE SUBSURFACE
  PROCESS_MODELS
    SUBSURFACE_FLOW flow
      MODE HYDRATE
      OPTIONS
        FIX_UPWIND_DIRECTION
      /
    /
  /
END

SUBSURFACE

HYDRATE
  HYDRATE_PHASE_BOUNDARY MORIDIS_SIMPLE
  EFFECTIVE_SAT_SCALING
  ADJUST_SOLUBILITY_WITHIN_GHSZ
  GT_3PHASE
  WITH_GIBBS_THOMSON
#  NO_PC
END

NUMERICAL_METHODS flow
  NEWTON_SOLVER
    USE_INFINITY_NORM_CONVERGENCE
    CENTRAL_DIFFERENCE_JACOBIAN
  END
  LINEAR_SOLVER FLOW
    SOLVER DIRECT
  END

END

#========================== discretization
===================================

GRID
  TYPE STRUCTURED CYLINDRICAL
  NXYZ 1500 1 1
DXYZ
    1000@0.02d0 \
    0.0200000000000000\
0.0202600212511425\
0.0205234230548373\
0.0207902493618595\
0.0210605446943913\
0.0213343541534502\
0.0216117234264150\
0.0218926987946491\
0.0221773271412226\
0.0224656559587354\
0.0227577333572418\
0.0230536080722776\
0.0233533294729928\
0.0236569475703883\
0.0239645130256615\
0.0242760771586591\
0.0245916919564404\
0.0249114100819516\
0.0252352848828133\
0.0255633704002216\
0.0258957213779658\
0.0262323932715626\
0.0265734422575092\
0.0269189252426573\
0.0272688998737076\
0.0276234245468296\
0.0279825584174049\
0.0283463614098980\
0.0287148942278549\
0.0290882183640325\
0.0294663961106586\
0.0298494905698262\
0.0302375656640228\
0.0306306861467960\
0.0310289176135581\
0.0314323265125318\
0.0318409801558372\
0.0322549467307234\
0.0326742953109462\
0.0330990958682938\
0.0335294192842617\
0.0339653373618804\
0.0344069228376961\
0.0348542493939071\
0.0353073916706589\
0.0357664252784980\
0.0362314268109885\
0.0367024738574920\
0.0371796450161145\
0.0376630199068207\
0.0381526791847194\
0.0386487045535219\
0.0391511787791740\
0.0396601857036672\
0.0401758102590278\
0.0406981384814885\
0.0412272575258448\
0.0417632556799970\
0.0423062223796818\
0.0428562482233957\
0.0434134249875117\
0.0439778456415934\
0.0445496043639073\
0.0451287965571376\
0.0457155188643046\
0.0463098691848909\
0.0469119466911759\
0.0475218518447843\
0.0481396864134487\
0.0487655534879903\
```

0.0493995574995205\
0.0500418042368660\
0.0506924008642208\
0.0513514559390274\
0.0520190794300901\
0.0526953827359247\
0.0533804787033461\
0.0540744816462975\
0.0547775073649251\
0.0554896731648998\
0.0562110978769910\
0.0569419018768944\
0.0576822071053175\
0.0584321370883268\
0.0591918169579586\
0.0599613734730988\
0.0607409350406337\
0.0615306317368752\
0.0623305953292656\
0.0631409592983642\
0.0639618588601191\
0.0647934309884295\
0.0656358144380007\
0.0664891497674970\
0.0673535793629942\
0.0682292474617387\
0.0691163001762143\
0.0700148855185222\
0.0709251534250784\
0.0718472557816315\
0.0727813464486062\
0.0737275812867762\
0.0746861181832711\
0.0756571170779206\
0.0766407399899423\
0.0776371510449758\
0.0786465165024684\
0.0796690047834169\
0.0807047864984699\
0.0817540344763959\
0.0828169237929209\
0.0838936317999411\
0.0849843381551166\
0.0860892248518470\
0.0872084762496402\
0.0883422791048732\
0.0894908226019546\
0.0906542983848912\
0.0918329005892653\
0.0930268258746285\
0.0942362734573153\
0.0954614451436841\
0.0967025453637906\
0.0979597812054984\
0.0992333624490332\
0.100523501601987\
0.101830413934776\
0.103154317516559\
0.104495433251630\
0.105853984916268\
0.107230199196085\
0.108624305723846\
0.110036537117786\
0.111467129020424\

0.112916320137881\
0.114384352279714\
0.115871470399259\
0.117377922634506\
0.118903960349502\
0.120449838176296\
0.122015814057421\
0.123602149288940\
0.125209108564041\
0.126836960017204\
0.128485975268943\
0.130156429471128\
0.131848601352894\
0.133562773267152\
0.135299231237701\
0.137058265006953\
0.138840168084280\
0.140645237794985\
0.142473775329919\
0.144326085795733\
0.146202478265788\
0.148103265831728\
0.150028765655721\
0.151979299023379\
0.153955191397370\
0.155956772471721\
0.157984376226833\
0.160038340985207\
0.162119009467894\
0.164226728851685\
0.166361850827037\
0.168524731656759\
0.170715732235451\
0.172935218149729\
0.175183559739224\
0.177461132158373\
0.179768315439022\
0.182105494553834\
0.184473059480524\
0.186871405266934\
0.189300932096948\
0.191762045357262\
0.194255155705034\
0.196780679136399\
0.199339037055884\
0.201930656346725\
0.204555969442090\
0.207215414397240\
0.209909434962619\
0.212638480657898\
0.215403006846983\
0.218203474813994\
0.221040351840232\
0.223914111282156\
0.226825232650358\
0.229774201689580\
0.232761510459759\
0.235787657418137\
0.238853147502428\
0.241958492215073\
0.245104209708589\
0.248290824872024\
0.251518869418546\
0.254788881974153\

0.258101408167559\
0.261457000721227\
0.264856219543602\
0.268299631822532\
0.271787812119910\
0.275321342467545\
0.278900812464277\
0.282526819374358\
0.286199968227109\
0.289920871917876\
0.293690151310297\
0.297508435339893\
0.301376361119019\
0.305294574043166\
0.309263727898652\
0.313284484971712\
0.317357516159005\
0.321483501079562\
0.325663128188181\
0.329897094890304\
0.334186107658386\
0.338530882149775\
0.342932143326123\
0.347390625574354\
0.351907072829205\
0.356482238697352\
0.361116886583160\
0.365811789816061\
0.370567731779594\
0.375385506042112\
0.380265916489203\
0.385209777457821\
0.390217913872166\
0.395291161381329\
0.400430366498726\
0.405636386743348\
0.410910090782844\
0.416252358578465\
0.421664081531894\
0.427146162633983\
0.432699516615423\
0.438325070099377\
0.444023761756095\
0.449796542459536\
0.455644375446030\
0.461568236475006\
0.467569113991799\
0.473648009292585\
0.479805936691456\
0.486043923689661\
0.492363011147060\
0.498764253455797\
0.505248718716233\
0.511817488915170\
0.518471660106386\
0.525212342593525\
0.532040661115358\
0.538957755033452\
0.545964778522289\
0.553062900761844\
0.560253306132673\
0.567537194413540\
0.574915780981605\
0.582390297015225\

0.589961989699382\
0.597632122433789\
0.605401975043697\
0.613272843993447\
0.621246042602791\
0.629322901266036\
0.637504767674027\
0.645793007039021\
0.654189002322489\
0.662694154465866\
0.671309882624318\
0.680037624403532\
0.688878836099601\
0.697834992942010\
0.706907589339800\
0.716098139130912\
0.725408175834793\
0.734839252908271\
0.744392944004762\
0.754070843236849\
0.763874565442275\
0.773805746453387\
0.783866043370089\
0.794057134836349\
0.804380721320287\
0.814838525397917\
0.825432292040570\
0.836163788906060\
0.847034806633629\
0.858047159142735\
0.869202683935712\
0.880503242404381\
0.891950720140631\
0.903547027251051\
0.915294098675645\
0.927193894510694\
0.939248400335811\
0.951459627545256\
0.963829613683550\
0.976360422785458\
0.989054145720393\
1.00191290054129\
1.01493883283801\
1.02813411609540\
1.04150095205586\
1.05504157108685\
1.06875823255291\
1.08265322519278\
1.09672886750118\
1.11098750811577\
1.12543152620896\
1.14006333188497\
1.15488536658189\
1.16990010347912\
1.18511004791004\
1.20051773778000\
1.21612574398981\
1.23193667086475\
1.24795315658908\
1.26417787364626\
1.28061352926486\
1.29726286587034\
1.31412866154255\
1.33121373047937\

1.34852092346624\
1.36605312835181\
1.38381327052987\
1.40180431342741\
1.42002925899912\
1.43849114822832\
1.45719306163431\
1.47613811978642\
1.49532948382472\
1.51477035598744\
1.53446398014531\
1.55441364234283\
1.57462267134658\
1.59509443920062\
1.61583236178919\
1.63683989940663\
1.65812055733482\
1.67967788642798\
1.70151548370525\
1.72363699295082\
1.74604610532194\
1.76874655996486\
1.79174214463866\
1.81503669634734\
1.83863410198003\
1.86253829895953\
1.88675327589934\
1.91128307326917\
1.93613178406912\
1.96130355451263\
1.98680258471836\
2.01263312941094\
2.03879949863095\
2.06530605845409\
2.09215723171966\
2.11935749876859\
2.14691139819099\
2.17482352758347\
2.20309854431629\
2.23174116631045\
2.26075617282496\
2.29014840525427\
2.31992276793607\
2.35008422896971\
2.38063782104506\
2.41158864228232\
2.44294185708268\
2.47470269699003\
2.50687646156388\
2.53946851926366\
2.57248430834445\
2.60592933776445\
2.63980918810418\
2.67412951249759\
2.70889603757542\
2.74411456442069\
2.77979096953664\
2.81593120582731\
2.85254130359083\
2.88962737152559\
2.92719559774958\
2.96525225083286\
3.00380368084359\
3.04285632040756\

3.08241668578151\
3.12249137794049\
3.16308708367917\
3.20421057672771\
3.24586871888195\
3.28806846114835\
3.33081684490384\
3.37412100307076\
3.41798816130699\
3.46242563921165\
3.50744085154644\
3.55304130947280\
3.59923462180531\
3.64602849628116\
3.69343074084637\
3.74144926495852\
3.79009208090655\
3.83936730514768\
3.88928315966168\
3.93984797332281\
3.99107018328954\
4.04295833641236\
4.09552109065991\
4.14876721656360\
4.20270559868109\
4.25734523707872\
4.31269524883325\
4.36876486955314\
4.42556345491957\
4.48310048224750\
4.54138555206708\
4.60042838972552\
4.66023884700991\
4.72082690379103\
4.78220266968857\
4.84437638575804\
4.90735842619953\
4.97115930008878\
5.03578965313067\
5.10126026943554\
5.16758207331864\
5.23476613112293\
5.30282365306558\
5.37176599510848\
5.44160466085311\
5.51235130346001\
5.58401772759313\
5.65661589138966\
5.73015790845524\
5.80465604988527\
5.88012274631242\
5.95657058998079\
6.03401233684706\
6.11246090870887\
6.19192939536097\
6.27243105677935\
6.35397932533379\
6.43658780802913\
6.52027028877573\
6.60504073068947\
6.69091327842151\
6.77790226051857\
6.86602219181364\
6.95528777584801\

```
7.04571390732461\
7.13731567459334\
7.23010836216867\
7.32410745328001\
7.41932863245520\
7.51578778813762\
7.61350101533726\
7.71248461831639\
7.81275511330999\
7.91432923128162\
8.01722392071518\
8.12145635044288\
8.22704391250994\
8.33400422507668\
8.44235513535825\
8.55211472260250\
8.66330130110676\
8.77593342327366\
8.89002988270680\
9.00560971734657\
9.12269221264684\
9.24129690479285\
9.36144358396102\
9.48315229762109\
9.60644335388120\
9.73133732487647\
9.85785505020167\
9.98601764038841\
10.1158464804276\
10.2473632333379\
10.3805898437801\
10.5155485417190\
10.6522618461323\
10.7907525687688\
10.9310438179538\
11.0731590024457\
11.2171218353415\
11.3629563380336\
11.5106868442183\
11.6603380039554\
11.8119347877820\
11.9655024908787\
12.1210667372900\
12.2786534842006\
12.4382890262659\
12.6000000000000

   1@1.d0
   1@1.d0
  /
END

#========================== fluid properties
================================
FLUID_PROPERTY
  PHASE LIQUID
  DIFFUSION_COEFFICIENT 1.d-9
END

FLUID_PROPERTY
  PHASE GAS
  DIFFUSION_COEFFICIENT 2.d-5
END
```

```
#========================== more fluid properties
============================
EOS WATER
  DENSITY IF97
  ENTHALPY IF97
  STEAM_DENSITY IF97
  STEAM_ENTHALPY IF97
END

EOS GAS
  DENSITY IDEAL # PR_METHANE
  ENTHALPY IDEAL_METHANE
  VISCOSITY DEFAULT #CONSTANT 1.1d-5 Pa-s #DEFAULT
END


#========================== material properties
============================
MATERIAL_PROPERTY soil1
  ID 1000
  CHARACTERISTIC_CURVES default
  POROSITY 0.3
  TORTUOSITY 1.0
  ROCK_DENSITY 2600.d0
  THERMAL_CONDUCTIVITY_DRY 2.d0 #W/m-C
  THERMAL_CONDUCTIVITY_WET 2.18d0 #W/m-C
  HEAT_CAPACITY 1000 J/kg-C
  PERMEABILITY
    PERM_ISO 1.d-12
  /
  #SOIL_REFERENCE_PRESSURE INITIAL_PRESSURE
  #POROSITY_COMPRESSIBILITY 1.d-9
END


#========================== characteristic curves
============================

CHARACTERISTIC_CURVES default
  SATURATION_FUNCTION IGHCC2_COMP #VAN_GENUCHTEN
    ALPHA 8.d-5
    M 0.45
    LIQUID_RESIDUAL_SATURATION 0.12d0
    MAX_CAPILLARY_PRESSURE 1.d9 #0.d0
    #CALCULATE_INTERFACIAL_TENSION
  /
  PERMEABILITY_FUNCTION IGHCC2_COMP_LIQ
#BURDINE_BC_LIQ
    PHASE LIQUID
    LAMBDA 3
    LIQUID_RESIDUAL_SATURATION 0.12
  /
  PERMEABILITY_FUNCTION IGHCC2_COMP_GAS
#BURDINE_BC_GAS
    PHASE GAS
    LAMBDA 3
    LIQUID_RESIDUAL_SATURATION 0.12
    GAS_RESIDUAL_SATURATION 0.02
  /
END

#========================== output options
===================================
OUTPUT
```

```
  SNAPSHOT_FILE
   TIMES d 2 5 10 20 30 60
   FORMAT TECPLOT POINT
  /
  UNFILTER_NON_STATE_VARIABLES

  VARIABLES
   TEMPERATURE
   LIQUID_PRESSURE
   GAS_PRESSURE
   LIQUID_SATURATION
   GAS_SATURATION
   HYDRATE_SATURATION
   ICE_SATURATION
   LIQUID_MASS_FRACTIONS
   LIQUID_MOLE_FRACTIONS
   GAS_MASS_FRACTIONS
   LIQUID_DENSITY
   LIQUID_DENSITY MOLAR
   GAS_DENSITY
   GAS_DENSITY MOLAR
   PERMEABILITY
   LIQUID_RELATIVE_PERMEABILITY
   GAS_RELATIVE_PERMEABILITY
   POROSITY
   #EFFECTIVE_POROSITY
  /
END

#=========================== times
=========================================
TIME
  FINAL_TIME 60 d
  INITIAL_TIMESTEP_SIZE 1.d-6 h
  #MAXIMUM_TIMESTEP_SIZE 8.d-3 d #8.d-3 d #1.d-2 d #5.d-3
d
  MAXIMUM_TIMESTEP_SIZE 1.d-1 d
END

#=========================== regions
=======================================
REGION all
  COORDINATES
    0.d0 0.d0 0.d0
    1.d3 1.d0 1.d0
  /
END

REGION edge
  FACE EAST
  COORDINATES
    1.0d3 0.d0 0.d0
    1.0d3 1.d0 1.d0
  /
END

REGION center
  COORDINATES
    0.d0 0.d0 0.d0
    0.d0 1.d0 1.d0
  /
END
```

```
#=========================== flow conditions
=================================

FLOW_CONDITION initial
  TYPE
    GAS_PRESSURE DIRICHLET
    HYDRATE_SATURATION DIRICHLET
    TEMPERATURE DIRICHLET
  /
  GAS_PRESSURE 4.6d6
  HYDRATE_SATURATION 5.d-1
  TEMPERATURE 3.d0
END

FLOW_CONDITION edge
  TYPE
    GAS_PRESSURE DIRICHLET
    HYDRATE_SATURATION DIRICHLET
    TEMPERATURE DIRICHLET
  /
  GAS_PRESSURE 4.6d6
  HYDRATE_SATURATION 5.d-1
  TEMPERATURE 3.d0
END

FLOW_CONDITION center
  SYNC_TIMESTEP_WITH_UPDATE
  TYPE
    RATE MASS_RATE
  /
  RATE 0.d0 0.d0 150.d0 g/s g/s W
END

#=========================== condition couplers
===============================
# initial condition
INITIAL_CONDITION all
  FLOW_CONDITION initial
  REGION all
END

SOURCE_SINK center
  FLOW_CONDITION center
  REGION center
END

BOUNDARY_CONDITION edge
  FLOW_CONDITION edge
  REGION edge
END

#=========================== stratigraphy couplers
============================
STRATA
  REGION all
  MATERIAL soil1
END

#=========================== convergence criteria
============================

END_SUBSURFACE
```

A.2. hydrate_ice.in (Section 2.3.5.2)

```
#Description: Gas hydrate example
SIMULATION
  SIMULATION_TYPE SUBSURFACE
  PROCESS_MODELS
    SUBSURFACE_FLOW flow
      MODE HYDRATE
    /
  /
END

SUBSURFACE

NUMERICAL_METHODS flow
    NEWTON_SOLVER
      USE_INFINITY_NORM_CONVERGENCE
      PRES_ABS_UPDATE_INF_TOL 1.d-1
      PRES_REL_UPDATE_INF_TOL 1.d-4
      SAT_ABS_UPDATE_INF_TOL 1.d-6
      SAT_REL_UPDATE_INF_TOL 1.d-4
      RESIDUAL_ABS_INF_TOL 1.d-6
      RESIDUAL_SCALED_INF_TOL 1.d-7
      XMOL_ABS_UPDATE_INF_TOL 1.d-10
      XMOL_REL_UPDATE_INF_TOL 1.d-5
      CENTRAL_DIFFERENCE_JACOBIAN
    /
END

HYDRATE
   HYDRATE_PHASE_BOUNDARY MORIDIS
   WITH_GIBBS_THOMSON
   GT_3PHASE
   SCALE_PERM_BY_HYD_SAT
   EFFECTIVE_SAT_SCALING
   ADJUST_SOLUBILITY_WITHIN_GHSZ
   BC_REFERENCE_PRESSURE 1.d20
END

#========================== discretization ===================================
GRID
  TYPE STRUCTURED
  NXYZ 1 1 1000
  DXYZ
    1@1.d1
    1@1.d1
    1000@1.d0
  /
END

#========================== fluid properties =================================
FLUID_PROPERTY
  PHASE LIQUID
  DIFFUSION_COEFFICIENT 1.d-9
```

```
END

FLUID_PROPERTY
  PHASE GAS
  DIFFUSION_COEFFICIENT 1.d-5
END

#========================== more fluid properties ============================
EOS WATER
  DENSITY IF97
  ENTHALPY IF97
  STEAM_DENSITY IF97
  STEAM_ENTHALPY IF97
END

EOS GAS
  DENSITY DEFAULT
  VISCOSITY DEFAULT
  HENRYS_CONSTANT DEFAULT #CONSTANT 1.d11
END


#========================== material properties ==============================

MATERIAL_PROPERTY marine_sediments
  ID 10
  CHARACTERISTIC_CURVES marine_sediments
  POROSITY 0.4
  TORTUOSITY_FUNCTION_OF_POROSITY 1.4 #Van Loon and Mibus 2015
  ROCK_DENSITY 2700.d0
  THERMAL_CONDUCTIVITY_DRY 4.0 W/m-C
  THERMAL_CONDUCTIVITY_WET 1.0 W/m-C
  HEAT_CAPACITY 830 J/kg-C
  PERMEABILITY
    PERM_ISO 1.d-15
  /
END

#========================== characteristic curves ============================

CHARACTERISTIC_CURVES marine_sediments
  SATURATION_FUNCTION VAN_GENUCHTEN
    LOOP_INVARIANT
    UNSATURATED_EXTENSION LCPC
    ALPHA 1.d-4
    M 0.2
    LIQUID_RESIDUAL_SATURATION 0.1d0
    MAX_CAPILLARY_PRESSURE 1.d8
  /
  PERMEABILITY_FUNCTION MUALEM_VG_LIQ
    PHASE LIQUID
    M 0.2
    LIQUID_RESIDUAL_SATURATION 0.1d0
  /
  PERMEABILITY_FUNCTION MUALEM_VG_GAS
    PHASE GAS
```

```
    M 0.2
    LIQUID_RESIDUAL_SATURATION 0.1d0
    GAS_RESIDUAL_SATURATION 0.1d0
  /
  TEST
END

#========================== output options ===================================
OUTPUT
  SNAPSHOT_FILE
    TIMES y 1 10 100 1000 10000
    FORMAT TECPLOT POINT
  /
  UNFILTER_NON_STATE_VARIABLES

  VARIABLES
   TEMPERATURE
   LIQUID_PRESSURE
   GAS_PRESSURE
   LIQUID_SATURATION
   GAS_SATURATION
   HYDRATE_SATURATION
   ICE_SATURATION
   LIQUID_MOLE_FRACTIONS
  /
END

#========================== times ============================================
TIME
  FINAL_TIME 10000 y
  INITIAL_TIMESTEP_SIZE 1.d0 h
  MAXIMUM_TIMESTEP_SIZE 1.d2 y

END

#========================== regions ==========================================
REGION all
  COORDINATES
    0.d0 0.d0 0.d0
    1.d1 1.d1 1000.d0
  /
END

REGION top
  FACE TOP
  COORDINATES
    0.0d0 0.d0 1000.d0
    1.0d1 1.d1 1000.d0
  /
END

REGION bottom
  FACE BOTTOM
  COORDINATES
    0.d0 0.d0 0.d0
    1.d1 1.d1 0.d0
```

```
  /
END

REGION methanogen
  COORDINATES
    0.d0 0.d0 700.d0
    1.d1 1.d1 800.d0
  /
END

#========================== flow conditions ===================================

FLOW_CONDITION initial
  TYPE
    LIQUID_PRESSURE HYDROSTATIC
    MOLE_FRACTION DIRICHLET
    TEMPERATURE DIRICHLET
  /
  DATUM 0.d0 0.d0 0.d0
  LIQUID_PRESSURE 20.d6  #Pa
  MOLE_FRACTION 1.d-4
  TEMPERATURE 2.d0
END

FLOW_CONDITION bcB
  TYPE
    LIQUID_PRESSURE DIRICHLET
    MOLE_FRACTION DIRICHLET
    TEMPERATURE DIRICHLET
  /
  LIQUID_PRESSURE 20.d6 #Pa
  MOLE_FRACTION 1.d-4
  TEMPERATURE 2.d0
END

FLOW_CONDITION bcT
  TYPE
    GAS_PRESSURE DIRICHLET_SEEPAGE
    RELATIVE_HUMIDITY DIRICHLET
    TEMPERATURE DIRICHLET
  /
  GAS_PRESSURE 10.d6  #Pa
  RELATIVE_HUMIDITY 10
  TEMPERATURE -10.d0
END

#========================== condition couplers ================================
# initial condition
INITIAL_CONDITION all
  FLOW_CONDITION initial
  REGION all
END

BOUNDARY_CONDITION top
  FLOW_CONDITION bcT
  REGION top
```

```
END


BOUNDARY_CONDITION bottom
  FLOW_CONDITION bcB
  REGION bottom
END
#========================== stratigraphy couplers ============================
STRATA
  REGION all
  MATERIAL marine_sediments
END

END_SUBSURFACE
```

A.3. hydrate_ice_with_gas.in (Section 2.3.5.3)

```
#Description: Gas hydrate example
SIMULATION
  SIMULATION_TYPE SUBSURFACE
  PROCESS_MODELS
    SUBSURFACE_FLOW flow
      MODE HYDRATE
    /
  /
END

SUBSURFACE

NUMERICAL_METHODS flow
    NEWTON_SOLVER
      USE_INFINITY_NORM_CONVERGENCE
      PRES_ABS_UPDATE_INF_TOL 1.d-1
      PRES_REL_UPDATE_INF_TOL 1.d-4
      SAT_ABS_UPDATE_INF_TOL 1.d-6
      SAT_REL_UPDATE_INF_TOL 1.d-4
      RESIDUAL_ABS_INF_TOL 1.d-6
      RESIDUAL_SCALED_INF_TOL 1.d-7
      XMOL_ABS_UPDATE_INF_TOL 1.d-10
      XMOL_REL_UPDATE_INF_TOL 1.d-5
      CENTRAL_DIFFERENCE_JACOBIAN
    /
END

HYDRATE
  HYDRATE_PHASE_BOUNDARY MORIDIS
  WITH_GIBBS_THOMSON
  GT_3PHASE
  SCALE_PERM_BY_HYD_SAT
  EFFECTIVE_SAT_SCALING
  ADJUST_SOLUBILITY_WITHIN_GHSZ
END

#========================== discretization ===================================
GRID
  TYPE STRUCTURED
  NXYZ 1 1 1000
  DXYZ
    1@1.d1
    1@1.d1
    1000@1.d0
  /
END

#========================== fluid properties =================================
FLUID_PROPERTY
  PHASE LIQUID
  DIFFUSION_COEFFICIENT 1.d-9
END

FLUID_PROPERTY
```

```
  PHASE GAS
  DIFFUSION_COEFFICIENT 1.d-5
END

#========================== more fluid properties ===========================
EOS WATER
  DENSITY IF97
  ENTHALPY IF97
  STEAM_DENSITY IF97
  STEAM_ENTHALPY IF97
END

EOS GAS
  DENSITY DEFAULT
  VISCOSITY DEFAULT
  HENRYS_CONSTANT DEFAULT #CONSTANT 1.d11
END


#========================== material properties ==============================

MATERIAL_PROPERTY marine_sediments
  ID 10
  CHARACTERISTIC_CURVES marine_sediments
  POROSITY 0.4
  TORTUOSITY_FUNCTION_OF_POROSITY 1.4 #Van Loon and Mibus 2015
  ROCK_DENSITY 2700.d0
  THERMAL_CONDUCTIVITY_DRY 4.0 W/m-C
  THERMAL_CONDUCTIVITY_WET 1.0 W/m-C
  HEAT_CAPACITY 830 J/kg-C
  PERMEABILITY
    PERM_ISO 1.d-15
  /
END

#========================== characteristic curves ===========================

CHARACTERISTIC_CURVES marine_sediments
  SATURATION_FUNCTION VAN_GENUCHTEN
    LOOP_INVARIANT
    UNSATURATED_EXTENSION LCPC
    ALPHA 1.d-1
    M .05
    LIQUID_RESIDUAL_SATURATION 0.1d0
    MAX_CAPILLARY_PRESSURE 1.d8
  /
  PERMEABILITY_FUNCTION MUALEM_VG_LIQ
    PHASE LIQUID
    M 0.05
    LIQUID_RESIDUAL_SATURATION 0.1d0
  /
  PERMEABILITY_FUNCTION MUALEM_VG_GAS
    PHASE GAS
    M 0.05
    LIQUID_RESIDUAL_SATURATION 0.1d0
    GAS_RESIDUAL_SATURATION 0.1d0
```

```
 /
 TEST
END

#========================== output options ===================================
OUTPUT
 SNAPSHOT_FILE
  TIMES y 1 10 100 1000 10000
  FORMAT TECPLOT POINT
 /
 UNFILTER_NON_STATE_VARIABLES

 VARIABLES
  TEMPERATURE
  LIQUID_PRESSURE
  GAS_PRESSURE
  LIQUID_SATURATION
  GAS_SATURATION
  HYDRATE_SATURATION
  ICE_SATURATION
  LIQUID_MOLE_FRACTIONS
 /
END

#========================== times ===========================================
TIME
 FINAL_TIME 10000 y
 INITIAL_TIMESTEP_SIZE 1.d0 h
 MAXIMUM_TIMESTEP_SIZE 1.d2 y
END

#========================== regions =========================================
REGION all
 COORDINATES
  0.d0 0.d0 0.d0
  1.d1 1.d1 1000.d0
 /
END

REGION top
 FACE TOP
 COORDINATES
  0.0d0 0.d0 1000.d0
  1.0d1 1.d1 1000.d0
 /
END

REGION bottom
 FACE BOTTOM
 COORDINATES
  0.d0 0.d0 0.d0
  1.d1 1.d1 0.d0
 /
END

REGION methanogen
```

```
  COORDINATES
    0.d0 0.d0 700.d0
    1.d1 1.d1 800.d0
  /
END

#========================== flow conditions =================================

FLOW_CONDITION initial
  TYPE
    LIQUID_PRESSURE HYDROSTATIC
    MOLE_FRACTION DIRICHLET
    TEMPERATURE DIRICHLET
  /
  DATUM 0.d0 0.d0 0.d0
  LIQUID_PRESSURE 20.d6
  MOLE_FRACTION 5.d-4
  TEMPERATURE 2.d0
END

FLOW_CONDITION bcB
  TYPE
    LIQUID_PRESSURE DIRICHLET
    MOLE_FRACTION DIRICHLET
    TEMPERATURE DIRICHLET
  /
  LIQUID_PRESSURE 20.d6 #Pa
  MOLE_FRACTION 5.d-4
  TEMPERATURE 2.d0
END

FLOW_CONDITION bcT
  TYPE
    GAS_PRESSURE DIRICHLET
    RELATIVE_HUMIDITY DIRICHLET
    TEMPERATURE DIRICHLET
  /
  GAS_PRESSURE 10.d6 #Pa
  RELATIVE_HUMIDITY 10
  TEMPERATURE -10.d0
END


FLOW_CONDITION methanogen
  SYNC_TIMESTEP_WITH_UPDATE
  TYPE
    RATE MASS_RATE
  /
 #RATE 0.d0 1.d-4 0.d0 g/s g/s MW
 INTERPOLATION LINEAR
 RATE FILE ./methanogen.gen
END

#========================== condition couplers ==============================
# initial condition
INITIAL_CONDITION all
```

```
  FLOW_CONDITION initial
  REGION all
END

BOUNDARY_CONDITION top
  FLOW_CONDITION bcT
  REGION top
END

SOURCE_SINK methanogen
  FLOW_CONDITION methanogen
  REGION methanogen
END

BOUNDARY_CONDITION bottom
  FLOW_CONDITION bcB
  REGION bottom
END

#========================== stratigraphy couplers ============================
STRATA
  REGION all
  MATERIAL marine_sediments
END


END_SUBSURFACE
```

methanogen.gen

```
TIME_UNITS y
DATA_UNITS g/s g/s MW
0.000E+00  0.d0  1.d-4  0.d0
1.E+03     0.d0  1.d-4  0.d0
1.0E+03    0.d0  0.d0   0.d0
1.0E+05    0.d0  0.d0   0.d0
```

A.4. ice_run.in

```
WALLCLOCK_STOP 0.5 min
/
END

SIMULATION
  SIMULATION_TYPE SUBSURFACE
  PROCESS_MODELS
    SUBSURFACE_FLOW flow
      MODE HYDRATE
      OPTIONS
      /
    /
  /
CHECKPOINT
```

```
TIMES y 135000 270000 405000 510000 645000
FORMAT HDF5
TIME_UNITS y
/
END

SUBSURFACE
  NUMERICAL_METHODS flow
    NEWTON_SOLVER
      USE_INFINITY_NORM_CONVERGENCE
      SAT_ABS_UPDATE_INF_TOL 1.d-7
      SAT_REL_UPDATE_INF_TOL 1.d-8
    /
    TIMESTEPPER
      PRESSURE_CHANGE_GOVERNOR 1.0d5
      TEMPERATURE_CHANGE_GOVERNOR 1.0d0
    /
END

GRID
  TYPE STRUCTURED CARTESIAN
  NXYZ 1 1 1000
  DXYZ
    1@1.d0
    1@1.d0
    1000@1.d0
  /
 GRAVITY 0.d0 0.d0 -9.8d0
END

DATASET porosity
  FILENAME ../phi_k_dataset.h5
  HDF5_DATASET_NAME porosity
END


REGION all
  COORDINATES
    0.d0 0.d0 0.d0
    1.d0 1.d0 1000.d0
  /
END

REGION top
  FACE TOP
  COORDINATES
    0.0d0 0.d0 1000.d0
    1.0d0 1.d0 1000.d0
  /
END

REGION bottom
  FACE BOTTOM
  COORDINATES
    0.d0 0.d0 0.d0
    1.d0 1.d0 0.d0
  /

END

HYDRATE
   HYDRATE_PHASE_BOUNDARY MORIDIS_SIMPLE
   WITH_GIBBS_THOMSON
   GT_3PHASE
   BC_REFERENCE_PRESSURE 1.d20
   SCALE_PERM_BY_HYD_SAT
   EFFECTIVE_SAT_SCALING
   ADJUST_SOLUBILITY_WITHIN_GHSZ
```

```
  #WITH_SEDIMENTATION
  SALINITY 0.035
  #METHANOGENESIS
   #NAME ss_methanogenesis
   #ALPHA 0.0
   #K_ALPHA 2241
   #LAMBDA 1e-14
   #V_SED 0.0
   #SMT_DEPTH 15
  #/
  #PERM_SCALING_FUNCTION DAI_AND_SEOL
END

FLUID_PROPERTY
 PHASE LIQUID
 DIFFUSION_COEFFICIENT 1.d-9
END

FLUID_PROPERTY
 PHASE GAS
 DIFFUSION_COEFFICIENT 2.d-5
END

EOS WATER
 DENSITY IF97
 ENTHALPY IF97
 STEAM_DENSITY IF97
 STEAM_ENTHALPY IF97
END

EOS GAS
 DENSITY PR_METHANE
 ENTHALPY IDEAL_METHANE
 VISCOSITY DEFAULT #CONSTANT 1.1d-5 Pa-s #DEFAULT
END

MATERIAL_PROPERTY marine_sediments
 ID 1
 CHARACTERISTIC_CURVES marine_sediments
 POROSITY DATASET porosity
 TORTUOSITY_FUNCTION_OF_POROSITY 1.4 #Van Loon and Mibus 2015
 ROCK_DENSITY 2700.d0
 THERMAL_CONDUCTIVITY_DRY 1.0 W/m-C
 THERMAL_CONDUCTIVITY_WET 1.0 W/m-C
 HEAT_CAPACITY 830 J/kg-C
 PERMEABILITY
  PERM_ISO 1.d-15
 /
END

CHARACTERISTIC_CURVES marine_sediments
 SATURATION_FUNCTION VAN_GENUCHTEN
  LOOP_INVARIANT
  UNSATURATED_EXTENSION ECPC
  ALPHA 5.8d-4
  M 0.189
  LIQUID_RESIDUAL_SATURATION 0.1d0
  MAX_CAPILLARY_PRESSURE 1.d8 #roughly read from Jacinto et al. 2009
 /
 PERMEABILITY_FUNCTION MUALEM_VG_LIQ
  PHASE LIQUID
  M 0.189
  LIQUID_RESIDUAL_SATURATION 0.1d0
 /
 PERMEABILITY_FUNCTION MUALEM_VG_GAS
  PHASE GAS
  M 0.189
  LIQUID_RESIDUAL_SATURATION 0.1d0
```

```
    GAS_RESIDUAL_SATURATION 0.15d0
  /
END

STRATA
  REGION all
  MATERIAL marine_sediments
END

TIME
  FINAL_TIME 645000 y
  INITIAL_TIMESTEP_SIZE 1.d-3 y
  MAXIMUM_TIMESTEP_SIZE 250.0 y
END

OUTPUT
  SNAPSHOT_FILE
    PERIODIC TIME 15000 y
    FORMAT TECPLOT POINT
    #NO_PRINT_INITIAL
  /
  #UNFILTER_NON_STATE_VARIABLES

  VARIABLES
   GAS_SATURATION
   HYDRATE_SATURATION
   GAS_DENSITY
   POROSITY
   ICE_SATURATION
   TEMPERATURE
   THERMODYNAMIC_STATE
   LIQUID_SATURATION
   GAS_PRESSURE
   LIQUID_PRESSURE
   PERMEABILITY
  /
END

EXTERNAL_FILE flowConditions.txt

# initial condition
INITIAL_CONDITION all
  FLOW_CONDITION initial
  REGION all
END

BOUNDARY_CONDITION top
  FLOW_CONDITION top
  REGION top
END

BOUNDARY_CONDITION bottom
  FLOW_CONDITION bottom
  REGION bottom
END

END_SUBSURFACE
```

A.5. methane_run.in

```
SIMULATION
```

```
  SIMULATION_TYPE SUBSURFACE
  PROCESS_MODELS
    SUBSURFACE_FLOW flow
      MODE HYDRATE
      OPTIONS
        RESTRICT_STATE_CHANGE
      /
    /
  /
  RESTART
    FILENAME ../ice_run1/ice_run1-405000.0000y.h5
  /
END

SUBSURFACE
NUMERICAL_METHODS flow
  NEWTON_SOLVER
    USE_INFINITY_NORM_CONVERGENCE

    SAT_ABS_UPDATE_INF_TOL 1.d-2
    SAT_REL_UPDATE_INF_TOL 1.d-2

    GAS_PRES_ABS_UPDATE_INF_TOL 1.d+4
    GAS_PRES_REL_UPDATE_INF_TOL 1.d-2

    LIQUID_PRES_ABS_UPDATE_INF_TOL 1.d+4
    LIQUID_PRES_REL_UPDATE_INF_TOL 1.d-2

    GAS_RESIDUAL_ABS_INF_TOL 1.d-8
    GAS_RESIDUAL_SCALED_INF_TOL 1.d-5

    LIQUID_RESIDUAL_ABS_INF_TOL 1.d-7
    LIQUID_RESIDUAL_SCALED_INF_TOL 1.d-4
  /
  TIMESTEPPER
    PRESSURE_CHANGE_GOVERNOR 1.0d6
    SATURATION_CHANGE_GOVERNOR 0.05
    #TEMPERATURE_CHANGE_GOVERNOR 0.5d0
  /
END

WALLCLOCK_STOP 120 min

GRID
  TYPE STRUCTURED CARTESIAN
  NXYZ 1 1 1000
  DXYZ
    1@1.d0
    1@1.d0
    1000@1.d0
  /
 GRAVITY 0.d0 0.d0 -9.8d0
END

DATASET porosity
  FILENAME ../phi_k_dataset.h5
  HDF5_DATASET_NAME porosity
END


REGION all
  COORDINATES
    0.d0 0.d0 0.d0
    1.d0 1.d0 1000.d0
  /
END

REGION top
```

```
  FACE TOP
  COORDINATES
    0.0d0 0.d0 1000.d0
    1.0d0 1.d0 1000.d0
  /
END

REGION bottom
  FACE BOTTOM
  COORDINATES
    0.d0 0.d0 0.d0
    1.d0 1.d0 0.d0
  /

END

# positive flux is up
INTEGRAL_FLUX sediment_surface
  FLUXES_OPTION POSITIVE_FLUXES_ONLY
  PLANE
    0.d0 0.d0 1000.d0
    1.d0 1.d0 1000.d0
    0.d0 1.d0 1000.d0
  /
END

# positive flux is up
#INTEGRAL_FLUX ice_surface
#  CELL_IDS
#    327 328
#  /
#END

# This will be dynamic, find ice > 0 and make CELL_IDS
INTEGRAL_FLUX 5m_depth
  CELL_IDS
    322 323
  /
END

# positive flux is up
INTEGRAL_FLUX
  NAME 300m
  CELL_IDS
    700 701
  /
END

# positive flux is up
INTEGRAL_FLUX
  NAME 325m
  CELL_IDS
    675 676
  /
END

# positive flux is up
INTEGRAL_FLUX
  NAME 350m
  CELL_IDS
    650 651
  /
END

# positive flux is up
INTEGRAL_FLUX
  NAME 375m
  CELL_IDS
```

```
    625 626
  /
END

# positive flux is up
INTEGRAL_FLUX
  NAME 400m
  CELL_IDS
    600 601
  /
END

# positive flux is up
INTEGRAL_FLUX
  NAME 425m
  CELL_IDS
    575 576
  /
END

# positive flux is up
INTEGRAL_FLUX
  NAME 450m
  CELL_IDS
    550 551
  /
END

# positive flux is up
INTEGRAL_FLUX
  NAME 475m
  CELL_IDS
    525 526
  /
END

# positive flux is up
INTEGRAL_FLUX
  NAME 500m
  CELL_IDS
    500 501
  /
END

# positive flux is up
INTEGRAL_FLUX
  NAME 525m
  CELL_IDS
    475 476
  /
END

# positive flux is up
INTEGRAL_FLUX
  NAME 550m
  CELL_IDS
    450 451
  /
END

# positive flux is up
INTEGRAL_FLUX
  NAME 575m
  CELL_IDS
    425 426
  /
END
```

```
# positive flux is up
INTEGRAL_FLUX
  NAME 600m
  CELL_IDS
    400 401
  /
END

# positive flux is up
INTEGRAL_FLUX
  NAME 625m
  CELL_IDS
    375 376
  /
END

# positive flux is up
INTEGRAL_FLUX
  NAME 650m
  CELL_IDS
    350 351
  /
END

# positive flux is up
INTEGRAL_FLUX
  NAME 675m
  CELL_IDS
    325 326
  /
END

# positive flux is up
INTEGRAL_FLUX
  NAME 700m
  CELL_IDS
    300 301
  /
END

# positive flux is up
INTEGRAL_FLUX
  NAME 725m
  CELL_IDS
    275 276
  /
END

# positive flux is up
INTEGRAL_FLUX
  NAME 750m
  CELL_IDS
    250 251
  /
END

# positive flux is up
INTEGRAL_FLUX
  NAME 775m
  CELL_IDS
    225 226
  /
END

# positive flux is up
INTEGRAL_FLUX
  NAME 800m
  CELL_IDS
```

```
    200 201
  /
END

# positive flux is up
INTEGRAL_FLUX
  NAME 825m
  CELL_IDS
    175 176
  /
END

# positive flux is up
INTEGRAL_FLUX
  NAME 850m
  CELL_IDS
    150 151
  /
END

# positive flux is up
INTEGRAL_FLUX
  NAME 875m
  CELL_IDS
    125 126
  /
END

# positive flux is up
INTEGRAL_FLUX
  NAME 900m
  CELL_IDS
    100 101
  /
END

HYDRATE
   HYDRATE_PHASE_BOUNDARY MORIDIS
   WITH_GIBBS_THOMSON
   GT_3PHASE
   BC_REFERENCE_PRESSURE 1.d20
   SCALE_PERM_BY_HYD_SAT
   EFFECTIVE_SAT_SCALING
   ADJUST_SOLUBILITY_WITHIN_GHSZ
   WITH_SEDIMENTATION
   SALINITY 0.035
   METHANOGENESIS
    NAME ss_methanogenesis
    ALPHA 0.1597591273811524
    K_ALPHA 2241
    LAMBDA 1e-14
    V_SED 3.303563591360281e-13
    SMT_DEPTH 5.0
   /
   #PERM_SCALING_FUNCTION DAI_AND_SEOL
END

FLUID_PROPERTY
  PHASE LIQUID
  DIFFUSION_COEFFICIENT 1.d-9
END

FLUID_PROPERTY
  PHASE GAS
  DIFFUSION_COEFFICIENT 2.d-5
END

EOS WATER
```

```
  DENSITY IF97
  ENTHALPY IF97
  STEAM_DENSITY IF97
  STEAM_ENTHALPY IF97
END

EOS GAS
  DENSITY PR_METHANE
  ENTHALPY IDEAL_METHANE
  VISCOSITY DEFAULT #CONSTANT 1.1d-5 Pa-s #DEFAULT
END

MATERIAL_PROPERTY marine_sediments
  ID 1
  CHARACTERISTIC_CURVES marine_sediments
  POROSITY DATASET porosity
  TORTUOSITY_FUNCTION_OF_POROSITY 1.4 #Van Loon and Mibus 2015
  ROCK_DENSITY 2700.d0
  THERMAL_CONDUCTIVITY_DRY 1.0 W/m-C
  THERMAL_CONDUCTIVITY_WET 1.0 W/m-C
  HEAT_CAPACITY 830 J/kg-C
  PERMEABILITY
    PERM_ISO 5.d-14
  /
END

CHARACTERISTIC_CURVES marine_sediments
  PERMEABILITY_FUNCTION BURDINE_LINEAR_LIQ
    PHASE LIQUID
    LIQUID_RESIDUAL_SATURATION 0.2d0
  /
  PERMEABILITY_FUNCTION BURDINE_LINEAR_GAS
    PHASE GAS
    LIQUID_RESIDUAL_SATURATION 0.2d0
    GAS_RESIDUAL_SATURATION 0.10d0
  /
  SATURATION_FUNCTION VAN_GENUCHTEN
    LOOP_INVARIANT
    UNSATURATED_EXTENSION ECPC
    ALPHA 1.0e-5
    M 0.2
    LIQUID_RESIDUAL_SATURATION 0.1d0
    MAX_CAPILLARY_PRESSURE 5.d10
  /
END

STRATA
  REGION all
  MATERIAL marine_sediments
END

TIME
  FINAL_TIME 555000.0 y
  INITIAL_TIMESTEP_SIZE 1.d-3 y
  MAXIMUM_TIMESTEP_SIZE 100.0 y

END

OUTPUT
  SNAPSHOT_FILE
    TIMES y 507000.0
    PERIODIC TIME 5000 y
    FORMAT TECPLOT POINT
    #NO_PRINT_INITIAL
  /
  OBSERVATION_FILE
    TIMES y 507000.0
    PERIODIC TIME 5000 y
```

```
  /
  #UNFILTER_NON_STATE_VARIABLES

  VARIABLES
   GAS_SATURATION
   HYDRATE_SATURATION
   GAS_DENSITY
   POROSITY
   ICE_SATURATION
   TEMPERATURE
   THERMODYNAMIC_STATE
   LIQUID_SATURATION
   GAS_PRESSURE
   LIQUID_PRESSURE
   PERMEABILITY
  /
END

EXTERNAL_FILE flowConditions.txt

# initial condition
INITIAL_CONDITION all
  FLOW_CONDITION initial
  REGION all
END

BOUNDARY_CONDITION top
  FLOW_CONDITION top
  REGION top
END

BOUNDARY_CONDITION bottom
  FLOW_CONDITION bottom
  REGION bottom
END

END_SUBSURFACE
```

A.6. flowConditions.txt

Note this input deck is displayed in two-column format for space efficiency.

```
FLOW_CONDITION initial
  TYPE
    LIQUID_PRESSURE HYDROSTATIC
    MOLE_FRACTION DIRICHLET
    TEMPERATURE DIRICHLET
  /
  DATUM 0.d0 0.d0 1000.d0
  GRADIENT
    TEMPERATURE 0.d0 0.d0 -0.051790238209626256
  /
  LIQUID_PRESSURE 228791.4427924983
  MOLE_FRACTION 1.d-10
  TEMPERATURE 4.485964300000311
END

FLOW_CONDITION top
  TYPE
    GAS_PRESSURE DIRICHLET_SEEPAGE
    RELATIVE_HUMIDITY DIRICHLET
    TEMPERATURE DIRICHLET
  /
  GAS_PRESSURE LIST
    TIME_UNITS year
    DATA_UNITS Pa
    INTERPOLATION LINEAR
    0.d0 228791.4427924983d0
    500.d0 216079.41141697354d0
    1000.d0 204254.24913385956d0
    1500.d0 195348.21356150892d0
    2000.d0 186439.81370538234d0
    2500.d0 178040.14871894888d0
    3000.d0 170205.6557750324d0
    3500.d0 164602.3892874983d0
    4000.d0 159895.85107054017d0
    4500.d0 154968.39927724394d0
    5000.d0 149877.65678848544d0
    5500.d0 147933.47740728944d0
    6000.d0 145340.1116006376d0
    6500.d0 143319.08471963252d0
```

7000.d0 142189.29585391603d0
7500.d0 140447.22504305508d0
8000.d0 139028.5862147748d0
8500.d0 139035.1831686525d0
9000.d0 137756.4155298107d0
9500.d0 135860.22833514455d0
10000.d0 134443.6973206771d0
10500.d0 132296.14757278838d0
11000.d0 130349.20411701099d0
11500.d0 128086.24827501315d0
12000.d0 124684.03116551835d0
12500.d0 121664.86919777622d0
13000.d0 118553.90722993365d0
13500.d0 113995.92115036542d0
14000.d0 109679.31370196117d0
14500.d0 105693.31580100703d0
15000.d0 101325.0d0
15500.d0 101325.0d0
16000.d0 101325.0d0
16500.d0 101325.0d0
17000.d0 101325.0d0
17500.d0 101325.0d0
18000.d0 101325.0d0
18500.d0 101325.0d0
19000.d0 101325.0d0
19500.d0 101325.0d0
20000.d0 101325.0d0
20500.d0 101325.0d0
21000.d0 101325.0d0
21500.d0 101325.0d0
22000.d0 101325.0d0
22500.d0 101325.0d0
23000.d0 101325.0d0
23500.d0 101325.0d0
24000.d0 101325.0d0
24500.d0 101325.0d0
25000.d0 101325.0d0
25500.d0 101325.0d0
26000.d0 101325.0d0
26500.d0 101325.0d0
27000.d0 101325.0d0
27500.d0 101325.0d0
28000.d0 101325.0d0
28500.d0 101325.0d0
29000.d0 101325.0d0
29500.d0 101325.0d0
30000.d0 101325.0d0
30500.d0 101325.0d0
31000.d0 101325.0d0
31500.d0 101325.0d0
32000.d0 101325.0d0
32500.d0 101325.0d0
33000.d0 101325.0d0
33500.d0 101325.0d0
34000.d0 101325.0d0
34500.d0 101325.0d0
35000.d0 101325.0d0
35500.d0 101325.0d0
36000.d0 101325.0d0
36500.d0 101325.0d0
37000.d0 101325.0d0
37500.d0 101325.0d0
38000.d0 101325.0d0
38500.d0 101325.0d0
39000.d0 101325.0d0
39500.d0 101325.0d0
40000.d0 101325.0d0
40500.d0 101325.0d0
41000.d0 101325.0d0
41500.d0 101325.0d0
42000.d0 101325.0d0
42500.d0 101325.0d0
43000.d0 101325.0d0
43500.d0 101325.0d0
44000.d0 101325.0d0
44500.d0 101325.0d0
45000.d0 101325.0d0
45500.d0 101325.0d0
46000.d0 101325.0d0
46500.d0 101325.0d0
47000.d0 101325.0d0
47500.d0 101325.0d0
48000.d0 101325.0d0
48500.d0 101325.0d0
49000.d0 101325.0d0
49500.d0 101325.0d0
50000.d0 101325.0d0
50500.d0 101325.0d0
51000.d0 101325.0d0
51500.d0 101325.0d0
52000.d0 101325.0d0
52500.d0 101325.0d0
53000.d0 101325.0d0
53500.d0 101325.0d0
54000.d0 101325.0d0
54500.d0 101325.0d0
55000.d0 101325.0d0
55500.d0 101325.0d0
56000.d0 101325.0d0
56500.d0 101325.0d0
57000.d0 101325.0d0
57500.d0 101325.0d0
58000.d0 101325.0d0
58500.d0 101325.0d0
59000.d0 101325.0d0
59500.d0 101325.0d0
60000.d0 101325.0d0
60500.d0 101325.0d0
61000.d0 101325.0d0
61500.d0 101325.0d0
62000.d0 101325.0d0
62500.d0 101325.0d0
63000.d0 101325.0d0
63500.d0 101325.0d0
64000.d0 101325.0d0
64500.d0 101325.0d0
65000.d0 101325.0d0
65500.d0 101325.0d0
66000.d0 101325.0d0
66500.d0 101325.0d0
67000.d0 101325.0d0
67500.d0 101325.0d0
68000.d0 101325.0d0
68500.d0 101325.0d0
69000.d0 101325.0d0
69500.d0 101325.0d0
70000.d0 101325.0d0
70500.d0 101325.0d0
71000.d0 101325.0d0
71500.d0 101325.0d0
72000.d0 101325.0d0
72500.d0 101325.0d0
73000.d0 101325.0d0
73500.d0 101325.0d0
74000.d0 101325.0d0
74500.d0 101325.0d0

75000.d0 101325.0d0
75500.d0 101325.0d0
76000.d0 101325.0d0
76500.d0 101325.0d0
77000.d0 101325.0d0
77500.d0 101325.0d0
78000.d0 101325.0d0
78500.d0 101325.0d0
79000.d0 101325.0d0
79500.d0 101325.0d0
80000.d0 101325.0d0
80500.d0 101325.0d0
81000.d0 101325.0d0
81500.d0 101325.0d0
82000.d0 101325.0d0
82500.d0 101325.0d0
83000.d0 101325.0d0
83500.d0 101325.0d0
84000.d0 101325.0d0
84500.d0 101325.0d0
85000.d0 101325.0d0
85500.d0 101325.0d0
86000.d0 101325.0d0
86500.d0 101325.0d0
87000.d0 101325.0d0
87500.d0 101325.0d0
88000.d0 101325.0d0
88500.d0 101325.0d0
89000.d0 101325.0d0
89500.d0 101325.0d0
90000.d0 101325.0d0
90500.d0 101325.0d0
91000.d0 101325.0d0
91500.d0 101325.0d0
92000.d0 101325.0d0
92500.d0 101325.0d0
93000.d0 101325.0d0
93500.d0 101325.0d0
94000.d0 101325.0d0
94500.d0 101325.0d0
95000.d0 101325.0d0
95500.d0 101325.0d0
96000.d0 101325.0d0
96500.d0 101325.0d0
97000.d0 101325.0d0
97500.d0 101325.0d0
98000.d0 101325.0d0
98500.d0 101325.0d0
99000.d0 101325.0d0
99500.d0 101325.0d0
100000.d0 101325.0d0
100500.d0 101325.0d0
101000.d0 101325.0d0
101500.d0 101325.0d0
102000.d0 101325.0d0
102500.d0 114683.62337630425d0
103000.d0 142825.69745976117d0
103500.d0 169062.53769892064d0
104000.d0 193497.409290442d0
104500.d0 217307.69171576673d0
105000.d0 241411.80000000013d0
105500.d0 245797.68214455183d0
106000.d0 253844.65090038383d0
106500.d0 269774.2769149649d0
107000.d0 284755.1306861842d0
107500.d0 300272.25166315015d0
108000.d0 316352.38817811455d0
108500.d0 333506.8570924001d0
109000.d0 350869.0081508969d0
109500.d0 367989.968740548d0
110000.d0 385170.7769401565d0
110500.d0 401322.13684938423d0
111000.d0 417453.6042095362d0
111500.d0 433682.5747398268d0
112000.d0 449071.6901276747d0
112500.d0 462215.76948475064d0
113000.d0 474868.9443939842d0
113500.d0 487628.93212720985d0
114000.d0 499318.76683480304d0
114500.d0 508418.7506718697d0
115000.d0 516765.78645717644d0
115500.d0 525438.1141936843d0
116000.d0 533126.7747602843d0
116500.d0 538802.1731015407d0
117000.d0 543777.3894524488d0
117500.d0 548719.0826178014d0
118000.d0 552371.4150739119d0
118500.d0 555243.4824182974d0
119000.d0 557761.1270398516d0
119500.d0 560348.1629447096d0
120000.d0 561610.2000000002d0
120500.d0 560347.7005038051d0
121000.d0 557760.8765156117d0
121500.d0 555243.7657930969d0
122000.d0 552371.1557083392d0
122500.d0 548718.6316264215d0
123000.d0 543777.1076652851d0
123500.d0 538802.2391891903d0
124000.d0 533126.9873324714d0
124500.d0 525438.5303322929d0
125000.d0 516765.5101894857d0
125500.d0 508418.89753693575d0
126000.d0 499318.3411097474d0
126500.d0 487629.09900688176d0
127000.d0 474868.9031925703d0
127500.d0 462216.02242934395d0
128000.d0 449071.9306445766d0
128500.d0 433682.8151632949d0
129000.d0 417453.6148773002d0
129500.d0 401322.23714783275d0
130000.d0 385170.60403481725d0
130500.d0 367989.62843270693d0
131000.d0 350868.6081736669d0
131500.d0 333507.1308766445d0
132000.d0 316352.5741729917d0
132500.d0 300272.01659828494d0
133000.d0 284755.0282189866d0
133500.d0 269774.5679173274d0
134000.d0 253844.78124372096d0
134500.d0 241492.01399866963d0
135000.d0 228791.44279249868d0
135500.d0 216079.41141697404d0
136000.d0 204254.24913385956d0
136500.d0 195348.2135615086d0
137000.d0 186439.8137053813d0
137500.d0 178040.14871894865d0
138000.d0 170205.6557750324d0
138500.d0 164602.38928749776d0
139000.d0 159895.8510705401d0
139500.d0 154968.39927724376d0
140000.d0 149877.65678848536d0
140500.d0 147933.47740728947d0
141000.d0 145340.11160063773d0
141500.d0 143319.0847196329d0
142000.d0 142189.29585391603d0
142500.d0 140447.22504305525d0

143000.d0 139028.5862147748d0
143500.d0 139035.1831686525d0
144000.d0 137756.4155298107d0
144500.d0 135860.22833514435d0
145000.d0 134443.6973206771d0
145500.d0 132296.14757278838d0
146000.d0 130349.20411701087d0
146500.d0 128086.24827501309d0
147000.d0 124684.03116551835d0
147500.d0 121664.86919777622d0
148000.d0 118553.90722993365d0
148500.d0 113995.92115036582d0
149000.d0 109679.3137019612d0
149500.d0 105693.3158010066d0
150000.d0 101325.0d0
150500.d0 101325.0d0
151000.d0 101325.0d0
151500.d0 101325.0d0
152000.d0 101325.0d0
152500.d0 101325.0d0
153000.d0 101325.0d0
153500.d0 101325.0d0
154000.d0 101325.0d0
154500.d0 101325.0d0
155000.d0 101325.0d0
155500.d0 101325.0d0
156000.d0 101325.0d0
156500.d0 101325.0d0
157000.d0 101325.0d0
157500.d0 101325.0d0
158000.d0 101325.0d0
158500.d0 101325.0d0
159000.d0 101325.0d0
159500.d0 101325.0d0
160000.d0 101325.0d0
160500.d0 101325.0d0
161000.d0 101325.0d0
161500.d0 101325.0d0
162000.d0 101325.0d0
162500.d0 101325.0d0
163000.d0 101325.0d0
163500.d0 101325.0d0
164000.d0 101325.0d0
164500.d0 101325.0d0
165000.d0 101325.0d0
165500.d0 101325.0d0
166000.d0 101325.0d0
166500.d0 101325.0d0
167000.d0 101325.0d0
167500.d0 101325.0d0
168000.d0 101325.0d0
168500.d0 101325.0d0
169000.d0 101325.0d0
169500.d0 101325.0d0
170000.d0 101325.0d0
170500.d0 101325.0d0
171000.d0 101325.0d0
171500.d0 101325.0d0
172000.d0 101325.0d0
172500.d0 101325.0d0
173000.d0 101325.0d0
173500.d0 101325.0d0
174000.d0 101325.0d0
174500.d0 101325.0d0
175000.d0 101325.0d0
175500.d0 101325.0d0
176000.d0 101325.0d0
176500.d0 101325.0d0
177000.d0 101325.0d0
177500.d0 101325.0d0
178000.d0 101325.0d0
178500.d0 101325.0d0
179000.d0 101325.0d0
179500.d0 101325.0d0
180000.d0 101325.0d0
180500.d0 101325.0d0
181000.d0 101325.0d0
181500.d0 101325.0d0
182000.d0 101325.0d0
182500.d0 101325.0d0
183000.d0 101325.0d0
183500.d0 101325.0d0
184000.d0 101325.0d0
184500.d0 101325.0d0
185000.d0 101325.0d0
185500.d0 101325.0d0
186000.d0 101325.0d0
186500.d0 101325.0d0
187000.d0 101325.0d0
187500.d0 101325.0d0
188000.d0 101325.0d0
188500.d0 101325.0d0
189000.d0 101325.0d0
189500.d0 101325.0d0
190000.d0 101325.0d0
190500.d0 101325.0d0
191000.d0 101325.0d0
191500.d0 101325.0d0
192000.d0 101325.0d0
192500.d0 101325.0d0
193000.d0 101325.0d0
193500.d0 101325.0d0
194000.d0 101325.0d0
194500.d0 101325.0d0
195000.d0 101325.0d0
195500.d0 101325.0d0
196000.d0 101325.0d0
196500.d0 101325.0d0
197000.d0 101325.0d0
197500.d0 101325.0d0
198000.d0 101325.0d0
198500.d0 101325.0d0
199000.d0 101325.0d0
199500.d0 101325.0d0
200000.d0 101325.0d0
200500.d0 101325.0d0
201000.d0 101325.0d0
201500.d0 101325.0d0
202000.d0 101325.0d0
202500.d0 101325.0d0
203000.d0 101325.0d0
203500.d0 101325.0d0
204000.d0 101325.0d0
204500.d0 101325.0d0
205000.d0 101325.0d0
205500.d0 101325.0d0
206000.d0 101325.0d0
206500.d0 101325.0d0
207000.d0 101325.0d0
207500.d0 101325.0d0
208000.d0 101325.0d0
208500.d0 101325.0d0
209000.d0 101325.0d0
209500.d0 101325.0d0
210000.d0 101325.0d0
210500.d0 101325.0d0

211000.d0 101325.0d0
211500.d0 101325.0d0
212000.d0 101325.0d0
212500.d0 101325.0d0
213000.d0 101325.0d0
213500.d0 101325.0d0
214000.d0 101325.0d0
214500.d0 101325.0d0
215000.d0 101325.0d0
215500.d0 101325.0d0
216000.d0 101325.0d0
216500.d0 101325.0d0
217000.d0 101325.0d0
217500.d0 101325.0d0
218000.d0 101325.0d0
218500.d0 101325.0d0
219000.d0 101325.0d0
219500.d0 101325.0d0
220000.d0 101325.0d0
220500.d0 101325.0d0
221000.d0 101325.0d0
221500.d0 101325.0d0
222000.d0 101325.0d0
222500.d0 101325.0d0
223000.d0 101325.0d0
223500.d0 101325.0d0
224000.d0 101325.0d0
224500.d0 101325.0d0
225000.d0 101325.0d0
225500.d0 101325.0d0
226000.d0 101325.0d0
226500.d0 101325.0d0
227000.d0 101325.0d0
227500.d0 101325.0d0
228000.d0 101325.0d0
228500.d0 101325.0d0
229000.d0 101325.0d0
229500.d0 101325.0d0
230000.d0 101325.0d0
230500.d0 101325.0d0
231000.d0 101325.0d0
231500.d0 101325.0d0
232000.d0 101325.0d0
232500.d0 101325.0d0
233000.d0 101325.0d0
233500.d0 101325.0d0
234000.d0 101325.0d0
234500.d0 101325.0d0
235000.d0 101325.0d0
235500.d0 101325.0d0
236000.d0 101325.0d0
236500.d0 101325.0d0
237000.d0 101325.0d0
237500.d0 114683.62337630628d0
238000.d0 142825.69745976164d0
238500.d0 169062.53769892064d0
239000.d0 193497.40929044347d0
239500.d0 217307.69171576703d0
240000.d0 241411.80000000013d0
240500.d0 245797.68214455218d0
241000.d0 253844.65090038424d0
241500.d0 269774.2769149648d0
242000.d0 284755.1306861832d0
242500.d0 300272.25166315195d0
243000.d0 316352.38817811455d0
243500.d0 333506.85709240206d0
244000.d0 350869.0081508971d0
244500.d0 367989.96874054853d0
245000.d0 385170.7769401565d0
245500.d0 401322.1368493825d0
246000.d0 417453.6042095362d0
246500.d0 433682.5747398268d0
247000.d0 449071.6901276736d0
247500.d0 462215.76948475215d0
248000.d0 474868.94439398433d0
248500.d0 487628.9321272106d0
249000.d0 499318.76683480287d0
249500.d0 508418.75067187d0
250000.d0 516765.78645717556d0
250500.d0 525438.1141936843d0
251000.d0 533126.7747602841d0
251500.d0 538802.1731015404d0
252000.d0 543777.3894524485d0
252500.d0 548719.0826178014d0
253000.d0 552371.4150739119d0
253500.d0 555243.4824182978d0
254000.d0 557761.1270398519d0
254500.d0 560348.1629447096d0
255000.d0 561610.2000000002d0
255500.d0 560347.7005038051d0
256000.d0 557760.8765156117d0
256500.d0 555243.7657930969d0
257000.d0 552371.1557083392d0
257500.d0 548718.6316264215d0
258000.d0 543777.1076652851d0
258500.d0 538802.2391891903d0
259000.d0 533126.9873324714d0
259500.d0 525438.5303322929d0
260000.d0 516765.5101894857d0
260500.d0 508418.89753693575d0
261000.d0 499318.3411097474d0
261500.d0 487629.09900688176d0
262000.d0 474868.9031925703d0
262500.d0 462216.02242934395d0
263000.d0 449071.9306445766d0
263500.d0 433682.8151632949d0
264000.d0 417453.6148773002d0
264500.d0 401322.23714783275d0
265000.d0 385170.60403481725d0
265500.d0 367989.62843270693d0
266000.d0 350868.6081736669d0
266500.d0 333507.1308766445d0
267000.d0 316352.5741729917d0
267500.d0 300272.01659828494d0
268000.d0 284755.0282189866d0
268500.d0 269774.5679173274d0
269000.d0 253844.78124372096d0
269500.d0 241492.01399866963d0
270000.d0 228791.44279249868d0
270500.d0 216079.41141697404d0
271000.d0 204254.24913385956d0
271500.d0 195348.2135615086d0
272000.d0 186439.8137053813d0
272500.d0 178040.14871894865d0
273000.d0 170205.6557750324d0
273500.d0 164602.38928749776d0
274000.d0 159895.8510705401d0
274500.d0 154968.39927724376d0
275000.d0 149877.65678848536d0
275500.d0 147933.47740728947d0
276000.d0 145340.11160063773d0
276500.d0 143319.0847196329d0
277000.d0 142189.29585391603d0
277500.d0 140447.22504305525d0
278000.d0 139028.5862147748d0
278500.d0 139035.1831686525d0

279000.d0 137756.4155298107d0
279500.d0 135860.22833514435d0
280000.d0 134443.6973206771d0
280500.d0 132296.14757278838d0
281000.d0 130349.20411701087d0
281500.d0 128086.24827501309d0
282000.d0 124684.03116551835d0
282500.d0 121664.86919777622d0
283000.d0 118553.90722993365d0
283500.d0 113995.92115036582d0
284000.d0 109679.3137019612d0
284500.d0 105693.3158010066d0
285000.d0 101325.0d0
285500.d0 101325.0d0
286000.d0 101325.0d0
286500.d0 101325.0d0
287000.d0 101325.0d0
287500.d0 101325.0d0
288000.d0 101325.0d0
288500.d0 101325.0d0
289000.d0 101325.0d0
289500.d0 101325.0d0
290000.d0 101325.0d0
290500.d0 101325.0d0
291000.d0 101325.0d0
291500.d0 101325.0d0
292000.d0 101325.0d0
292500.d0 101325.0d0
293000.d0 101325.0d0
293500.d0 101325.0d0
294000.d0 101325.0d0
294500.d0 101325.0d0
295000.d0 101325.0d0
295500.d0 101325.0d0
296000.d0 101325.0d0
296500.d0 101325.0d0
297000.d0 101325.0d0
297500.d0 101325.0d0
298000.d0 101325.0d0
298500.d0 101325.0d0
299000.d0 101325.0d0
299500.d0 101325.0d0
300000.d0 101325.0d0
300500.d0 101325.0d0
301000.d0 101325.0d0
301500.d0 101325.0d0
302000.d0 101325.0d0
302500.d0 101325.0d0
303000.d0 101325.0d0
303500.d0 101325.0d0
304000.d0 101325.0d0
304500.d0 101325.0d0
305000.d0 101325.0d0
305500.d0 101325.0d0
306000.d0 101325.0d0
306500.d0 101325.0d0
307000.d0 101325.0d0
307500.d0 101325.0d0
308000.d0 101325.0d0
308500.d0 101325.0d0
309000.d0 101325.0d0
309500.d0 101325.0d0
310000.d0 101325.0d0
310500.d0 101325.0d0
311000.d0 101325.0d0
311500.d0 101325.0d0
312000.d0 101325.0d0
312500.d0 101325.0d0
313000.d0 101325.0d0
313500.d0 101325.0d0
314000.d0 101325.0d0
314500.d0 101325.0d0
315000.d0 101325.0d0
315500.d0 101325.0d0
316000.d0 101325.0d0
316500.d0 101325.0d0
317000.d0 101325.0d0
317500.d0 101325.0d0
318000.d0 101325.0d0
318500.d0 101325.0d0
319000.d0 101325.0d0
319500.d0 101325.0d0
320000.d0 101325.0d0
320500.d0 101325.0d0
321000.d0 101325.0d0
321500.d0 101325.0d0
322000.d0 101325.0d0
322500.d0 101325.0d0
323000.d0 101325.0d0
323500.d0 101325.0d0
324000.d0 101325.0d0
324500.d0 101325.0d0
325000.d0 101325.0d0
325500.d0 101325.0d0
326000.d0 101325.0d0
326500.d0 101325.0d0
327000.d0 101325.0d0
327500.d0 101325.0d0
328000.d0 101325.0d0
328500.d0 101325.0d0
329000.d0 101325.0d0
329500.d0 101325.0d0
330000.d0 101325.0d0
330500.d0 101325.0d0
331000.d0 101325.0d0
331500.d0 101325.0d0
332000.d0 101325.0d0
332500.d0 101325.0d0
333000.d0 101325.0d0
333500.d0 101325.0d0
334000.d0 101325.0d0
334500.d0 101325.0d0
335000.d0 101325.0d0
335500.d0 101325.0d0
336000.d0 101325.0d0
336500.d0 101325.0d0
337000.d0 101325.0d0
337500.d0 101325.0d0
338000.d0 101325.0d0
338500.d0 101325.0d0
339000.d0 101325.0d0
339500.d0 101325.0d0
340000.d0 101325.0d0
340500.d0 101325.0d0
341000.d0 101325.0d0
341500.d0 101325.0d0
342000.d0 101325.0d0
342500.d0 101325.0d0
343000.d0 101325.0d0
343500.d0 101325.0d0
344000.d0 101325.0d0
344500.d0 101325.0d0
345000.d0 101325.0d0
345500.d0 101325.0d0
346000.d0 101325.0d0
346500.d0 101325.0d0

347000.d0 101325.0d0
347500.d0 101325.0d0
348000.d0 101325.0d0
348500.d0 101325.0d0
349000.d0 101325.0d0
349500.d0 101325.0d0
350000.d0 101325.0d0
350500.d0 101325.0d0
351000.d0 101325.0d0
351500.d0 101325.0d0
352000.d0 101325.0d0
352500.d0 101325.0d0
353000.d0 101325.0d0
353500.d0 101325.0d0
354000.d0 101325.0d0
354500.d0 101325.0d0
355000.d0 101325.0d0
355500.d0 101325.0d0
356000.d0 101325.0d0
356500.d0 101325.0d0
357000.d0 101325.0d0
357500.d0 101325.0d0
358000.d0 101325.0d0
358500.d0 101325.0d0
359000.d0 101325.0d0
359500.d0 101325.0d0
360000.d0 101325.0d0
360500.d0 101325.0d0
361000.d0 101325.0d0
361500.d0 101325.0d0
362000.d0 101325.0d0
362500.d0 101325.0d0
363000.d0 101325.0d0
363500.d0 101325.0d0
364000.d0 101325.0d0
364500.d0 101325.0d0
365000.d0 101325.0d0
365500.d0 101325.0d0
366000.d0 101325.0d0
366500.d0 101325.0d0
367000.d0 101325.0d0
367500.d0 101325.0d0
368000.d0 101325.0d0
368500.d0 101325.0d0
369000.d0 101325.0d0
369500.d0 101325.0d0
370000.d0 101325.0d0
370500.d0 101325.0d0
371000.d0 101325.0d0
371500.d0 101325.0d0
372000.d0 101325.0d0
372500.d0 114683.62337630628d0
373000.d0 142825.69745976164d0
373500.d0 169062.53769892064d0
374000.d0 193497.40929044347d0
374500.d0 217307.69171576703d0
375000.d0 241411.80000000013d0
375500.d0 245797.68214455218d0
376000.d0 253844.65090038424d0
376500.d0 269774.2769149648d0
377000.d0 284755.1306861832d0
377500.d0 300272.25166315195d0
378000.d0 316352.38817811455d0
378500.d0 333506.85709240206d0
379000.d0 350869.0081508971d0
379500.d0 367989.96874054853d0
380000.d0 385170.7769401565d0
380500.d0 401322.1368493825d0
381000.d0 417453.6042095362d0
381500.d0 433682.5747398268d0
382000.d0 449071.6901276736d0
382500.d0 462215.76948475215d0
383000.d0 474868.9443939837d0
383500.d0 487628.93212721025d0
384000.d0 499318.7668348029d0
384500.d0 508418.75067186984d0
385000.d0 516765.78645717556d0
385500.d0 525438.1141936848d0
386000.d0 533126.774760284d0
386500.d0 538802.1731015402d0
387000.d0 543777.3894524486d0
387500.d0 548719.0826178014d0
388000.d0 552371.4150739119d0
388500.d0 555243.4824182977d0
389000.d0 557761.1270398517d0
389500.d0 560348.1629447098d0
390000.d0 561610.2000000002d0
390500.d0 560347.7005038052d0
391000.d0 557760.8765156115d0
391500.d0 555243.7657930966d0
392000.d0 552371.1557083392d0
392500.d0 548718.6316264215d0
393000.d0 543777.1076652852d0
393500.d0 538802.2391891903d0
394000.d0 533126.9873324712d0
394500.d0 525438.5303322931d0
395000.d0 516765.5101894857d0
395500.d0 508418.8975369356d0
396000.d0 499318.3411097475d0
396500.d0 487629.09900688136d0
397000.d0 474868.9031925697d0
397500.d0 462216.02242934355d0
398000.d0 449071.93064457644d0
398500.d0 433682.8151632941d0
399000.d0 417453.6148773002d0
399500.d0 401322.23714783275d0
400000.d0 385170.60403481714d0
400500.d0 367989.62843270676d0
401000.d0 350868.60817366757d0
401500.d0 333507.13087664347d0
402000.d0 316352.5741729913d0
402500.d0 300272.016598284d0
403000.d0 284755.0282189871d0
403500.d0 269774.5679173266d0
404000.d0 253844.78124372076d0
404500.d0 241492.0139986694d0
405000.d0 228791.4427924985d0
405500.d0 216079.41141697328d0
406000.d0 204254.24913385956d0
406500.d0 195348.2135615084d0
407000.d0 186439.81370538156d0
407500.d0 178040.14871894865d0
408000.d0 170205.65577503195d0
408500.d0 164602.38928749782d0
409000.d0 159895.85107054014d0
409500.d0 154968.39927724368d0
410000.d0 149877.65678848565d0
410500.d0 147933.4774072896d0
411000.d0 145340.11160063767d0
411500.d0 143319.08471963272d0
412000.d0 142189.29585391603d0
412500.d0 140447.22504305516d0
413000.d0 139028.5862147748d0
413500.d0 139035.1831686525d0
414000.d0 137756.4155298108d0
414500.d0 135860.22833514446d0

415000.d0 134443.69732067722d0
415500.d0 132296.1475727885d0
416000.d0 130349.20411701096d0
416500.d0 128086.248275013d0
417000.d0 124684.03116551835d0
417500.d0 121664.86919777622d0
418000.d0 118553.90722993379d0
418500.d0 113995.9211503657d0
419000.d0 109679.31370196119d0
419500.d0 105693.31580100664d0
420000.d0 101325.0d0
420500.d0 101325.0d0
421000.d0 101325.0d0
421500.d0 101325.0d0
422000.d0 101325.0d0
422500.d0 101325.0d0
423000.d0 101325.0d0
423500.d0 101325.0d0
424000.d0 101325.0d0
424500.d0 101325.0d0
425000.d0 101325.0d0
425500.d0 101325.0d0
426000.d0 101325.0d0
426500.d0 101325.0d0
427000.d0 101325.0d0
427500.d0 101325.0d0
428000.d0 101325.0d0
428500.d0 101325.0d0
429000.d0 101325.0d0
429500.d0 101325.0d0
430000.d0 101325.0d0
430500.d0 101325.0d0
431000.d0 101325.0d0
431500.d0 101325.0d0
432000.d0 101325.0d0
432500.d0 101325.0d0
433000.d0 101325.0d0
433500.d0 101325.0d0
434000.d0 101325.0d0
434500.d0 101325.0d0
435000.d0 101325.0d0
435500.d0 101325.0d0
436000.d0 101325.0d0
436500.d0 101325.0d0
437000.d0 101325.0d0
437500.d0 101325.0d0
438000.d0 101325.0d0
438500.d0 101325.0d0
439000.d0 101325.0d0
439500.d0 101325.0d0
440000.d0 101325.0d0
440500.d0 101325.0d0
441000.d0 101325.0d0
441500.d0 101325.0d0
442000.d0 101325.0d0
442500.d0 101325.0d0
443000.d0 101325.0d0
443500.d0 101325.0d0
444000.d0 101325.0d0
444500.d0 101325.0d0
445000.d0 101325.0d0
445500.d0 101325.0d0
446000.d0 101325.0d0
446500.d0 101325.0d0
447000.d0 101325.0d0
447500.d0 101325.0d0
448000.d0 101325.0d0
448500.d0 101325.0d0
449000.d0 101325.0d0
449500.d0 101325.0d0
450000.d0 101325.0d0
450500.d0 101325.0d0
451000.d0 101325.0d0
451500.d0 101325.0d0
452000.d0 101325.0d0
452500.d0 101325.0d0
453000.d0 101325.0d0
453500.d0 101325.0d0
454000.d0 101325.0d0
454500.d0 101325.0d0
455000.d0 101325.0d0
455500.d0 101325.0d0
456000.d0 101325.0d0
456500.d0 101325.0d0
457000.d0 101325.0d0
457500.d0 101325.0d0
458000.d0 101325.0d0
458500.d0 101325.0d0
459000.d0 101325.0d0
459500.d0 101325.0d0
460000.d0 101325.0d0
460500.d0 101325.0d0
461000.d0 101325.0d0
461500.d0 101325.0d0
462000.d0 101325.0d0
462500.d0 101325.0d0
463000.d0 101325.0d0
463500.d0 101325.0d0
464000.d0 101325.0d0
464500.d0 101325.0d0
465000.d0 101325.0d0
465500.d0 101325.0d0
466000.d0 101325.0d0
466500.d0 101325.0d0
467000.d0 101325.0d0
467500.d0 101325.0d0
468000.d0 101325.0d0
468500.d0 101325.0d0
469000.d0 101325.0d0
469500.d0 101325.0d0
470000.d0 101325.0d0
470500.d0 101325.0d0
471000.d0 101325.0d0
471500.d0 101325.0d0
472000.d0 101325.0d0
472500.d0 101325.0d0
473000.d0 101325.0d0
473500.d0 101325.0d0
474000.d0 101325.0d0
474500.d0 101325.0d0
475000.d0 101325.0d0
475500.d0 101325.0d0
476000.d0 101325.0d0
476500.d0 101325.0d0
477000.d0 101325.0d0
477500.d0 101325.0d0
478000.d0 101325.0d0
478500.d0 101325.0d0
479000.d0 101325.0d0
479500.d0 101325.0d0
480000.d0 101325.0d0
480500.d0 101325.0d0
481000.d0 101325.0d0
481500.d0 101325.0d0
482000.d0 101325.0d0
482500.d0 101325.0d0

483000.d0 101325.0d0
483500.d0 101325.0d0
484000.d0 101325.0d0
484500.d0 101325.0d0
485000.d0 101325.0d0
485500.d0 101325.0d0
486000.d0 101325.0d0
486500.d0 101325.0d0
487000.d0 101325.0d0
487500.d0 101325.0d0
488000.d0 101325.0d0
488500.d0 101325.0d0
489000.d0 101325.0d0
489500.d0 101325.0d0
490000.d0 101325.0d0
490500.d0 101325.0d0
491000.d0 101325.0d0
491500.d0 101325.0d0
492000.d0 101325.0d0
492500.d0 101325.0d0
493000.d0 101325.0d0
493500.d0 101325.0d0
494000.d0 101325.0d0
494500.d0 101325.0d0
495000.d0 101325.0d0
495500.d0 101325.0d0
496000.d0 101325.0d0
496500.d0 101325.0d0
497000.d0 101325.0d0
497500.d0 101325.0d0
498000.d0 101325.0d0
498500.d0 101325.0d0
499000.d0 101325.0d0
499500.d0 101325.0d0
500000.d0 101325.0d0
500500.d0 101325.0d0
501000.d0 101325.0d0
501500.d0 101325.0d0
502000.d0 101325.0d0
502500.d0 101325.0d0
503000.d0 101325.0d0
503500.d0 101325.0d0
504000.d0 101325.0d0
504500.d0 101325.0d0
505000.d0 101325.0d0
505500.d0 101325.0d0
506000.d0 101325.0d0
506500.d0 101325.0d0
507000.d0 101325.0d0
507500.d0 114683.62337630507d0
508000.d0 142825.6974597607d0
508500.d0 169062.53769892064d0
509000.d0 193497.40929044347d0
509500.d0 217307.69171576633d0
510000.d0 241411.80000000013d0
510500.d0 245797.682144552d0
511000.d0 253844.65090038403d0
511500.d0 269774.276914964d0
512000.d0 284755.1306861837d0
512500.d0 300272.2516631511d0
513000.d0 316352.3881781142d0
513500.d0 333506.8570924011d0
514000.d0 350869.0081508978d0
514500.d0 367989.9687405483d0
515000.d0 385170.77694015636d0
515500.d0 401322.1368493829d0
516000.d0 417453.6042095362d0
516500.d0 433682.5747398264d0
517000.d0 449071.6901276739d0
517500.d0 462215.7694847519d0
518000.d0 474868.9443939837d0
518500.d0 487628.93212721025d0
519000.d0 499318.7668348029d0
519500.d0 508418.7506718697d0
520000.d0 516765.78645717556d0
520500.d0 525438.1141936845d0
521000.d0 533126.774760284d0
521500.d0 538802.1731015404d0
522000.d0 543777.3894524486d0
522500.d0 548719.0826178014d0
523000.d0 552371.4150739119d0
523500.d0 555243.4824182977d0
524000.d0 557761.1270398517d0
524500.d0 560348.1629447096d0
525000.d0 561610.2000000002d0
525500.d0 560347.7005038052d0
526000.d0 557760.8765156115d0
526500.d0 555243.7657930967d0
527000.d0 552371.1557083391d0
527500.d0 548718.6316264215d0
528000.d0 543777.1076652852d0
528500.d0 538802.2391891903d0
529000.d0 533126.9873324712d0
529500.d0 525438.530332293d0
530000.d0 516765.5101894857d0
530500.d0 508418.89753693546d0
531000.d0 499318.3411097475d0
531500.d0 487629.09900688136d0
532000.d0 474868.9031925697d0
532500.d0 462216.0224293438d0
533000.d0 449071.93064457685d0
533500.d0 433682.8151632945d0
534000.d0 417453.6148773002d0
534500.d0 401322.23714783316d0
535000.d0 385170.60403481714d0
535500.d0 367989.62843270676d0
536000.d0 350868.60817366757d0
536500.d0 333507.13087664347d0
537000.d0 316352.57417299127d0
537500.d0 300272.016598284d0
538000.d0 284755.02821898705d0
538500.d0 269774.5679173266d0
539000.d0 253844.78124372076d0
539500.d0 241492.0139986694d0
540000.d0 228791.4427924985d0
540500.d0 216079.41141697328d0
541000.d0 204254.24913385956d0
541500.d0 195348.21356150857d0
542000.d0 186439.8137053817d0
542500.d0 178040.1487189487d0
543000.d0 170205.65577503195d0
543500.d0 164602.3892874978d0
544000.d0 159895.85107054014d0
544500.d0 154968.3992772437d0
545000.d0 149877.65678848565d0
545500.d0 147933.4774072896d0
546000.d0 145340.11160063767d0
546500.d0 143319.08471963275d0
547000.d0 142189.29585391603d0
547500.d0 140447.22504305516d0
548000.d0 139028.5862147748d0
548500.d0 139035.1831686525d0
549000.d0 137756.41552981077d0
549500.d0 135860.2283351444d0
550000.d0 134443.69732067717d0
550500.d0 132296.14757278847d0

551000.d0 130349.20411701096d0
551500.d0 128086.248275013d0
552000.d0 124684.03116551824d0
552500.d0 121664.86919777622d0
553000.d0 118553.90722993373d0
553500.d0 113995.92115036567d0
554000.d0 109679.31370196119d0
554500.d0 105693.31580100664d0
555000.d0 101325.0d0
555500.d0 101325.0d0
556000.d0 101325.0d0
556500.d0 101325.0d0
557000.d0 101325.0d0
557500.d0 101325.0d0
558000.d0 101325.0d0
558500.d0 101325.0d0
559000.d0 101325.0d0
559500.d0 101325.0d0
560000.d0 101325.0d0
560500.d0 101325.0d0
561000.d0 101325.0d0
561500.d0 101325.0d0
562000.d0 101325.0d0
562500.d0 101325.0d0
563000.d0 101325.0d0
563500.d0 101325.0d0
564000.d0 101325.0d0
564500.d0 101325.0d0
565000.d0 101325.0d0
565500.d0 101325.0d0
566000.d0 101325.0d0
566500.d0 101325.0d0
567000.d0 101325.0d0
567500.d0 101325.0d0
568000.d0 101325.0d0
568500.d0 101325.0d0
569000.d0 101325.0d0
569500.d0 101325.0d0
570000.d0 101325.0d0
570500.d0 101325.0d0
571000.d0 101325.0d0
571500.d0 101325.0d0
572000.d0 101325.0d0
572500.d0 101325.0d0
573000.d0 101325.0d0
573500.d0 101325.0d0
574000.d0 101325.0d0
574500.d0 101325.0d0
575000.d0 101325.0d0
575500.d0 101325.0d0
576000.d0 101325.0d0
576500.d0 101325.0d0
577000.d0 101325.0d0
577500.d0 101325.0d0
578000.d0 101325.0d0
578500.d0 101325.0d0
579000.d0 101325.0d0
579500.d0 101325.0d0
580000.d0 101325.0d0
580500.d0 101325.0d0
581000.d0 101325.0d0
581500.d0 101325.0d0
582000.d0 101325.0d0
582500.d0 101325.0d0
583000.d0 101325.0d0
583500.d0 101325.0d0
584000.d0 101325.0d0
584500.d0 101325.0d0
585000.d0 101325.0d0
585500.d0 101325.0d0
586000.d0 101325.0d0
586500.d0 101325.0d0
587000.d0 101325.0d0
587500.d0 101325.0d0
588000.d0 101325.0d0
588500.d0 101325.0d0
589000.d0 101325.0d0
589500.d0 101325.0d0
590000.d0 101325.0d0
590500.d0 101325.0d0
591000.d0 101325.0d0
591500.d0 101325.0d0
592000.d0 101325.0d0
592500.d0 101325.0d0
593000.d0 101325.0d0
593500.d0 101325.0d0
594000.d0 101325.0d0
594500.d0 101325.0d0
595000.d0 101325.0d0
595500.d0 101325.0d0
596000.d0 101325.0d0
596500.d0 101325.0d0
597000.d0 101325.0d0
597500.d0 101325.0d0
598000.d0 101325.0d0
598500.d0 101325.0d0
599000.d0 101325.0d0
599500.d0 101325.0d0
600000.d0 101325.0d0
600500.d0 101325.0d0
601000.d0 101325.0d0
601500.d0 101325.0d0
602000.d0 101325.0d0
602500.d0 101325.0d0
603000.d0 101325.0d0
603500.d0 101325.0d0
604000.d0 101325.0d0
604500.d0 101325.0d0
605000.d0 101325.0d0
605500.d0 101325.0d0
606000.d0 101325.0d0
606500.d0 101325.0d0
607000.d0 101325.0d0
607500.d0 101325.0d0
608000.d0 101325.0d0
608500.d0 101325.0d0
609000.d0 101325.0d0
609500.d0 101325.0d0
610000.d0 101325.0d0
610500.d0 101325.0d0
611000.d0 101325.0d0
611500.d0 101325.0d0
612000.d0 101325.0d0
612500.d0 101325.0d0
613000.d0 101325.0d0
613500.d0 101325.0d0
614000.d0 101325.0d0
614500.d0 101325.0d0
615000.d0 101325.0d0
615500.d0 101325.0d0
616000.d0 101325.0d0
616500.d0 101325.0d0
617000.d0 101325.0d0
617500.d0 101325.0d0
618000.d0 101325.0d0
618500.d0 101325.0d0

```
  619000.d0 101325.0d0
  619500.d0 101325.0d0
  620000.d0 101325.0d0
  620500.d0 101325.0d0
  621000.d0 101325.0d0
  621500.d0 101325.0d0
  622000.d0 101325.0d0
  622500.d0 101325.0d0
  623000.d0 101325.0d0
  623500.d0 101325.0d0
  624000.d0 101325.0d0
  624500.d0 101325.0d0
  625000.d0 101325.0d0
  625500.d0 101325.0d0
  626000.d0 101325.0d0
  626500.d0 101325.0d0
  627000.d0 101325.0d0
  627500.d0 101325.0d0
  628000.d0 101325.0d0
  628500.d0 101325.0d0
  629000.d0 101325.0d0
  629500.d0 101325.0d0
  630000.d0 101325.0d0
  630500.d0 101325.0d0
  631000.d0 101325.0d0
  631500.d0 101325.0d0
  632000.d0 101325.0d0
  632500.d0 101325.0d0
  633000.d0 101325.0d0
  633500.d0 101325.0d0
  634000.d0 101325.0d0
  634500.d0 101325.0d0
  635000.d0 101325.0d0
  635500.d0 101325.0d0
  636000.d0 101325.0d0
  636500.d0 101325.0d0
  637000.d0 101325.0d0
  637500.d0 101325.0d0
  638000.d0 101325.0d0
  638500.d0 101325.0d0
  639000.d0 101325.0d0
  639500.d0 101325.0d0
  640000.d0 101325.0d0
  640500.d0 101325.0d0
  641000.d0 101325.0d0
  641500.d0 101325.0d0
  642000.d0 101325.0d0
  642500.d0 114683.6233763056d0
  643000.d0 142825.6974597611d0
  643500.d0 169062.53769892076d0
  644000.d0 193497.40929044323d0
  644500.d0 217307.69171576656d0
  645000.d0 241411.80000000013d0

 /
 RELATIVE_HUMIDITY 1.d-10
 TEMPERATURE LIST
  TIME_UNITS year
  DATA_UNITS C
  INTERPOLATION LINEAR
  0.d0 4.485964300000311d0
  500.d0 4.485964300000311d0
  1000.d0 4.485964300000311d0
  1500.d0 4.485964300000311d0
  2000.d0 4.485964300000311d0
  2500.d0 4.485964300000311d0
  3000.d0 4.485964300000311d0
  3500.d0 4.485964300000311d0
```

```
  4000.d0 4.485964300000311d0
  4500.d0 4.485964300000311d0
  5000.d0 4.485964300000311d0
  5500.d0 4.485964300000311d0
  6000.d0 4.485964300000311d0
  6500.d0 4.485964300000311d0
  7000.d0 4.485964300000311d0
  7500.d0 4.485964300000311d0
  8000.d0 4.485964300000311d0
  8500.d0 4.485964300000311d0
  9000.d0 4.485964300000311d0
  9500.d0 4.485964300000311d0
  10000.d0 4.485964300000311d0
  10500.d0 4.485964300000311d0
  11000.d0 4.485964300000311d0
  11500.d0 4.485964300000311d0
  12000.d0 4.485964300000311d0
  12500.d0 4.485964300000311d0
  13000.d0 4.485964300000311d0
  13500.d0 4.485964300000311d0
  14000.d0 4.485964300000311d0
  14500.d0 4.485964300000311d0
  15000.d0 -17.4212d0
  15500.d0 -17.26013698630137d0
  16000.d0 -16.498857142857144d0
  16500.d0 -17.498d0
  17000.d0 -16.83d0
  17500.d0 -17.11d0
  18000.d0 -16.6056338028169d0
  18500.d0 -16.359142857142857d0
  19000.d0 -15.811044776119402d0
  19500.d0 -14.846935483870967d0
  20000.d0 -15.195076923076924d0
  20500.d0 -15.205373134328358d0
  21000.d0 -16.93041095890411d0
  21500.d0 -15.865588235294117d0
  22000.d0 -15.31846153846154d0
  22500.d0 -16.71d0
  23000.d0 -15.940000000000001d0
  23500.d0 -15.914d0
  24000.d0 -17.265d0
  24500.d0 -16.844594594594597d0
  25000.d0 -16.413424657534247d0
  25500.d0 -17.849493670886073d0
  26000.d0 -18.389518072289157d0
  26500.d0 -18.693411764705882d0
  27000.d0 -18.991264367816093d0
  27500.d0 -19.12125d0
  28000.d0 -17.875185185185185d0
  28500.d0 -17.515897435897436d0
  29000.d0 -17.43632911392405d0
  29500.d0 -17.696582278481014d0
  30000.d0 -17.972962962962963d0
  30500.d0 -17.394814814814815d0
  31000.d0 -18.884137931034484d0
  31500.d0 -19.661612903225805d0
  32000.d0 -18.152222222222225d0
  32500.d0 -18.97444938202247d0
  33000.d0 -17.926913580246914d0
  33500.d0 -17.041772151898734d0
  34000.d0 -18.093658536585366d0
  34500.d0 -19.043333333333337d0
  35000.d0 -19.938736842105264d0
  35500.d0 -19.900000000000002d0
  36000.d0 -18.257976190476192d0
  36500.d0 -20.293333333333333d0
  37000.d0 -20.095208333333332d0
  37500.d0 -20.163999999999998d0
```

```
38000.d0 -19.821075268817204d0
38500.d0 -19.428241758241757d0
39000.d0 -20.2303125d0
39500.d0 -19.973368421052633d0
40000.d0 -20.544795918367345d0
40500.d0 -20.255744680851063d0
41000.d0 -19.26752808988764d0
41500.d0 -19.16090909090909d0
42000.d0 -19.91d0
42500.d0 -20.48783505154639d0
43000.d0 -19.465555555555554d0
43500.d0 -19.411555555555555d0
44000.d0 -19.665714285714284d0
44500.d0 -18.684418604651164d0
45000.d0 -18.926744186046513d0
45500.d0 -18.282530120481930d0
46000.d0 -18.42168674698795d0
46500.d0 -17.5597435897435 9d0
47000.d0 -17.0425d0
47500.d0 -17.25d0
48000.d0 -16.12861111111111d0
48500.d0 -17.493766233766234d0
49000.d0 -17.45565789473684d0
49500.d0 -17.705696202531644d0
50000.d0 -18.95470588235294d0
50500.d0 -19.06344827586207d0
51000.d0 -18.648333333333333d0
51500.d0 -18.907142857142860d0
52000.d0 -19.526022727272725d0
52500.d0 -18.458024691358027d0
53000.d0 -17.96d0
53500.d0 -18.7725d0
54000.d0 -18.156666666666666d0
54500.d0 -18.006835443037975d0
55000.d0 -17.550394736842104d0
55500.d0 -18.36d0
56000.d0 -18.361481481481484d0
56500.d0 -18.214624999999998d0
57000.d0 -19.092142857142857d0
57500.d0 -19.054047619047620d0
58000.d0 -19.218809523809526d0
58500.d0 -19.365d0
59000.d0 -19.417906976744188d0
59500.d0 -20.05d0
60000.d0 -19.093493975903613d0
60500.d0 -19.750227272727273d0
61000.d0 -19.18857142857143d0
61500.d0 -17.843684210526316d0
62000.d0 -18.320126582278480d0
62500.d0 -17.858026315789473d0
63000.d0 -17.662027027027030d0
63500.d0 -17.5472d0
64000.d0 -18.522784810126580d0
64500.d0 -19.232891566265060d0
65000.d0 -19.342530120481930d0
65500.d0 -18.638625d0
66000.d0 -18.973333333333333d0
66500.d0 -19.58d0
67000.d0 -18.766624999999998d0
67500.d0 -18.979367088607596d0
68000.d0 -19.045925925925925d0
68500.d0 -19.709302325581394d0
69000.d0 -18.57909090909091d0
69500.d0 -17.813783783783784d0
70000.d0 -17.707534246575342d0
70500.d0 -18.423636363636366d0
71000.d0 -19.253950617283950d0
71500.d0 -19.888235294117650d0
```

```
72000.d0 -19.850714285714286d0
72500.d0 -19.667108433734942d0
73000.d0 -19.155d0
73500.d0 -20.482758620689655d0
74000.d0 -20.375d0
74500.d0 -20.089176470588235d0
75000.d0 -20.494827586206895d0
75500.d0 -20.732758620689655d0
76000.d0 -19.11d0
76500.d0 -20.90888888888889d0
77000.d0 -20.474534883720928d0
77500.d0 -20.434117647058823d0
78000.d0 -20.876511627906975d0
78500.d0 -20.422941176470587d0
79000.d0 -19.832222222222224d0
79500.d0 -20.580465116279072d0
80000.d0 -20.375180722891564d0
80500.d0 -20.339642857142856d0
81000.d0 -20.695581395348840d0
81500.d0 -20.175714285714285d0
82000.d0 -20.511058823529410d0
82500.d0 -20.735d0
83000.d0 -20.541785714285716d0
83500.d0 -20.238433734939758d0
84000.d0 -20.506265060240963d0
84500.d0 -20.446666666666665d0
85000.d0 -20.177926829268294d0
85500.d0 -20.412804878048780d0
86000.d0 -20.322682926829270d0
86500.d0 -20.710714285714285d0
87000.d0 -20.423658536585364d0
87500.d0 -20.396585365853660d0
88000.d0 -20.764523809523810d0
88500.d0 -19.143684210526317d0
89000.d0 -18.345428571428570d0
89500.d0 -18.101884057971013d0
90000.d0 -16.95d0
90500.d0 -16.142d0
91000.d0 -14.755714285714287d0
91500.d0 -16.580952380952382d0
92000.d0 -16.087704918032788d0
92500.d0 -16.142786852459000d0
93000.d0 -14.903392857142856d0
93500.d0 -13.770769230769230d0
94000.d0 -12.618541666666667d0
94500.d0 -13.167d0
95000.d0 -12.883877551020408d0
95500.d0 -12.56d0
96000.d0 -12.953469387755103d0
96500.d0 -12.996938775510204d0
97000.d0 -12.952244897959183d0
97500.d0 -12.420425531914894d0
98000.d0 -13.2384d0
98500.d0 -12.800416666666667d0
99000.d0 -13.081020408163266d0
99500.d0 -12.246956521739131d0
100000.d0 -12.90375d0
100500.d0 -11.27d0
101000.d0 -13.116595744680852d0
101500.d0 -13.046000000000001d0
102000.d0 -13.514347826086958d0
102500.d0 4.485964300000311d0
103000.d0 4.485964300000311d0
103500.d0 4.485964300000311d0
104000.d0 4.485964300000311d0
104500.d0 4.485964300000311d0
105000.d0 4.485964300000311d0
105500.d0 4.485964300000311d0
```

106000.d0 4.485964300000311d0
106500.d0 4.485964300000311d0
107000.d0 4.485964300000311d0
107500.d0 4.485964300000311d0
108000.d0 4.485964300000311d0
108500.d0 4.485964300000311d0
109000.d0 4.485964300000311d0
109500.d0 4.485964300000311d0
110000.d0 4.485964300000311d0
110500.d0 4.485964300000311d0
111000.d0 4.485964300000311d0
111500.d0 4.485964300000311d0
112000.d0 4.485964300000311d0
112500.d0 4.485964300000311d0
113000.d0 4.485964300000311d0
113500.d0 4.485964300000311d0
114000.d0 4.485964300000311d0
114500.d0 4.485964300000311d0
115000.d0 4.485964300000311d0
115500.d0 4.485964300000311d0
116000.d0 4.485964300000311d0
116500.d0 4.485964300000311d0
117000.d0 4.485964300000311d0
117500.d0 4.485964300000311d0
118000.d0 4.485964300000311d0
118500.d0 4.485964300000311d0
119000.d0 4.485964300000311d0
119500.d0 4.485964300000311d0
120000.d0 4.485964300000311d0
120500.d0 4.485964300000311d0
121000.d0 4.485964300000311d0
121500.d0 4.485964300000311d0
122000.d0 4.485964300000311d0
122500.d0 4.485964300000311d0
123000.d0 4.485964300000311d0
123500.d0 4.485964300000311d0
124000.d0 4.485964300000311d0
124500.d0 4.485964300000311d0
125000.d0 4.485964300000311d0
125500.d0 4.485964300000311d0
126000.d0 4.485964300000311d0
126500.d0 4.485964300000311d0
127000.d0 4.485964300000311d0
127500.d0 4.485964300000311d0
128000.d0 4.485964300000311d0
128500.d0 4.485964300000311d0
129000.d0 4.485964300000311d0
129500.d0 4.485964300000311d0
130000.d0 4.485964300000311d0
130500.d0 4.485964300000311d0
131000.d0 4.485964300000311d0
131500.d0 4.485964300000311d0
132000.d0 4.485964300000311d0
132500.d0 4.485964300000311d0
133000.d0 4.485964300000311d0
133500.d0 4.485964300000311d0
134000.d0 4.485964300000311d0
134500.d0 4.485964300000311d0
135000.d0 4.485964300000311d0
135500.d0 4.485964300000311d0
136000.d0 4.485964300000311d0
136500.d0 4.485964300000311d0
137000.d0 4.485964300000311d0
137500.d0 4.485964300000311d0
138000.d0 4.485964300000311d0
138500.d0 4.485964300000311d0
139000.d0 4.485964300000311d0
139500.d0 4.485964300000311d0

140000.d0 4.485964300000311d0
140500.d0 4.485964300000311d0
141000.d0 4.485964300000311d0
141500.d0 4.485964300000311d0
142000.d0 4.485964300000311d0
142500.d0 4.485964300000311d0
143000.d0 4.485964300000311d0
143500.d0 4.485964300000311d0
144000.d0 4.485964300000311d0
144500.d0 4.485964300000311d0
145000.d0 4.485964300000311d0
145500.d0 4.485964300000311d0
146000.d0 4.485964300000311d0
146500.d0 4.485964300000311d0
147000.d0 4.485964300000311d0
147500.d0 4.485964300000311d0
148000.d0 4.485964300000311d0
148500.d0 4.485964300000311d0
149000.d0 4.485964300000311d0
149500.d0 4.485964300000311d0
150000.d0 -17.4212d0
150500.d0 -17.26013698630137d0
151000.d0 -16.498857142857144d0
151500.d0 -17.498d0
152000.d0 -16.83d0
152500.d0 -17.11d0
153000.d0 -16.6056338028169d0
153500.d0 -16.359142857142857d0
154000.d0 -15.811044776119402d0
154500.d0 -14.846935483870967d0
155000.d0 -15.195076923076924d0
155500.d0 -15.205373134328358d0
156000.d0 -16.93041095890411d0
156500.d0 -15.865588235294117d0
157000.d0 -15.31846153846154d0
157500.d0 -16.71d0
158000.d0 -15.940000000000001d0
158500.d0 -15.914d0
159000.d0 -17.265d0
159500.d0 -16.844594594594597d0
160000.d0 -16.413424657534247d0
160500.d0 -17.849493670886073d0
161000.d0 -18.389518072289157d0
161500.d0 -18.693411764705882d0
162000.d0 -18.991264367816093d0
162500.d0 -19.12125d0
163000.d0 -17.875185185185185d0
163500.d0 -17.515897435897436d0
164000.d0 -17.43632911392405d0
164500.d0 -17.696582278481014d0
165000.d0 -17.972962962962963d0
165500.d0 -17.394814814814815d0
166000.d0 -18.884137931034484d0
166500.d0 -19.661612903225805d0
167000.d0 -18.152222222222225d0
167500.d0 -18.97449438202247d0
168000.d0 -17.926913580246914d0
168500.d0 -17.041772151898734d0
169000.d0 -18.093658536585366d0
169500.d0 -19.043333333333337d0
170000.d0 -19.938736842105264d0
170500.d0 -19.900000000000002d0
171000.d0 -18.257976190476192d0
171500.d0 -20.293333333333333d0
172000.d0 -20.095208333333332d0
172500.d0 -20.163999999999998d0
173000.d0 -19.821075268817204d0
173500.d0 -19.428241758241757d0

174000.d0 -20.2303125d0
174500.d0 -19.973368421052633d0
175000.d0 -20.544795918367345d0
175500.d0 -20.255744680851063d0
176000.d0 -19.267528088764d0
176500.d0 -19.16090909090909d0
177000.d0 -19.91d0
177500.d0 -20.48783505154639d0
178000.d0 -19.465555555555554d0
178500.d0 -19.411555555555555d0
179000.d0 -19.665714285714284d0
179500.d0 -18.684418604651164d0
180000.d0 -18.926744186046513d0
180500.d0 -18.28253012048193d0
181000.d0 -18.42168674698795d0
181500.d0 -17.55974358974359d0
182000.d0 -17.0425d0
182500.d0 -17.25d0
183000.d0 -16.12861111111111d0
183500.d0 -17.493766233766234d0
184000.d0 -17.455657894736 84d0
184500.d0 -17.705696202531644d0
185000.d0 -18.95470588235294d0
185500.d0 -19.06344827586207d0
186000.d0 -18.648333333333333d0
186500.d0 -18.907142857142 86d0
187000.d0 -19.526022727272725d0
187500.d0 -18.458024691358027d0
188000.d0 -17.96d0
188500.d0 -18.7725d0
189000.d0 -18.156666666666666d0
189500.d0 -18.006835443037975d0
190000.d0 -17.550394736842104d0
190500.d0 -18.36d0
191000.d0 -18.361481481481484d0
191500.d0 -18.214624999999998d0
192000.d0 -19.092142857142857d0
192500.d0 -19.05404761904762d0
193000.d0 -19.218809523809526d0
193500.d0 -19.365d0
194000.d0 -19.417906976744188d0
194500.d0 -20.05d0
195000.d0 -19.093493975903613d0
195500.d0 -19.750227272727273d0
196000.d0 -19.18857142857143d0
196500.d0 -17.843684210526316d0
197000.d0 -18.320126582278 48d0
197500.d0 -17.858026315789473d0
198000.d0 -17.66202702702703d0
198500.d0 -17.5472d0
199000.d0 -18.522784810126 58d0
199500.d0 -19.232891566265 06d0
200000.d0 -19.342530120481 93d0
200500.d0 -18.638625d0
201000.d0 -18.973333333333333d0
201500.d0 -19.58d0
202000.d0 -18.766624999999998d0
202500.d0 -18.979367088607596d0
203000.d0 -19.045925925925925d0
203500.d0 -19.709302325581394d0
204000.d0 -18.57909090909091d0
204500.d0 -17.813783783783784d0
205000.d0 -17.707534246575342d0
205500.d0 -18.423636363636366d0
206000.d0 -19.25395061728395d0
206500.d0 -19.88823529411765d0
207000.d0 -19.850714285714286d0
207500.d0 -19.667108433734942d0
208000.d0 -19.155d0
208500.d0 -20.482758620689655d0
209000.d0 -20.375d0
209500.d0 -20.089176470588235d0
210000.d0 -20.494827586206895d0
210500.d0 -20.732758620689655d0
211000.d0 -19.11d0
211500.d0 -20.90888888888889d0
212000.d0 -20.4745348837209 28d0
212500.d0 -20.434117647058823d0
213000.d0 -20.876511627906975d0
213500.d0 -20.422941176470587d0
214000.d0 -19.832222222222224d0
214500.d0 -20.580465116279072d0
215000.d0 -20.375180722891564d0
215500.d0 -20.339642857142856d0
216000.d0 -20.6955813953488 4d0
216500.d0 -20.175714285714285d0
217000.d0 -20.51105882352941d0
217500.d0 -20.735d0
218000.d0 -20.541785714285716d0
218500.d0 -20.238433734939758d0
219000.d0 -20.506265060240963d0
219500.d0 -20.446666666666665d0
220000.d0 -20.177926829268294d0
220500.d0 -20.412804878048 78d0
221000.d0 -20.322682926829 27d0
221500.d0 -20.710714285714285d0
222000.d0 -20.423658536585364d0
222500.d0 -20.396585365853 66d0
223000.d0 -20.764523809523 81d0
223500.d0 -19.143684210526317d0
224000.d0 -18.345428571428 57d0
224500.d0 -18.101884057971013d0
225000.d0 -16.95d0
225500.d0 -16.142d0
226000.d0 -14.755714285714287d0
226500.d0 -16.580952380952382d0
227000.d0 -16.087704918032788d0
227500.d0 -16.1427868852459d0
228000.d0 -14.903392857142856d0
228500.d0 -13.770769230769 23d0
229000.d0 -12.618541666666667d0
229500.d0 -13.167d0
230000.d0 -12.883877551020408d0
230500.d0 -12.56d0
231000.d0 -12.953469387755103d0
231500.d0 -12.996938775510204d0
232000.d0 -12.952244897959183d0
232500.d0 -12.420425531914894d0
233000.d0 -13.2384d0
233500.d0 -12.800416666666667d0
234000.d0 -13.081020408163266d0
234500.d0 -12.246956521739131d0
235000.d0 -12.90375d0
235500.d0 -11.27d0
236000.d0 -13.116595744680852d0
236500.d0 -13.046000000000001d0
237000.d0 -13.514347826086958d0
237500.d0 4.485964300000311d0
238000.d0 4.485964300000311d0
238500.d0 4.485964300000311d0
239000.d0 4.485964300000311d0
239500.d0 4.485964300000311d0
240000.d0 4.485964300000311d0
240500.d0 4.485964300000311d0
241000.d0 4.485964300000311d0
241500.d0 4.485964300000311d0

242000.d0 4.485964300000311d0
242500.d0 4.485964300000311d0
243000.d0 4.485964300000311d0
243500.d0 4.485964300000311d0
244000.d0 4.485964300000311d0
244500.d0 4.485964300000311d0
245000.d0 4.485964300000311d0
245500.d0 4.485964300000311d0
246000.d0 4.485964300000311d0
246500.d0 4.485964300000311d0
247000.d0 4.485964300000311d0
247500.d0 4.485964300000311d0
248000.d0 4.485964300000311d0
248500.d0 4.485964300000311d0
249000.d0 4.485964300000311d0
249500.d0 4.485964300000311d0
250000.d0 4.485964300000311d0
250500.d0 4.485964300000311d0
251000.d0 4.485964300000311d0
251500.d0 4.485964300000311d0
252000.d0 4.485964300000311d0
252500.d0 4.485964300000311d0
253000.d0 4.485964300000311d0
253500.d0 4.485964300000311d0
254000.d0 4.485964300000311d0
254500.d0 4.485964300000311d0
255000.d0 4.485964300000311d0
255500.d0 4.485964300000311d0
256000.d0 4.485964300000311d0
256500.d0 4.485964300000311d0
257000.d0 4.485964300000311d0
257500.d0 4.485964300000311d0
258000.d0 4.485964300000311d0
258500.d0 4.485964300000311d0
259000.d0 4.485964300000311d0
259500.d0 4.485964300000311d0
260000.d0 4.485964300000311d0
260500.d0 4.485964300000311d0
261000.d0 4.485964300000311d0
261500.d0 4.485964300000311d0
262000.d0 4.485964300000311d0
262500.d0 4.485964300000311d0
263000.d0 4.485964300000311d0
263500.d0 4.485964300000311d0
264000.d0 4.485964300000311d0
264500.d0 4.485964300000311d0
265000.d0 4.485964300000311d0
265500.d0 4.485964300000311d0
266000.d0 4.485964300000311d0
266500.d0 4.485964300000311d0
267000.d0 4.485964300000311d0
267500.d0 4.485964300000311d0
268000.d0 4.485964300000311d0
268500.d0 4.485964300000311d0
269000.d0 4.485964300000311d0
269500.d0 4.485964300000311d0
270000.d0 4.485964300000311d0
270500.d0 4.485964300000311d0
271000.d0 4.485964300000311d0
271500.d0 4.485964300000311d0
272000.d0 4.485964300000311d0
272500.d0 4.485964300000311d0
273000.d0 4.485964300000311d0
273500.d0 4.485964300000311d0
274000.d0 4.485964300000311d0
274500.d0 4.485964300000311d0
275000.d0 4.485964300000311d0
275500.d0 4.485964300000311d0
276000.d0 4.485964300000311d0
276500.d0 4.485964300000311d0
277000.d0 4.485964300000311d0
277500.d0 4.485964300000311d0
278000.d0 4.485964300000311d0
278500.d0 4.485964300000311d0
279000.d0 4.485964300000311d0
279500.d0 4.485964300000311d0
280000.d0 4.485964300000311d0
280500.d0 4.485964300000311d0
281000.d0 4.485964300000311d0
281500.d0 4.485964300000311d0
282000.d0 4.485964300000311d0
282500.d0 4.485964300000311d0
283000.d0 4.485964300000311d0
283500.d0 4.485964300000311d0
284000.d0 4.485964300000311d0
284500.d0 4.485964300000311d0
285000.d0 -17.4212d0
285500.d0 -17.26013698630137d0
286000.d0 -16.498857142857144d0
286500.d0 -17.498d0
287000.d0 -16.83d0
287500.d0 -17.11d0
288000.d0 -16.6056338028169d0
288500.d0 -16.359142857142857d0
289000.d0 -15.811044776119402d0
289500.d0 -14.846935483870967d0
290000.d0 -15.195076923076924d0
290500.d0 -15.205373134328358d0
291000.d0 -16.93041095890411d0
291500.d0 -15.865588235294117d0
292000.d0 -15.31846153846154d0
292500.d0 -16.71d0
293000.d0 -15.940000000000001d0
293500.d0 -15.914d0
294000.d0 -17.265d0
294500.d0 -16.844594594594597d0
295000.d0 -16.413424657534247d0
295500.d0 -17.849493670886073d0
296000.d0 -18.389518072289157d0
296500.d0 -18.693411764705882d0
297000.d0 -18.991264367816093d0
297500.d0 -19.12125d0
298000.d0 -17.875185185185185d0
298500.d0 -17.515897435897436d0
299000.d0 -17.43632911392405d0
299500.d0 -17.696582278481014d0
300000.d0 -17.972962962962963d0
300500.d0 -17.394814814814815d0
301000.d0 -18.884137931034484d0
301500.d0 -19.661612903225805d0
302000.d0 -18.152222222222225d0
302500.d0 -18.97449438202247d0
303000.d0 -17.926913580246914d0
303500.d0 -17.041772151898734d0
304000.d0 -18.093658536585366d0
304500.d0 -19.043333333333337d0
305000.d0 -19.938736842105264d0
305500.d0 -19.900000000000002d0
306000.d0 -18.257976190476192d0
306500.d0 -20.293333333333333d0
307000.d0 -20.095208333333332d0
307500.d0 -20.163999999999998d0
308000.d0 -19.8210752688172O4d0
308500.d0 -19.428241758241757d0
309000.d0 -20.2303125d0
309500.d0 -19.973368421052633d0

310000.d0 -20.544795918367345d0
310500.d0 -20.255744680851063d0
311000.d0 -19.26752808988764d0
311500.d0 -19.16090909090909d0
312000.d0 -19.91d0
312500.d0 -20.48783505154639d0
313000.d0 -19.465555555555554d0
313500.d0 -19.411555555555555d0
314000.d0 -19.6657142857142 84d0
314500.d0 -18.684418604651164d0
315000.d0 -18.926744186046513d0
315500.d0 -18.28253012048193d0
316000.d0 -18.42168674698795d0
316500.d0 -17.559743589743 59d0
317000.d0 -17.0425d0
317500.d0 -17.25d0
318000.d0 -16.12861111111111d0
318500.d0 -17.493766233766234d0
319000.d0 -17.455657894736 84d0
319500.d0 -17.705696202531644d0
320000.d0 -18.954705882352 94d0
320500.d0 -19.06344827586207d0
321000.d0 -18.648333333333333d0
321500.d0 -18.907142857142 86d0
322000.d0 -19.526022727272725d0
322500.d0 -18.458024691358027d0
323000.d0 -17.96d0
323500.d0 -18.7725d0
324000.d0 -18.156666666666666d0
324500.d0 -18.006835443037975d0
325000.d0 -17.550394736842104d0
325500.d0 -18.36d0
326000.d0 -18.361481481481484d0
326500.d0 -18.214624999999998d0
327000.d0 -19.092142857142857d0
327500.d0 -19.05404761904762d0
328000.d0 -19.218809523809526d0
328500.d0 -19.365d0
329000.d0 -19.417906976744188d0
329500.d0 -20.05d0
330000.d0 -19.093493975903613d0
330500.d0 -19.750227272727273d0
331000.d0 -19.18857142857143d0
331500.d0 -17.843684210526316d0
332000.d0 -18.320126582278 48d0
332500.d0 -17.858026315789473d0
333000.d0 -17.66202702702703d0
333500.d0 -17.5472d0
334000.d0 -18.52278481012658d0
334500.d0 -19.232891566265 06d0
335000.d0 -19.34253012048193d0
335500.d0 -18.638625d0
336000.d0 -18.973333333333333d0
336500.d0 -19.58d0
337000.d0 -18.766624999999998d0
337500.d0 -18.979367088607596d0
338000.d0 -19.045925925925925d0
338500.d0 -19.709302325581394d0
339000.d0 -18.57909090909091d0
339500.d0 -17.813783783783784d0
340000.d0 -17.707534246575342d0
340500.d0 -18.423636363636366d0
341000.d0 -19.25395061728395d0
341500.d0 -19.888235294117 65d0
342000.d0 -19.850714285714286d0
342500.d0 -19.667108433734942d0
343000.d0 -19.155d0
343500.d0 -20.482758620689655d0

344000.d0 -20.375d0
344500.d0 -20.089176470588235d0
345000.d0 -20.494827586206895d0
345500.d0 -20.732758620689655d0
346000.d0 -19.11d0
346500.d0 -20.90888888888889d0
347000.d0 -20.474534883720928d0
347500.d0 -20.434117647058823d0
348000.d0 -20.876511627906975d0
348500.d0 -20.422941176470587d0
349000.d0 -19.832222222222224d0
349500.d0 -20.580465116279072d0
350000.d0 -20.375180722891564d0
350500.d0 -20.339642857142856d0
351000.d0 -20.69558139534884d0
351500.d0 -20.175714285714285d0
352000.d0 -20.51105882352941d0
352500.d0 -20.735d0
353000.d0 -20.541785714285716d0
353500.d0 -20.238433734939758d0
354000.d0 -20.506265060240963d0
354500.d0 -20.446666666666665d0
355000.d0 -20.177926829268294d0
355500.d0 -20.412804878048 78d0
356000.d0 -20.32268292682927d0
356500.d0 -20.710714285714285d0
357000.d0 -20.423658536585364d0
357500.d0 -20.396585365853 66d0
358000.d0 -20.76452380952381d0
358500.d0 -19.143684210526317d0
359000.d0 -18.34542857142857d0
359500.d0 -18.101884057971013d0
360000.d0 -16.95d0
360500.d0 -16.142d0
361000.d0 -14.755714285714287d0
361500.d0 -16.580952380952382d0
362000.d0 -16.087704918032788d0
362500.d0 -16.1427868852459d0
363000.d0 -14.903392857142856d0
363500.d0 -13.770769230769 23d0
364000.d0 -12.618541666666667d0
364500.d0 -13.167d0
365000.d0 -12.883877551020408d0
365500.d0 -12.56d0
366000.d0 -12.953469387755103d0
366500.d0 -12.996938775510204d0
367000.d0 -12.952244897959183d0
367500.d0 -12.420425531914894d0
368000.d0 -13.2384d0
368500.d0 -12.800416666666667d0
369000.d0 -13.081020408163266d0
369500.d0 -12.246956521739131d0
370000.d0 -12.90375d0
370500.d0 -11.27d0
371000.d0 -13.116595744680852d0
371500.d0 -13.046000000000001d0
372000.d0 -13.514347826086958d0
372500.d0 4.485964300000311d0
373000.d0 4.485964300000311d0
373500.d0 4.485964300000311d0
374000.d0 4.485964300000311d0
374500.d0 4.485964300000311d0
375000.d0 4.485964300000311d0
375500.d0 4.485964300000311d0
376000.d0 4.485964300000311d0
376500.d0 4.485964300000311d0
377000.d0 4.485964300000311d0
377500.d0 4.485964300000311d0

378000.d0 4.485964300000311d0
378500.d0 4.485964300000311d0
379000.d0 4.485964300000311d0
379500.d0 4.485964300000311d0
380000.d0 4.485964300000311d0
380500.d0 4.485964300000311d0
381000.d0 4.485964300000311d0
381500.d0 4.485964300000311d0
382000.d0 4.485964300000311d0
382500.d0 4.485964300000311d0
383000.d0 4.485964300000311d0
383500.d0 4.485964300000311d0
384000.d0 4.485964300000311d0
384500.d0 4.485964300000311d0
385000.d0 4.485964300000311d0
385500.d0 4.485964300000311d0
386000.d0 4.485964300000311d0
386500.d0 4.485964300000311d0
387000.d0 4.485964300000311d0
387500.d0 4.485964300000311d0
388000.d0 4.485964300000311d0
388500.d0 4.485964300000311d0
389000.d0 4.485964300000311d0
389500.d0 4.485964300000311d0
390000.d0 4.485964300000311d0
390500.d0 4.485964300000311d0
391000.d0 4.485964300000311d0
391500.d0 4.485964300000311d0
392000.d0 4.485964300000311d0
392500.d0 4.485964300000311d0
393000.d0 4.485964300000311d0
393500.d0 4.485964300000311d0
394000.d0 4.485964300000311d0
394500.d0 4.485964300000311d0
395000.d0 4.485964300000311d0
395500.d0 4.485964300000311d0
396000.d0 4.485964300000311d0
396500.d0 4.485964300000311d0
397000.d0 4.485964300000311d0
397500.d0 4.485964300000311d0
398000.d0 4.485964300000311d0
398500.d0 4.485964300000311d0
399000.d0 4.485964300000311d0
399500.d0 4.485964300000311d0
400000.d0 4.485964300000311d0
400500.d0 4.485964300000311d0
401000.d0 4.485964300000311d0
401500.d0 4.485964300000311d0
402000.d0 4.485964300000311d0
402500.d0 4.485964300000311d0
403000.d0 4.485964300000311d0
403500.d0 4.485964300000311d0
404000.d0 4.485964300000311d0
404500.d0 4.485964300000311d0
405000.d0 4.485964300000311d0
405500.d0 4.485964300000311d0
406000.d0 4.485964300000311d0
406500.d0 4.485964300000311d0
407000.d0 4.485964300000311d0
407500.d0 4.485964300000311d0
408000.d0 4.485964300000311d0
408500.d0 4.485964300000311d0
409000.d0 4.485964300000311d0
409500.d0 4.485964300000311d0
410000.d0 4.485964300000311d0
410500.d0 4.485964300000311d0
411000.d0 4.485964300000311d0
411500.d0 4.485964300000311d0

412000.d0 4.485964300000311d0
412500.d0 4.485964300000311d0
413000.d0 4.485964300000311d0
413500.d0 4.485964300000311d0
414000.d0 4.485964300000311d0
414500.d0 4.485964300000311d0
415000.d0 4.485964300000311d0
415500.d0 4.485964300000311d0
416000.d0 4.485964300000311d0
416500.d0 4.485964300000311d0
417000.d0 4.485964300000311d0
417500.d0 4.485964300000311d0
418000.d0 4.485964300000311d0
418500.d0 4.485964300000311d0
419000.d0 4.485964300000311d0
419500.d0 4.485964300000311d0
420000.d0 -17.4212d0
420500.d0 -17.26013698630137d0
421000.d0 -16.498857142857144d0
421500.d0 -17.498d0
422000.d0 -16.83d0
422500.d0 -17.11d0
423000.d0 -16.6056338028169d0
423500.d0 -16.359142857142857d0
424000.d0 -15.811044776119402d0
424500.d0 -14.846935483870967d0
425000.d0 -15.195076923076924d0
425500.d0 -15.205373134328358d0
426000.d0 -16.93041095890411d0
426500.d0 -15.865588235294117d0
427000.d0 -15.31846153846154d0
427500.d0 -16.71d0
428000.d0 -15.940000000000001d0
428500.d0 -15.914d0
429000.d0 -17.265d0
429500.d0 -16.844594594594597d0
430000.d0 -16.413424657534247d0
430500.d0 -17.849493670886073d0
431000.d0 -18.389518072289157d0
431500.d0 -18.693411764705882d0
432000.d0 -18.991264367816093d0
432500.d0 -19.12125d0
433000.d0 -17.875185185185185d0
433500.d0 -17.515897435897436d0
434000.d0 -17.43632911392405d0
434500.d0 -17.696582278481014d0
435000.d0 -17.972962962962963d0
435500.d0 -17.394814814814815d0
436000.d0 -18.8841379310344 84d0
436500.d0 -19.661612903225805d0
437000.d0 -18.152222222222225d0
437500.d0 -18.97449438202247d0
438000.d0 -17.926913580246914d0
438500.d0 -17.041772151898734d0
439000.d0 -18.093658536585366d0
439500.d0 -19.043333333333337d0
440000.d0 -19.938736842105264d0
440500.d0 -19.900000000000002d0
441000.d0 -18.257976190476192d0
441500.d0 -20.293333333333333d0
442000.d0 -20.095208333333332d0
442500.d0 -20.163999999999998d0
443000.d0 -19.821075268817204d0
443500.d0 -19.428241758241757d0
444000.d0 -20.2303125d0
444500.d0 -19.973368421052633d0
445000.d0 -20.544795918367345d0
445500.d0 -20.255744680851063d0

446000.d0 -19.26752808988764d0
446500.d0 -19.16090909090909d0
447000.d0 -19.91d0
447500.d0 -20.48783505154639d0
448000.d0 -19.465555555555554d0
448500.d0 -19.411555555555555d0
449000.d0 -19.665714285714284d0
449500.d0 -18.684418604651164d0
450000.d0 -18.926744186046513d0
450500.d0 -18.28253012048193d0
451000.d0 -18.42168674698795d0
451500.d0 -17.55974358974359d0
452000.d0 -17.0425d0
452500.d0 -17.25d0
453000.d0 -16.12861111111111d0
453500.d0 -17.493766233766234d0
454000.d0 -17.455657894736 84d0
454500.d0 -17.705696202531644d0
455000.d0 -18.95470588235294d0
455500.d0 -19.06344827586207d0
456000.d0 -18.648333333333333d0
456500.d0 -18.907142857142 86d0
457000.d0 -19.526022727272725d0
457500.d0 -18.458024691358027d0
458000.d0 -17.96d0
458500.d0 -18.7725d0
459000.d0 -18.156666666666666d0
459500.d0 -18.006835443037975d0
460000.d0 -17.55039473684 2104d0
460500.d0 -18.36d0
461000.d0 -18.361481481481484d0
461500.d0 -18.214624999999998d0
462000.d0 -19.092142857142857d0
462500.d0 -19.05404761904762d0
463000.d0 -19.218809523809526d0
463500.d0 -19.365d0
464000.d0 -19.417906976744188d0
464500.d0 -20.05d0
465000.d0 -19.093493975903613d0
465500.d0 -19.750227272727273d0
466000.d0 -19.18857142857143d0
466500.d0 -17.843684210526316d0
467000.d0 -18.32012658227848d0
467500.d0 -17.858026315789473d0
468000.d0 -17.66202702702703d0
468500.d0 -17.5472d0
469000.d0 -18.522784810126 58d0
469500.d0 -19.232891566265 06d0
470000.d0 -19.342530120481 93d0
470500.d0 -18.638625d0
471000.d0 -18.973333333333333d0
471500.d0 -19.58d0
472000.d0 -18.766624999999998d0
472500.d0 -18.979367088607596d0
473000.d0 -19.045925925925925d0
473500.d0 -19.709302325581394d0
474000.d0 -18.579090909090 91d0
474500.d0 -17.813783783783784d0
475000.d0 -17.707534246575342d0
475500.d0 -18.423636363636366d0
476000.d0 -19.25395061728395d0
476500.d0 -19.88823529411765d0
477000.d0 -19.850714285714286d0
477500.d0 -19.667108433734942d0
478000.d0 -19.155d0
478500.d0 -20.482758620689655d0
479000.d0 -20.375d0
479500.d0 -20.089176470588235d0
480000.d0 -20.494827586206895d0
480500.d0 -20.732758620689655d0
481000.d0 -19.11d0
481500.d0 -20.90888888888889d0
482000.d0 -20.474534883720928d0
482500.d0 -20.434117647058823d0
483000.d0 -20.876511627906975d0
483500.d0 -20.422941176470587d0
484000.d0 -19.832222222222224d0
484500.d0 -20.580465116279072d0
485000.d0 -20.375180722891564d0
485500.d0 -20.339642857142856d0
486000.d0 -20.695581395348 84d0
486500.d0 -20.175714285714285d0
487000.d0 -20.511058823529 41d0
487500.d0 -20.735d0
488000.d0 -20.541785714285716d0
488500.d0 -20.238433734939758d0
489000.d0 -20.506265060240963d0
489500.d0 -20.446666666666665d0
490000.d0 -20.177926829268294d0
490500.d0 -20.412804878048 78d0
491000.d0 -20.322682926829 27d0
491500.d0 -20.710714285714285d0
492000.d0 -20.423658536585364d0
492500.d0 -20.396585365853 66d0
493000.d0 -20.764523809523 81d0
493500.d0 -19.143684210526317d0
494000.d0 -18.345428571428 57d0
494500.d0 -18.101884057971013d0
495000.d0 -16.95d0
495500.d0 -16.142d0
496000.d0 -14.755714285714287d0
496500.d0 -16.580952380952382d0
497000.d0 -16.087704918032788d0
497500.d0 -16.142786885245 9d0
498000.d0 -14.903392857142856d0
498500.d0 -13.770769230769 23d0
499000.d0 -12.618541666666667d0
499500.d0 -13.167d0
500000.d0 -12.883877551020408d0
500500.d0 -12.56d0
501000.d0 -12.953469387755103d0
501500.d0 -12.996938775510204d0
502000.d0 -12.952244897959183d0
502500.d0 -12.420425531914894d0
503000.d0 -13.2384d0
503500.d0 -12.800416666666667d0
504000.d0 -13.081020408163266d0
504500.d0 -12.246956521739131d0
505000.d0 -12.90375d0
505500.d0 -11.27d0
506000.d0 -13.116595744680852d0
506500.d0 -13.046000000000001d0
507000.d0 -13.514347826086958d0
507500.d0 4.485964300000311d0
508000.d0 4.485964300000311d0
508500.d0 4.485964300000311d0
509000.d0 4.485964300000311d0
509500.d0 4.485964300000311d0
510000.d0 4.485964300000311d0
510500.d0 4.485964300000311d0
511000.d0 4.485964300000311d0
511500.d0 4.485964300000311d0
512000.d0 4.485964300000311d0
512500.d0 4.485964300000311d0
513000.d0 4.485964300000311d0
513500.d0 4.485964300000311d0

514000.d0 4.485964300000311d0
514500.d0 4.485964300000311d0
515000.d0 4.485964300000311d0
515500.d0 4.485964300000311d0
516000.d0 4.485964300000311d0
516500.d0 4.485964300000311d0
517000.d0 4.485964300000311d0
517500.d0 4.485964300000311d0
518000.d0 4.485964300000311d0
518500.d0 4.485964300000311d0
519000.d0 4.485964300000311d0
519500.d0 4.485964300000311d0
520000.d0 4.485964300000311d0
520500.d0 4.485964300000311d0
521000.d0 4.485964300000311d0
521500.d0 4.485964300000311d0
522000.d0 4.485964300000311d0
522500.d0 4.485964300000311d0
523000.d0 4.485964300000311d0
523500.d0 4.485964300000311d0
524000.d0 4.485964300000311d0
524500.d0 4.485964300000311d0
525000.d0 4.485964300000311d0
525500.d0 4.485964300000311d0
526000.d0 4.485964300000311d0
526500.d0 4.485964300000311d0
527000.d0 4.485964300000311d0
527500.d0 4.485964300000311d0
528000.d0 4.485964300000311d0
528500.d0 4.485964300000311d0
529000.d0 4.485964300000311d0
529500.d0 4.485964300000311d0
530000.d0 4.485964300000311d0
530500.d0 4.485964300000311d0
531000.d0 4.485964300000311d0
531500.d0 4.485964300000311d0
532000.d0 4.485964300000311d0
532500.d0 4.485964300000311d0
533000.d0 4.485964300000311d0
533500.d0 4.485964300000311d0
534000.d0 4.485964300000311d0
534500.d0 4.485964300000311d0
535000.d0 4.485964300000311d0
535500.d0 4.485964300000311d0
536000.d0 4.485964300000311d0
536500.d0 4.485964300000311d0
537000.d0 4.485964300000311d0
537500.d0 4.485964300000311d0
538000.d0 4.485964300000311d0
538500.d0 4.485964300000311d0
539000.d0 4.485964300000311d0
539500.d0 4.485964300000311d0
540000.d0 4.485964300000311d0
540500.d0 4.485964300000311d0
541000.d0 4.485964300000311d0
541500.d0 4.485964300000311d0
542000.d0 4.485964300000311d0
542500.d0 4.485964300000311d0
543000.d0 4.485964300000311d0
543500.d0 4.485964300000311d0
544000.d0 4.485964300000311d0
544500.d0 4.485964300000311d0
545000.d0 4.485964300000311d0
545500.d0 4.485964300000311d0
546000.d0 4.485964300000311d0
546500.d0 4.485964300000311d0
547000.d0 4.485964300000311d0
547500.d0 4.485964300000311d0

548000.d0 4.485964300000311d0
548500.d0 4.485964300000311d0
549000.d0 4.485964300000311d0
549500.d0 4.485964300000311d0
550000.d0 4.485964300000311d0
550500.d0 4.485964300000311d0
551000.d0 4.485964300000311d0
551500.d0 4.485964300000311d0
552000.d0 4.485964300000311d0
552500.d0 4.485964300000311d0
553000.d0 4.485964300000311d0
553500.d0 4.485964300000311d0
554000.d0 4.485964300000311d0
554500.d0 4.485964300000311d0
555000.d0 -17.4212d0
555500.d0 -17.26013698630137d0
556000.d0 -16.498857142857144d0
556500.d0 -17.498d0
557000.d0 -16.83d0
557500.d0 -17.11d0
558000.d0 -16.6056338028169d0
558500.d0 -16.359142857142857d0
559000.d0 -15.811044776119402d0
559500.d0 -14.846935483870967d0
560000.d0 -15.195076923076924d0
560500.d0 -15.205373134328358d0
561000.d0 -16.9304109589041d0
561500.d0 -15.865588235294117d0
562000.d0 -15.31846153846154d0
562500.d0 -16.71d0
563000.d0 -15.940000000000001d0
563500.d0 -15.914d0
564000.d0 -17.265d0
564500.d0 -16.844594594594597d0
565000.d0 -16.413424657534247d0
565500.d0 -17.849493670886073d0
566000.d0 -18.389518072289157d0
566500.d0 -18.693411764705882d0
567000.d0 -18.991264367816093d0
567500.d0 -19.12125d0
568000.d0 -17.875185185185185d0
568500.d0 -17.515897435897436d0
569000.d0 -17.43632911392405d0
569500.d0 -17.696582278481014d0
570000.d0 -17.972962962962963d0
570500.d0 -17.394814814814815d0
571000.d0 -18.884137931034484d0
571500.d0 -19.661612903225805d0
572000.d0 -18.152222222222225d0
572500.d0 -18.97449438202247d0
573000.d0 -17.926913580246914d0
573500.d0 -17.041772151898734d0
574000.d0 -18.093658536585366d0
574500.d0 -19.043333333333337d0
575000.d0 -19.938736842105264d0
575500.d0 -19.900000000000002d0
576000.d0 -18.257976190476192d0
576500.d0 -20.293333333333333d0
577000.d0 -20.095208333333332d0
577500.d0 -20.163999999999998d0
578000.d0 -19.8210752688172O4d0
578500.d0 -19.428241758241757d0
579000.d0 -20.2303125d0
579500.d0 -19.973368421052633d0
580000.d0 -20.5447959183673450
580500.d0 -20.255744680851063d0
581000.d0 -19.26752808988764d0
581500.d0 -19.16090909090909d0

```
582000.d0 -19.91d0
582500.d0 -20.48783505154639d0
583000.d0 -19.465555555555554d0
583500.d0 -19.411555555555555d0
584000.d0 -19.665714285714284d0
584500.d0 -18.684418604651164d0
585000.d0 -18.926744186046513d0
585500.d0 -18.28253012048193d0
586000.d0 -18.42168674698795d0
586500.d0 -17.559743589743590d0
587000.d0 -17.0425d0
587500.d0 -17.25d0
588000.d0 -16.12861111111111d0
588500.d0 -17.493766233766234d0
589000.d0 -17.45565789473684d0
589500.d0 -17.705696202531644d0
590000.d0 -18.954705882352940d0
590500.d0 -19.06344827586207d0
591000.d0 -18.648333333333333d0
591500.d0 -18.907142857142860d0
592000.d0 -19.526022727272725d0
592500.d0 -18.458024691358027d0
593000.d0 -17.96d0
593500.d0 -18.7725d0
594000.d0 -18.156666666666666d0
594500.d0 -18.006835443037975d0
595000.d0 -17.550394736842104d0
595500.d0 -18.36d0
596000.d0 -18.361481481481484d0
596500.d0 -18.214624999999998d0
597000.d0 -19.092142857142857d0
597500.d0 -19.05404761904762d0
598000.d0 -19.218809523809526d0
598500.d0 -19.365d0
599000.d0 -19.417906976744188d0
599500.d0 -20.05d0
600000.d0 -19.093493975903613d0
600500.d0 -19.750227272727273d0
601000.d0 -19.18857142857143d0
601500.d0 -17.843684210526316d0
602000.d0 -18.3201265822784 8d0
602500.d0 -17.858026315789473d0
603000.d0 -17.66202702702703d0
603500.d0 -17.5472d0
604000.d0 -18.52278481012658d0
604500.d0 -19.23289156626506d0
605000.d0 -19.34253012048193d0
605500.d0 -18.638625d0
606000.d0 -18.973333333333333d0
606500.d0 -19.58d0
607000.d0 -18.766624999999998d0
607500.d0 -18.979367088607596d0
608000.d0 -19.045925925925925d0
608500.d0 -19.709302325581394d0
609000.d0 -18.57909090909091d0
609500.d0 -17.813783783783784d0
610000.d0 -17.707534246575342d0
610500.d0 -18.423636363636366d0
611000.d0 -19.25395061728395d0
611500.d0 -19.88823529411765d0
612000.d0 -19.850714285714286d0
612500.d0 -19.667108433734942d0
613000.d0 -19.155d0
613500.d0 -20.482758620689655d0
614000.d0 -20.375d0
614500.d0 -20.089176470588235d0
615000.d0 -20.494827586206895d0
615500.d0 -20.732758620689655d0
```

```
616000.d0 -19.11d0
616500.d0 -20.90888888888889d0
617000.d0 -20.474534883720928d0
617500.d0 -20.434117647058823d0
618000.d0 -20.876511627906975d0
618500.d0 -20.422941176470587d0
619000.d0 -19.832222222222224d0
619500.d0 -20.580465116279072d0
620000.d0 -20.3751807228915 64d0
620500.d0 -20.339642857142856d0
621000.d0 -20.69558139534884d0
621500.d0 -20.175714285714285d0
622000.d0 -20.51105882352941d0
622500.d0 -20.735d0
623000.d0 -20.541785714285716d0
623500.d0 -20.238433734939758d0
624000.d0 -20.506265060240963d0
624500.d0 -20.446666666666665d0
625000.d0 -20.177926829268294d0
625500.d0 -20.41280487804878d0
626000.d0 -20.32268292682927d0
626500.d0 -20.710714285714285d0
627000.d0 -20.423658536585364d0
627500.d0 -20.396585365853 66d0
628000.d0 -20.76452380952381d0
628500.d0 -19.143684210526317d0
629000.d0 -18.34542857142857d0
629500.d0 -18.101884057971013d0
630000.d0 -16.95d0
630500.d0 -16.142d0
631000.d0 -14.755714285714287d0
631500.d0 -16.580952380952382d0
632000.d0 -16.087704918032788d0
632500.d0 -16.1427868852459d0
633000.d0 -14.903392857142856d0
633500.d0 -13.77076923076923d0
634000.d0 -12.618541666666667d0
634500.d0 -13.167d0
635000.d0 -12.883877551020408d0
635500.d0 -12.56d0
636000.d0 -12.953469387755103d0
636500.d0 -12.996938775510204d0
637000.d0 -12.952244897959183d0
637500.d0 -12.420425531914894d0
638000.d0 -13.2384d0
638500.d0 -12.800416666666667d0
639000.d0 -13.08102040816326 6d0
639500.d0 -12.246956521739131d0
640000.d0 -12.90375d0
640500.d0 -11.27d0
641000.d0 -13.116595744680852d0
641500.d0 -13.046000000000001d0
642000.d0 -13.514347826086958d0
642500.d0 4.485964300000311d0
643000.d0 4.485964300000311d0
643500.d0 4.485964300000311d0
644000.d0 4.485964300000311d0
644500.d0 4.485964300000311d0
645000.d0 4.485964300000311d0

 /
END

FLOW_CONDITION bottom
  TYPE
    LIQUID_PRESSURE HYDROSTATIC
    MOLE_FRACTION DIRICHLET
    TEMPERATURE DIRICHLET
```

```
/
DATUM 0.d0 0.d0 1000.d0
GRADIENT
  TEMPERATURE 0.d0 0.d0 -0.051790238209626256
/
LIQUID_PRESSURE LIST
  TIME_UNITS year
  DATA_UNITS Pa
  INTERPOLATION LINEAR
  0.d0 228791.4427924983d0
  500.d0 216079.41141697354d0
  1000.d0 204254.24913385956d0
  1500.d0 195348.21356150892d0
  2000.d0 186439.81370538234d0
  2500.d0 178040.14871894888d0
  3000.d0 170205.6557750324d0
  3500.d0 164602.3892874983d0
  4000.d0 159895.85107054017d0
  4500.d0 154968.39927724394d0
  5000.d0 149877.65678848544d0
  5500.d0 147933.47740728944d0
  6000.d0 145340.1116006376d0
  6500.d0 143319.08471963252d0
  7000.d0 142189.29585391603d0
  7500.d0 140447.22504305508d0
  8000.d0 139028.5862147748d0
  8500.d0 139035.1831686525d0
  9000.d0 137756.4155298107d0
  9500.d0 135860.22833514455d0
  10000.d0 134443.6973206771d0
  10500.d0 132296.14757278838d0
  11000.d0 130349.20411701099d0
  11500.d0 128086.24827501315d0
  12000.d0 124684.03116551835d0
  12500.d0 121664.86919777622d0
  13000.d0 118553.90722993365d0
  13500.d0 113995.92115036542d0
  14000.d0 109679.31370196117d0
  14500.d0 105693.31580100703d0
  15000.d0 101325.0d0
  15500.d0 101325.0d0
  16000.d0 101325.0d0
  16500.d0 101325.0d0
  17000.d0 101325.0d0
  17500.d0 101325.0d0
  18000.d0 101325.0d0
  18500.d0 101325.0d0
  19000.d0 101325.0d0
  19500.d0 101325.0d0
  20000.d0 101325.0d0
  20500.d0 101325.0d0
  21000.d0 101325.0d0
  21500.d0 101325.0d0
  22000.d0 101325.0d0
  22500.d0 101325.0d0
  23000.d0 101325.0d0
  23500.d0 101325.0d0
  24000.d0 101325.0d0
  24500.d0 101325.0d0
  25000.d0 101325.0d0
  25500.d0 101325.0d0
  26000.d0 101325.0d0
  26500.d0 101325.0d0
  27000.d0 101325.0d0
  27500.d0 101325.0d0
  28000.d0 101325.0d0
  28500.d0 101325.0d0
  29000.d0 101325.0d0
  29500.d0 101325.0d0
  30000.d0 101325.0d0
  30500.d0 101325.0d0
  31000.d0 101325.0d0
  31500.d0 101325.0d0
  32000.d0 101325.0d0
  32500.d0 101325.0d0
  33000.d0 101325.0d0
  33500.d0 101325.0d0
  34000.d0 101325.0d0
  34500.d0 101325.0d0
  35000.d0 101325.0d0
  35500.d0 101325.0d0
  36000.d0 101325.0d0
  36500.d0 101325.0d0
  37000.d0 101325.0d0
  37500.d0 101325.0d0
  38000.d0 101325.0d0
  38500.d0 101325.0d0
  39000.d0 101325.0d0
  39500.d0 101325.0d0
  40000.d0 101325.0d0
  40500.d0 101325.0d0
  41000.d0 101325.0d0
  41500.d0 101325.0d0
  42000.d0 101325.0d0
  42500.d0 101325.0d0
  43000.d0 101325.0d0
  43500.d0 101325.0d0
  44000.d0 101325.0d0
  44500.d0 101325.0d0
  45000.d0 101325.0d0
  45500.d0 101325.0d0
  46000.d0 101325.0d0
  46500.d0 101325.0d0
  47000.d0 101325.0d0
  47500.d0 101325.0d0
  48000.d0 101325.0d0
  48500.d0 101325.0d0
  49000.d0 101325.0d0
  49500.d0 101325.0d0
  50000.d0 101325.0d0
  50500.d0 101325.0d0
  51000.d0 101325.0d0
  51500.d0 101325.0d0
  52000.d0 101325.0d0
  52500.d0 101325.0d0
  53000.d0 101325.0d0
  53500.d0 101325.0d0
  54000.d0 101325.0d0
  54500.d0 101325.0d0
  55000.d0 101325.0d0
  55500.d0 101325.0d0
  56000.d0 101325.0d0
  56500.d0 101325.0d0
  57000.d0 101325.0d0
  57500.d0 101325.0d0
  58000.d0 101325.0d0
  58500.d0 101325.0d0
  59000.d0 101325.0d0
  59500.d0 101325.0d0
  60000.d0 101325.0d0
  60500.d0 101325.0d0
  61000.d0 101325.0d0
  61500.d0 101325.0d0
  62000.d0 101325.0d0
  62500.d0 101325.0d0
  63000.d0 101325.0d0
```

63500.d0 101325.0d0
64000.d0 101325.0d0
64500.d0 101325.0d0
65000.d0 101325.0d0
65500.d0 101325.0d0
66000.d0 101325.0d0
66500.d0 101325.0d0
67000.d0 101325.0d0
67500.d0 101325.0d0
68000.d0 101325.0d0
68500.d0 101325.0d0
69000.d0 101325.0d0
69500.d0 101325.0d0
70000.d0 101325.0d0
70500.d0 101325.0d0
71000.d0 101325.0d0
71500.d0 101325.0d0
72000.d0 101325.0d0
72500.d0 101325.0d0
73000.d0 101325.0d0
73500.d0 101325.0d0
74000.d0 101325.0d0
74500.d0 101325.0d0
75000.d0 101325.0d0
75500.d0 101325.0d0
76000.d0 101325.0d0
76500.d0 101325.0d0
77000.d0 101325.0d0
77500.d0 101325.0d0
78000.d0 101325.0d0
78500.d0 101325.0d0
79000.d0 101325.0d0
79500.d0 101325.0d0
80000.d0 101325.0d0
80500.d0 101325.0d0
81000.d0 101325.0d0
81500.d0 101325.0d0
82000.d0 101325.0d0
82500.d0 101325.0d0
83000.d0 101325.0d0
83500.d0 101325.0d0
84000.d0 101325.0d0
84500.d0 101325.0d0
85000.d0 101325.0d0
85500.d0 101325.0d0
86000.d0 101325.0d0
86500.d0 101325.0d0
87000.d0 101325.0d0
87500.d0 101325.0d0
88000.d0 101325.0d0
88500.d0 101325.0d0
89000.d0 101325.0d0
89500.d0 101325.0d0
90000.d0 101325.0d0
90500.d0 101325.0d0
91000.d0 101325.0d0
91500.d0 101325.0d0
92000.d0 101325.0d0
92500.d0 101325.0d0
93000.d0 101325.0d0
93500.d0 101325.0d0
94000.d0 101325.0d0
94500.d0 101325.0d0
95000.d0 101325.0d0
95500.d0 101325.0d0
96000.d0 101325.0d0
96500.d0 101325.0d0
97000.d0 101325.0d0
97500.d0 101325.0d0
98000.d0 101325.0d0
98500.d0 101325.0d0
99000.d0 101325.0d0
99500.d0 101325.0d0
100000.d0 101325.0d0
100500.d0 101325.0d0
101000.d0 101325.0d0
101500.d0 101325.0d0
102000.d0 101325.0d0
102500.d0 114683.62337630425d0
103000.d0 142825.69745976117d0
103500.d0 169062.53769892064d0
104000.d0 193497.409290442d0
104500.d0 217307.69171576673d0
105000.d0 241411.80000000013d0
105500.d0 245797.68214455183d0
106000.d0 253844.65090038383d0
106500.d0 269774.2769149649d0
107000.d0 284755.1306861842d0
107500.d0 300272.25166315015d0
108000.d0 316352.38817811455d0
108500.d0 333506.8570924001d0
109000.d0 350869.0081508969d0
109500.d0 367989.968740548d0
110000.d0 385170.7769401565d0
110500.d0 401322.13684938423d0
111000.d0 417453.6042095362d0
111500.d0 433682.5747398268d0
112000.d0 449071.6901276747d0
112500.d0 462215.76948475064d0
113000.d0 474868.9443939842d0
113500.d0 487628.93212720985d0
114000.d0 499318.76683480304d0
114500.d0 508418.7506718697d0
115000.d0 516765.78645717644d0
115500.d0 525438.1141936843d0
116000.d0 533126.7747602843d0
116500.d0 538802.1731015407d0
117000.d0 543777.3894524488d0
117500.d0 548719.0826178014d0
118000.d0 552371.4150739119d0
118500.d0 555243.4824182974d0
119000.d0 557761.1270398516d0
119500.d0 560348.1629447096d0
120000.d0 561610.2000000002d0
120500.d0 560347.7005038051d0
121000.d0 557760.8765156117d0
121500.d0 555243.7657930969d0
122000.d0 552371.1557083392d0
122500.d0 548718.6316264215d0
123000.d0 543777.1076652851d0
123500.d0 538802.2391891903d0
124000.d0 533126.9873324714d0
124500.d0 525438.5303322929d0
125000.d0 516765.5101894857d0
125500.d0 508418.89753693575d0
126000.d0 499318.3411097474d0
126500.d0 487629.09900688176d0
127000.d0 474868.9031925703d0
127500.d0 462216.02242934395d0
128000.d0 449071.9306445766d0
128500.d0 433682.8151632949d0
129000.d0 417453.6148773002d0
129500.d0 401322.23714783275d0
130000.d0 385170.60403481725d0
130500.d0 367989.62843270693d0
131000.d0 350868.6081736669d0

131500.d0 333507.1308766445d0
132000.d0 316352.5741729917d0
132500.d0 300272.01659828494d0
133000.d0 284755.0282189866d0
133500.d0 269774.5679173274d0
134000.d0 253844.78124372096d0
134500.d0 241492.01399866963d0
135000.d0 228791.44279249868d0
135500.d0 216079.41141697404d0
136000.d0 204254.24913385956d0
136500.d0 195348.2135615086d0
137000.d0 186439.8137053813d0
137500.d0 178040.14871894865d0
138000.d0 170205.6557750324d0
138500.d0 164602.38928749776d0
139000.d0 159895.8510705401d0
139500.d0 154968.39927724376d0
140000.d0 149877.65678848536d0
140500.d0 147933.47740728947d0
141000.d0 145340.11160063773d0
141500.d0 143319.0847196329d0
142000.d0 142189.29585391603d0
142500.d0 140447.22504305525d0
143000.d0 139028.5862147748d0
143500.d0 139035.1831686525d0
144000.d0 137756.4155298107d0
144500.d0 135860.22833514435d0
145000.d0 134443.6973206771d0
145500.d0 132296.14757278838d0
146000.d0 130349.20411701087d0
146500.d0 128086.24827501309d0
147000.d0 124684.03116551835d0
147500.d0 121664.86919777622d0
148000.d0 118553.90722993365d0
148500.d0 113995.92115036582d0
149000.d0 109679.3137019612d0
149500.d0 105693.3158010066d0
150000.d0 101325.0d0
150500.d0 101325.0d0
151000.d0 101325.0d0
151500.d0 101325.0d0
152000.d0 101325.0d0
152500.d0 101325.0d0
153000.d0 101325.0d0
153500.d0 101325.0d0
154000.d0 101325.0d0
154500.d0 101325.0d0
155000.d0 101325.0d0
155500.d0 101325.0d0
156000.d0 101325.0d0
156500.d0 101325.0d0
157000.d0 101325.0d0
157500.d0 101325.0d0
158000.d0 101325.0d0
158500.d0 101325.0d0
159000.d0 101325.0d0
159500.d0 101325.0d0
160000.d0 101325.0d0
160500.d0 101325.0d0
161000.d0 101325.0d0
161500.d0 101325.0d0
162000.d0 101325.0d0
162500.d0 101325.0d0
163000.d0 101325.0d0
163500.d0 101325.0d0
164000.d0 101325.0d0
164500.d0 101325.0d0
165000.d0 101325.0d0
165500.d0 101325.0d0
166000.d0 101325.0d0
166500.d0 101325.0d0
167000.d0 101325.0d0
167500.d0 101325.0d0
168000.d0 101325.0d0
168500.d0 101325.0d0
169000.d0 101325.0d0
169500.d0 101325.0d0
170000.d0 101325.0d0
170500.d0 101325.0d0
171000.d0 101325.0d0
171500.d0 101325.0d0
172000.d0 101325.0d0
172500.d0 101325.0d0
173000.d0 101325.0d0
173500.d0 101325.0d0
174000.d0 101325.0d0
174500.d0 101325.0d0
175000.d0 101325.0d0
175500.d0 101325.0d0
176000.d0 101325.0d0
176500.d0 101325.0d0
177000.d0 101325.0d0
177500.d0 101325.0d0
178000.d0 101325.0d0
178500.d0 101325.0d0
179000.d0 101325.0d0
179500.d0 101325.0d0
180000.d0 101325.0d0
180500.d0 101325.0d0
181000.d0 101325.0d0
181500.d0 101325.0d0
182000.d0 101325.0d0
182500.d0 101325.0d0
183000.d0 101325.0d0
183500.d0 101325.0d0
184000.d0 101325.0d0
184500.d0 101325.0d0
185000.d0 101325.0d0
185500.d0 101325.0d0
186000.d0 101325.0d0
186500.d0 101325.0d0
187000.d0 101325.0d0
187500.d0 101325.0d0
188000.d0 101325.0d0
188500.d0 101325.0d0
189000.d0 101325.0d0
189500.d0 101325.0d0
190000.d0 101325.0d0
190500.d0 101325.0d0
191000.d0 101325.0d0
191500.d0 101325.0d0
192000.d0 101325.0d0
192500.d0 101325.0d0
193000.d0 101325.0d0
193500.d0 101325.0d0
194000.d0 101325.0d0
194500.d0 101325.0d0
195000.d0 101325.0d0
195500.d0 101325.0d0
196000.d0 101325.0d0
196500.d0 101325.0d0
197000.d0 101325.0d0
197500.d0 101325.0d0
198000.d0 101325.0d0
198500.d0 101325.0d0
199000.d0 101325.0d0

199500.d0 101325.0d0
200000.d0 101325.0d0
200500.d0 101325.0d0
201000.d0 101325.0d0
201500.d0 101325.0d0
202000.d0 101325.0d0
202500.d0 101325.0d0
203000.d0 101325.0d0
203500.d0 101325.0d0
204000.d0 101325.0d0
204500.d0 101325.0d0
205000.d0 101325.0d0
205500.d0 101325.0d0
206000.d0 101325.0d0
206500.d0 101325.0d0
207000.d0 101325.0d0
207500.d0 101325.0d0
208000.d0 101325.0d0
208500.d0 101325.0d0
209000.d0 101325.0d0
209500.d0 101325.0d0
210000.d0 101325.0d0
210500.d0 101325.0d0
211000.d0 101325.0d0
211500.d0 101325.0d0
212000.d0 101325.0d0
212500.d0 101325.0d0
213000.d0 101325.0d0
213500.d0 101325.0d0
214000.d0 101325.0d0
214500.d0 101325.0d0
215000.d0 101325.0d0
215500.d0 101325.0d0
216000.d0 101325.0d0
216500.d0 101325.0d0
217000.d0 101325.0d0
217500.d0 101325.0d0
218000.d0 101325.0d0
218500.d0 101325.0d0
219000.d0 101325.0d0
219500.d0 101325.0d0
220000.d0 101325.0d0
220500.d0 101325.0d0
221000.d0 101325.0d0
221500.d0 101325.0d0
222000.d0 101325.0d0
222500.d0 101325.0d0
223000.d0 101325.0d0
223500.d0 101325.0d0
224000.d0 101325.0d0
224500.d0 101325.0d0
225000.d0 101325.0d0
225500.d0 101325.0d0
226000.d0 101325.0d0
226500.d0 101325.0d0
227000.d0 101325.0d0
227500.d0 101325.0d0
228000.d0 101325.0d0
228500.d0 101325.0d0
229000.d0 101325.0d0
229500.d0 101325.0d0
230000.d0 101325.0d0
230500.d0 101325.0d0
231000.d0 101325.0d0
231500.d0 101325.0d0
232000.d0 101325.0d0
232500.d0 101325.0d0
233000.d0 101325.0d0
233500.d0 101325.0d0
234000.d0 101325.0d0
234500.d0 101325.0d0
235000.d0 101325.0d0
235500.d0 101325.0d0
236000.d0 101325.0d0
236500.d0 101325.0d0
237000.d0 101325.0d0
237500.d0 114683.62337630628d0
238000.d0 142825.69745976164d0
238500.d0 169062.53769892064d0
239000.d0 193497.40929044347d0
239500.d0 217307.69171576703d0
240000.d0 241411.80000000013d0
240500.d0 245797.68214455218d0
241000.d0 253844.65090038424d0
241500.d0 269774.2769149648d0
242000.d0 284755.1306861832d0
242500.d0 300272.25166315195d0
243000.d0 316352.38817811455d0
243500.d0 333506.85709240206d0
244000.d0 350869.0081508971d0
244500.d0 367989.96874054853d0
245000.d0 385170.7769401565d0
245500.d0 401322.1368493825d0
246000.d0 417453.6042095362d0
246500.d0 433682.5747398268d0
247000.d0 449071.6901276736d0
247500.d0 462215.76948475215d0
248000.d0 474868.94439398433d0
248500.d0 487628.9321272106d0
249000.d0 499318.76683480287d0
249500.d0 508418.75067187d0
250000.d0 516765.78645717556d0
250500.d0 525438.1141936843d0
251000.d0 533126.7747602841d0
251500.d0 538802.1731015404d0
252000.d0 543777.3894524485d0
252500.d0 548719.0826178014d0
253000.d0 552371.4150739119d0
253500.d0 555243.4824182978d0
254000.d0 557761.1270398519d0
254500.d0 560348.1629447096d0
255000.d0 561610.2000000002d0
255500.d0 560347.7005038051d0
256000.d0 557760.8765156117d0
256500.d0 555243.7657930969d0
257000.d0 552371.1557083392d0
257500.d0 548718.6316264215d0
258000.d0 543777.1076652851d0
258500.d0 538802.2391891903d0
259000.d0 533126.9873324714d0
259500.d0 525438.5303322929d0
260000.d0 516765.5101894857d0
260500.d0 508418.89753693575d0
261000.d0 499318.3411097474d0
261500.d0 487629.09900688176d0
262000.d0 474868.9031925703d0
262500.d0 462216.02242934395d0
263000.d0 449071.9306445766d0
263500.d0 433682.8151632949d0
264000.d0 417453.6148773002d0
264500.d0 401322.23714783275d0
265000.d0 385170.60403481725d0
265500.d0 367989.62843270693d0
266000.d0 350868.6081736669d0
266500.d0 333507.1308766445d0
267000.d0 316352.5741729917d0

267500.d0 300272.01659828494d0
268000.d0 284755.0282189866d0
268500.d0 269774.5679173274d0
269000.d0 253844.78124372096d0
269500.d0 241492.01399866963d0
270000.d0 228791.44279249868d0
270500.d0 216079.41141697404d0
271000.d0 204254.24913385956d0
271500.d0 195348.2135615086d0
272000.d0 186439.8137053813d0
272500.d0 178040.14871894865d0
273000.d0 170205.6557750324d0
273500.d0 164602.38928749776d0
274000.d0 159895.8510705401d0
274500.d0 154968.39927724376d0
275000.d0 149877.65678848536d0
275500.d0 147933.47740728947d0
276000.d0 145340.11160063773d0
276500.d0 143319.0847196329d0
277000.d0 142189.29585391603d0
277500.d0 140447.22504305525d0
278000.d0 139028.5862147748d0
278500.d0 139035.1831686525d0
279000.d0 137756.4155298107d0
279500.d0 135860.22833514435d0
280000.d0 134443.6973206771d0
280500.d0 132296.14757278838d0
281000.d0 130349.20411701087d0
281500.d0 128086.24827501309d0
282000.d0 124684.03116551835d0
282500.d0 121664.86919777622d0
283000.d0 118553.90722993365d0
283500.d0 113995.92115036582d0
284000.d0 109679.3137019612d0
284500.d0 105693.3158010066d0
285000.d0 101325.0d0
285500.d0 101325.0d0
286000.d0 101325.0d0
286500.d0 101325.0d0
287000.d0 101325.0d0
287500.d0 101325.0d0
288000.d0 101325.0d0
288500.d0 101325.0d0
289000.d0 101325.0d0
289500.d0 101325.0d0
290000.d0 101325.0d0
290500.d0 101325.0d0
291000.d0 101325.0d0
291500.d0 101325.0d0
292000.d0 101325.0d0
292500.d0 101325.0d0
293000.d0 101325.0d0
293500.d0 101325.0d0
294000.d0 101325.0d0
294500.d0 101325.0d0
295000.d0 101325.0d0
295500.d0 101325.0d0
296000.d0 101325.0d0
296500.d0 101325.0d0
297000.d0 101325.0d0
297500.d0 101325.0d0
298000.d0 101325.0d0
298500.d0 101325.0d0
299000.d0 101325.0d0
299500.d0 101325.0d0
300000.d0 101325.0d0
300500.d0 101325.0d0
301000.d0 101325.0d0

301500.d0 101325.0d0
302000.d0 101325.0d0
302500.d0 101325.0d0
303000.d0 101325.0d0
303500.d0 101325.0d0
304000.d0 101325.0d0
304500.d0 101325.0d0
305000.d0 101325.0d0
305500.d0 101325.0d0
306000.d0 101325.0d0
306500.d0 101325.0d0
307000.d0 101325.0d0
307500.d0 101325.0d0
308000.d0 101325.0d0
308500.d0 101325.0d0
309000.d0 101325.0d0
309500.d0 101325.0d0
310000.d0 101325.0d0
310500.d0 101325.0d0
311000.d0 101325.0d0
311500.d0 101325.0d0
312000.d0 101325.0d0
312500.d0 101325.0d0
313000.d0 101325.0d0
313500.d0 101325.0d0
314000.d0 101325.0d0
314500.d0 101325.0d0
315000.d0 101325.0d0
315500.d0 101325.0d0
316000.d0 101325.0d0
316500.d0 101325.0d0
317000.d0 101325.0d0
317500.d0 101325.0d0
318000.d0 101325.0d0
318500.d0 101325.0d0
319000.d0 101325.0d0
319500.d0 101325.0d0
320000.d0 101325.0d0
320500.d0 101325.0d0
321000.d0 101325.0d0
321500.d0 101325.0d0
322000.d0 101325.0d0
322500.d0 101325.0d0
323000.d0 101325.0d0
323500.d0 101325.0d0
324000.d0 101325.0d0
324500.d0 101325.0d0
325000.d0 101325.0d0
325500.d0 101325.0d0
326000.d0 101325.0d0
326500.d0 101325.0d0
327000.d0 101325.0d0
327500.d0 101325.0d0
328000.d0 101325.0d0
328500.d0 101325.0d0
329000.d0 101325.0d0
329500.d0 101325.0d0
330000.d0 101325.0d0
330500.d0 101325.0d0
331000.d0 101325.0d0
331500.d0 101325.0d0
332000.d0 101325.0d0
332500.d0 101325.0d0
333000.d0 101325.0d0
333500.d0 101325.0d0
334000.d0 101325.0d0
334500.d0 101325.0d0
335000.d0 101325.0d0

335500.d0 101325.0d0
336000.d0 101325.0d0
336500.d0 101325.0d0
337000.d0 101325.0d0
337500.d0 101325.0d0
338000.d0 101325.0d0
338500.d0 101325.0d0
339000.d0 101325.0d0
339500.d0 101325.0d0
340000.d0 101325.0d0
340500.d0 101325.0d0
341000.d0 101325.0d0
341500.d0 101325.0d0
342000.d0 101325.0d0
342500.d0 101325.0d0
343000.d0 101325.0d0
343500.d0 101325.0d0
344000.d0 101325.0d0
344500.d0 101325.0d0
345000.d0 101325.0d0
345500.d0 101325.0d0
346000.d0 101325.0d0
346500.d0 101325.0d0
347000.d0 101325.0d0
347500.d0 101325.0d0
348000.d0 101325.0d0
348500.d0 101325.0d0
349000.d0 101325.0d0
349500.d0 101325.0d0
350000.d0 101325.0d0
350500.d0 101325.0d0
351000.d0 101325.0d0
351500.d0 101325.0d0
352000.d0 101325.0d0
352500.d0 101325.0d0
353000.d0 101325.0d0
353500.d0 101325.0d0
354000.d0 101325.0d0
354500.d0 101325.0d0
355000.d0 101325.0d0
355500.d0 101325.0d0
356000.d0 101325.0d0
356500.d0 101325.0d0
357000.d0 101325.0d0
357500.d0 101325.0d0
358000.d0 101325.0d0
358500.d0 101325.0d0
359000.d0 101325.0d0
359500.d0 101325.0d0
360000.d0 101325.0d0
360500.d0 101325.0d0
361000.d0 101325.0d0
361500.d0 101325.0d0
362000.d0 101325.0d0
362500.d0 101325.0d0
363000.d0 101325.0d0
363500.d0 101325.0d0
364000.d0 101325.0d0
364500.d0 101325.0d0
365000.d0 101325.0d0
365500.d0 101325.0d0
366000.d0 101325.0d0
366500.d0 101325.0d0
367000.d0 101325.0d0
367500.d0 101325.0d0
368000.d0 101325.0d0
368500.d0 101325.0d0
369000.d0 101325.0d0
369500.d0 101325.0d0
370000.d0 101325.0d0
370500.d0 101325.0d0
371000.d0 101325.0d0
371500.d0 101325.0d0
372000.d0 101325.0d0
372500.d0 114683.62337630628d0
373000.d0 142825.69745976164d0
373500.d0 169062.53769892064d0
374000.d0 193497.40929044347d0
374500.d0 217307.69171576703d0
375000.d0 241411.80000000013d0
375500.d0 245797.68214455218d0
376000.d0 253844.65090038424d0
376500.d0 269774.2769149648d0
377000.d0 284755.1306861832d0
377500.d0 300272.25166315195d0
378000.d0 316352.38817811455d0
378500.d0 333506.85709240206d0
379000.d0 350869.0081508971d0
379500.d0 367989.96874054853d0
380000.d0 385170.7769401565d0
380500.d0 401322.1368493825d0
381000.d0 417453.6042095362d0
381500.d0 433682.5747398268d0
382000.d0 449071.6901276736d0
382500.d0 462215.76948475215d0
383000.d0 474868.9443939837d0
383500.d0 487628.93212721025d0
384000.d0 499318.7668348029d0
384500.d0 508418.75067186984d0
385000.d0 516765.78645717556d0
385500.d0 525438.1141936848d0
386000.d0 533126.774760284d0
386500.d0 538802.1731015402d0
387000.d0 543777.3894524486d0
387500.d0 548719.0826178014d0
388000.d0 552371.4150739119d0
388500.d0 555243.4824182977d0
389000.d0 557761.1270398517d0
389500.d0 560348.1629447098d0
390000.d0 561610.2000000002d0
390500.d0 560347.7005038052d0
391000.d0 557760.8765156115d0
391500.d0 555243.7657930966d0
392000.d0 552371.1557083392d0
392500.d0 548718.6316264215d0
393000.d0 543777.1076652852d0
393500.d0 538802.2391891903d0
394000.d0 533126.9873324712d0
394500.d0 525438.5303322931d0
395000.d0 516765.5101894857d0
395500.d0 508418.8975369356d0
396000.d0 499318.3411097475d0
396500.d0 487629.09900688136d0
397000.d0 474868.9031925697d0
397500.d0 462216.02242934355d0
398000.d0 449071.93064457644d0
398500.d0 433682.8151632941d0
399000.d0 417453.6148773002d0
399500.d0 401322.23714783275d0
400000.d0 385170.60403481714d0
400500.d0 367989.62843270676d0
401000.d0 350868.60817366757d0
401500.d0 333507.13087664347d0
402000.d0 316352.5741729913d0
402500.d0 300272.016598284d0
403000.d0 284755.0282189871d0

403500.d0 269774.5679173266d0
404000.d0 253844.78124372076d0
404500.d0 241492.0139986694d0
405000.d0 228791.4427924985d0
405500.d0 216079.41141697328d0
406000.d0 204254.24913385956d0
406500.d0 195348.2135615084d0
407000.d0 186439.81370538156d0
407500.d0 178040.14871894865d0
408000.d0 170205.65577503195d0
408500.d0 164602.38928749782d0
409000.d0 159895.85107054014d0
409500.d0 154968.39927724368d0
410000.d0 149877.65678848565d0
410500.d0 147933.4774072896d0
411000.d0 145340.11160063767d0
411500.d0 143319.08471963272d0
412000.d0 142189.29585391603d0
412500.d0 140447.22504305516d0
413000.d0 139028.5862147748d0
413500.d0 139035.1831686525d0
414000.d0 137756.4155298108d0
414500.d0 135860.22833514446d0
415000.d0 134443.69732067722d0
415500.d0 132296.1475727885d0
416000.d0 130349.20411701096d0
416500.d0 128086.248275013d0
417000.d0 124684.03116551835d0
417500.d0 121664.86919777622d0
418000.d0 118553.90722993379d0
418500.d0 113995.9211503657d0
419000.d0 109679.31370196119d0
419500.d0 105693.31580100664d0
420000.d0 101325.0d0
420500.d0 101325.0d0
421000.d0 101325.0d0
421500.d0 101325.0d0
422000.d0 101325.0d0
422500.d0 101325.0d0
423000.d0 101325.0d0
423500.d0 101325.0d0
424000.d0 101325.0d0
424500.d0 101325.0d0
425000.d0 101325.0d0
425500.d0 101325.0d0
426000.d0 101325.0d0
426500.d0 101325.0d0
427000.d0 101325.0d0
427500.d0 101325.0d0
428000.d0 101325.0d0
428500.d0 101325.0d0
429000.d0 101325.0d0
429500.d0 101325.0d0
430000.d0 101325.0d0
430500.d0 101325.0d0
431000.d0 101325.0d0
431500.d0 101325.0d0
432000.d0 101325.0d0
432500.d0 101325.0d0
433000.d0 101325.0d0
433500.d0 101325.0d0
434000.d0 101325.0d0
434500.d0 101325.0d0
435000.d0 101325.0d0
435500.d0 101325.0d0
436000.d0 101325.0d0
436500.d0 101325.0d0
437000.d0 101325.0d0
437500.d0 101325.0d0
438000.d0 101325.0d0
438500.d0 101325.0d0
439000.d0 101325.0d0
439500.d0 101325.0d0
440000.d0 101325.0d0
440500.d0 101325.0d0
441000.d0 101325.0d0
441500.d0 101325.0d0
442000.d0 101325.0d0
442500.d0 101325.0d0
443000.d0 101325.0d0
443500.d0 101325.0d0
444000.d0 101325.0d0
444500.d0 101325.0d0
445000.d0 101325.0d0
445500.d0 101325.0d0
446000.d0 101325.0d0
446500.d0 101325.0d0
447000.d0 101325.0d0
447500.d0 101325.0d0
448000.d0 101325.0d0
448500.d0 101325.0d0
449000.d0 101325.0d0
449500.d0 101325.0d0
450000.d0 101325.0d0
450500.d0 101325.0d0
451000.d0 101325.0d0
451500.d0 101325.0d0
452000.d0 101325.0d0
452500.d0 101325.0d0
453000.d0 101325.0d0
453500.d0 101325.0d0
454000.d0 101325.0d0
454500.d0 101325.0d0
455000.d0 101325.0d0
455500.d0 101325.0d0
456000.d0 101325.0d0
456500.d0 101325.0d0
457000.d0 101325.0d0
457500.d0 101325.0d0
458000.d0 101325.0d0
458500.d0 101325.0d0
459000.d0 101325.0d0
459500.d0 101325.0d0
460000.d0 101325.0d0
460500.d0 101325.0d0
461000.d0 101325.0d0
461500.d0 101325.0d0
462000.d0 101325.0d0
462500.d0 101325.0d0
463000.d0 101325.0d0
463500.d0 101325.0d0
464000.d0 101325.0d0
464500.d0 101325.0d0
465000.d0 101325.0d0
465500.d0 101325.0d0
466000.d0 101325.0d0
466500.d0 101325.0d0
467000.d0 101325.0d0
467500.d0 101325.0d0
468000.d0 101325.0d0
468500.d0 101325.0d0
469000.d0 101325.0d0
469500.d0 101325.0d0
470000.d0 101325.0d0
470500.d0 101325.0d0
471000.d0 101325.0d0

```
471500.d0 101325.0d0
472000.d0 101325.0d0
472500.d0 101325.0d0
473000.d0 101325.0d0
473500.d0 101325.0d0
474000.d0 101325.0d0
474500.d0 101325.0d0
475000.d0 101325.0d0
475500.d0 101325.0d0
476000.d0 101325.0d0
476500.d0 101325.0d0
477000.d0 101325.0d0
477500.d0 101325.0d0
478000.d0 101325.0d0
478500.d0 101325.0d0
479000.d0 101325.0d0
479500.d0 101325.0d0
480000.d0 101325.0d0
480500.d0 101325.0d0
481000.d0 101325.0d0
481500.d0 101325.0d0
482000.d0 101325.0d0
482500.d0 101325.0d0
483000.d0 101325.0d0
483500.d0 101325.0d0
484000.d0 101325.0d0
484500.d0 101325.0d0
485000.d0 101325.0d0
485500.d0 101325.0d0
486000.d0 101325.0d0
486500.d0 101325.0d0
487000.d0 101325.0d0
487500.d0 101325.0d0
488000.d0 101325.0d0
488500.d0 101325.0d0
489000.d0 101325.0d0
489500.d0 101325.0d0
490000.d0 101325.0d0
490500.d0 101325.0d0
491000.d0 101325.0d0
491500.d0 101325.0d0
492000.d0 101325.0d0
492500.d0 101325.0d0
493000.d0 101325.0d0
493500.d0 101325.0d0
494000.d0 101325.0d0
494500.d0 101325.0d0
495000.d0 101325.0d0
495500.d0 101325.0d0
496000.d0 101325.0d0
496500.d0 101325.0d0
497000.d0 101325.0d0
497500.d0 101325.0d0
498000.d0 101325.0d0
498500.d0 101325.0d0
499000.d0 101325.0d0
499500.d0 101325.0d0
500000.d0 101325.0d0
500500.d0 101325.0d0
501000.d0 101325.0d0
501500.d0 101325.0d0
502000.d0 101325.0d0
502500.d0 101325.0d0
503000.d0 101325.0d0
503500.d0 101325.0d0
504000.d0 101325.0d0
504500.d0 101325.0d0
505000.d0 101325.0d0
```

```
505500.d0 101325.0d0
506000.d0 101325.0d0
506500.d0 101325.0d0
507000.d0 101325.0d0
507500.d0 114683.62337630507d0
508000.d0 142825.6974597607d0
508500.d0 169062.53769892064d0
509000.d0 193497.40929044347d0
509500.d0 217307.69171576633d0
510000.d0 241411.80000000013d0
510500.d0 245797.682144552d0
511000.d0 253844.65090038403d0
511500.d0 269774.276914964d0
512000.d0 284755.1306861837d0
512500.d0 300272.2516631511d0
513000.d0 316352.3881781142d0
513500.d0 333506.8570924011d0
514000.d0 350869.0081508978d0
514500.d0 367989.9687405483d0
515000.d0 385170.77694015636d0
515500.d0 401322.1368493829d0
516000.d0 417453.6042095362d0
516500.d0 433682.5747398264d0
517000.d0 449071.6901276739d0
517500.d0 462215.7694847519d0
518000.d0 474868.9443939837d0
518500.d0 487628.93212721025d0
519000.d0 499318.7668348029d0
519500.d0 508418.7506718697d0
520000.d0 516765.78645717556d0
520500.d0 525438.1141936845d0
521000.d0 533126.774760284d0
521500.d0 538802.1731015404d0
522000.d0 543777.3894524486d0
522500.d0 548719.0826178014d0
523000.d0 552371.4150739119d0
523500.d0 555243.4824182977d0
524000.d0 557761.1270398517d0
524500.d0 560348.1629447096d0
525000.d0 561610.2000000002d0
525500.d0 560347.7005038052d0
526000.d0 557760.8765156115d0
526500.d0 555243.7657930967d0
527000.d0 552371.1557083391d0
527500.d0 548718.6316264215d0
528000.d0 543777.1076652852d0
528500.d0 538802.2391891903d0
529000.d0 533126.9873324712d0
529500.d0 525438.530332293d0
530000.d0 516765.5101894857d0
530500.d0 508418.89753693546d0
531000.d0 499318.3411097475d0
531500.d0 487629.09900688136d0
532000.d0 474868.9031925697d0
532500.d0 462216.0224293438d0
533000.d0 449071.93064457685d0
533500.d0 433682.8151632945d0
534000.d0 417453.6148773002d0
534500.d0 401322.23714783316d0
535000.d0 385170.60403481714d0
535500.d0 367989.62843270676d0
536000.d0 350868.60817366757d0
536500.d0 333507.13087664347d0
537000.d0 316352.57417299127d0
537500.d0 300272.016598284d0
538000.d0 284755.02821898705d0
538500.d0 269774.5679173266d0
539000.d0 253844.78124372076d0
```

539500.d0 241492.0139986694d0
540000.d0 228791.4427924985d0
540500.d0 216079.41141697328d0
541000.d0 204254.24913385956d0
541500.d0 195348.21356150857d0
542000.d0 186439.8137053817d0
542500.d0 178040.1487189487d0
543000.d0 170205.65577503195d0
543500.d0 164602.3892874978d0
544000.d0 159895.85107054014d0
544500.d0 154968.3992772437d0
545000.d0 149877.65678848565d0
545500.d0 147933.4774072896d0
546000.d0 145340.11160063767d0
546500.d0 143319.08471963275d0
547000.d0 142189.29585391603d0
547500.d0 140447.22504305516d0
548000.d0 139028.5862147748d0
548500.d0 139035.1831686525d0
549000.d0 137756.41552981077d0
549500.d0 135860.2283351444d0
550000.d0 134443.69732067717d0
550500.d0 132296.14757278847d0
551000.d0 130349.20411701096d0
551500.d0 128086.248275013d0
552000.d0 124684.03116551824d0
552500.d0 121664.86919777622d0
553000.d0 118553.90722993373d0
553500.d0 113995.92115036567d0
554000.d0 109679.31370196119d0
554500.d0 105693.31580100664d0
555000.d0 101325.0d0
555500.d0 101325.0d0
556000.d0 101325.0d0
556500.d0 101325.0d0
557000.d0 101325.0d0
557500.d0 101325.0d0
558000.d0 101325.0d0
558500.d0 101325.0d0
559000.d0 101325.0d0
559500.d0 101325.0d0
560000.d0 101325.0d0
560500.d0 101325.0d0
561000.d0 101325.0d0
561500.d0 101325.0d0
562000.d0 101325.0d0
562500.d0 101325.0d0
563000.d0 101325.0d0
563500.d0 101325.0d0
564000.d0 101325.0d0
564500.d0 101325.0d0
565000.d0 101325.0d0
565500.d0 101325.0d0
566000.d0 101325.0d0
566500.d0 101325.0d0
567000.d0 101325.0d0
567500.d0 101325.0d0
568000.d0 101325.0d0
568500.d0 101325.0d0
569000.d0 101325.0d0
569500.d0 101325.0d0
570000.d0 101325.0d0
570500.d0 101325.0d0
571000.d0 101325.0d0
571500.d0 101325.0d0
572000.d0 101325.0d0
572500.d0 101325.0d0
573000.d0 101325.0d0
573500.d0 101325.0d0
574000.d0 101325.0d0
574500.d0 101325.0d0
575000.d0 101325.0d0
575500.d0 101325.0d0
576000.d0 101325.0d0
576500.d0 101325.0d0
577000.d0 101325.0d0
577500.d0 101325.0d0
578000.d0 101325.0d0
578500.d0 101325.0d0
579000.d0 101325.0d0
579500.d0 101325.0d0
580000.d0 101325.0d0
580500.d0 101325.0d0
581000.d0 101325.0d0
581500.d0 101325.0d0
582000.d0 101325.0d0
582500.d0 101325.0d0
583000.d0 101325.0d0
583500.d0 101325.0d0
584000.d0 101325.0d0
584500.d0 101325.0d0
585000.d0 101325.0d0
585500.d0 101325.0d0
586000.d0 101325.0d0
586500.d0 101325.0d0
587000.d0 101325.0d0
587500.d0 101325.0d0
588000.d0 101325.0d0
588500.d0 101325.0d0
589000.d0 101325.0d0
589500.d0 101325.0d0
590000.d0 101325.0d0
590500.d0 101325.0d0
591000.d0 101325.0d0
591500.d0 101325.0d0
592000.d0 101325.0d0
592500.d0 101325.0d0
593000.d0 101325.0d0
593500.d0 101325.0d0
594000.d0 101325.0d0
594500.d0 101325.0d0
595000.d0 101325.0d0
595500.d0 101325.0d0
596000.d0 101325.0d0
596500.d0 101325.0d0
597000.d0 101325.0d0
597500.d0 101325.0d0
598000.d0 101325.0d0
598500.d0 101325.0d0
599000.d0 101325.0d0
599500.d0 101325.0d0
600000.d0 101325.0d0
600500.d0 101325.0d0
601000.d0 101325.0d0
601500.d0 101325.0d0
602000.d0 101325.0d0
602500.d0 101325.0d0
603000.d0 101325.0d0
603500.d0 101325.0d0
604000.d0 101325.0d0
604500.d0 101325.0d0
605000.d0 101325.0d0
605500.d0 101325.0d0
606000.d0 101325.0d0
606500.d0 101325.0d0
607000.d0 101325.0d0

```
607500.d0 101325.0d0
608000.d0 101325.0d0
608500.d0 101325.0d0
609000.d0 101325.0d0
609500.d0 101325.0d0
610000.d0 101325.0d0
610500.d0 101325.0d0
611000.d0 101325.0d0
611500.d0 101325.0d0
612000.d0 101325.0d0
612500.d0 101325.0d0
613000.d0 101325.0d0
613500.d0 101325.0d0
614000.d0 101325.0d0
614500.d0 101325.0d0
615000.d0 101325.0d0
615500.d0 101325.0d0
616000.d0 101325.0d0
616500.d0 101325.0d0
617000.d0 101325.0d0
617500.d0 101325.0d0
618000.d0 101325.0d0
618500.d0 101325.0d0
619000.d0 101325.0d0
619500.d0 101325.0d0
620000.d0 101325.0d0
620500.d0 101325.0d0
621000.d0 101325.0d0
621500.d0 101325.0d0
622000.d0 101325.0d0
622500.d0 101325.0d0
623000.d0 101325.0d0
623500.d0 101325.0d0
624000.d0 101325.0d0
624500.d0 101325.0d0
625000.d0 101325.0d0
625500.d0 101325.0d0
626000.d0 101325.0d0
626500.d0 101325.0d0
627000.d0 101325.0d0
627500.d0 101325.0d0
```

```
628000.d0 101325.0d0
628500.d0 101325.0d0
629000.d0 101325.0d0
629500.d0 101325.0d0
630000.d0 101325.0d0
630500.d0 101325.0d0
631000.d0 101325.0d0
631500.d0 101325.0d0
632000.d0 101325.0d0
632500.d0 101325.0d0
633000.d0 101325.0d0
633500.d0 101325.0d0
634000.d0 101325.0d0
634500.d0 101325.0d0
635000.d0 101325.0d0
635500.d0 101325.0d0
636000.d0 101325.0d0
636500.d0 101325.0d0
637000.d0 101325.0d0
637500.d0 101325.0d0
638000.d0 101325.0d0
638500.d0 101325.0d0
639000.d0 101325.0d0
639500.d0 101325.0d0
640000.d0 101325.0d0
640500.d0 101325.0d0
641000.d0 101325.0d0
641500.d0 101325.0d0
642000.d0 101325.0d0
642500.d0 114683.6233763056d0
643000.d0 142825.6974597611d0
643500.d0 169062.53769892076d0
644000.d0 193497.40929044323d0
644500.d0 217307.69171576656d0
645000.d0 241411.80000000013d0

 /
 TEMPERATURE 4.485964300000311
 MOLE_FRACTION 1.d-10
END
```

This page left blank.

DISTRIBUTION

Email—Internal

Name	Org.	Sandia Email Address
Ethan W. Conley	08844	ewconle@sandia.gov
Carmen M. Mendez	08844	cmmende@sandia.gov
Michael A. Nole	08844	mnole@sandia.gov
Benjamin K. Cook	08910	bkcook@sandia.gov
Andrew Glen	08913	aglen@sandia.gov
Benjamin M. Wagman	08917	bmwagma@sandia.gov
Technical Library	01911	sanddocs@sandia.gov

Email—External

Name	Company Email Address	Company Name
Professor Thomas Marchitto	tom.marchitto@colorado.edu	University of Colorado, Boulder

This page left blank.

This page left blank.

Sandia National Laboratories

Sandia National Laboratories is a multimission laboratory managed and operated by National Technology & Engineering Solutions of Sandia LLC, a wholly owned subsidiary of Honeywell International Inc. for the U.S. Department of Energy's National Nuclear Security Administration under contract DE-NA0003525.